

# MODELLING ACTIVATED CARBON ADSORPTION KINETICS FOR REMOVAL OF MICROPOLLUTANTS FROM WASTEWATER

Mathieu Coghe

Student number: 02207820

Promotors: Dr. Ir. Saba Daneshgar, Dr. Ir. Giacomo Bellandi

Tutors: Ir. Daniel Illana González, Ir. Simon Duchi

Master's Dissertation submitted to Ghent University in partial fulfilment of the requirements for the degree of  
Master of Science in Environmental Science and Technology

Academic year: 2023 - 2024

## Copyright

---

The author and the promoter give the permission to use this master dissertation for consultation and to copy parts of it for personal use. Every other use is subject to the copyright laws, more specifically the source must be extensively stated when using from this thesis.

De auteur en de promotor geven de toelating deze masterproef voor consultatie beschikbaar te stellen en delen van de masterproef te kopiëren voor persoonlijk gebruik. Elk ander gebruik valt onder de beperkingen van het auteursrecht, in het bijzonder met betrekking tot de verplichting de bron uitdrukkelijk te vermelden bij het aanhalen van resultaten uit deze masterproef.

Gent, 3 June 2024

The promoter(s),

The author,

*'Signature'*

*Prof. + Name*

*'Signature'*

*'Name'*

# PREFACE

# TABLE OF CONTENTS

<b>ABSTRACT</b>	<b>6</b>
<b>INTRODUCTION</b>	<b>7</b>
1.1    Problem statement: organic micropollutants	7
1.2    Modelling removal of organic micropollutants	8
1.3    Aim of the thesis	8
<b>LITERATURE REVIEW</b>	<b>9</b>
1 <b>Principles of micropollutant removal</b>	<b>9</b>
1.1    Classification of MPs	9
1.2    The fate of micropollutants in WWTPs	10
1.3    Tertiary treatment methods for MP removal in WWTPs	12
1.4    The adsorption process	17
1.5    Types of adsorbents	18
1.6    Types of adsorption set-ups	21
1.7    Adsorption equilibrium	22
1.8    Adsorption kinetics	23
1.9    The breakthrough curve	24
2 <b>Adsorption on activated carbon: breakthrough curve models</b>	<b>26</b>
2.1    Opportunities and challenges	26
2.2    Components of fixed-bed BTC models	27
2.3    Equilibrium relationship: isotherm equations	27
2.4    Fixed-bed BTC models	30
2.5    Conclusion BTC models	38
<b>MATERIALS AND METHODS</b>	<b>39</b>
3 <b>PSDM by USEPA model</b>	<b>39</b>
4 <b>modelling PFAS removal using GAC</b>	<b>41</b>
<b>RESULTS AND DISCUSSION</b>	<b>44</b>
5 <b>Testing the PSDM by USEPA model</b>	<b>44</b>
5.1    Isotherm fitting tool	44
5.2    Example modelling of compound TCE	45
5.3    Pilot modelling of compound PFHpA	46

5.4	USEPA fouling approach	47
<b>6</b>	<b>Extending USEPA PSDM model</b>	<b>50</b>
6.1	Extending the USEPA fouling approach	50
6.2	Alternative fouling approach	58
6.3	Scenario analysis on the Freundlich parameters	61
<b>CONCLUSION AND PERSPECTIVES</b>		<b>63</b>
<b>REFERENCE LIST</b>		<b>65</b>
<b>APPENDIX A: K FITTING TOOL</b>		<b>73</b>

## ABSTRACT

Organic micropollutants (e.g. antibiotics, PFAS compounds) in our aquatic effluents are of increasing concern and therefore advanced treatment is needed in wastewater treatment plants. From a wide range of potential treatment systems, fixed-bed adsorption onto granular activated carbon is effective and economic for the removal of micropollutants. Modelling is a tool that can help find optimal solutions for this purpose. However the adsorption process of a single micropollutant is already a very complex process and consists of different steps. When modelling this process, it is important to describe these steps and make the right choices from a theoretical perspective. A fixed-bed breakthrough curve model consists of three components including mass balance equation, adsorption kinetics described by uptake rate equation(s) and equilibrium described by an isotherm equation. The pore and surface diffusion model (PSDM) is a versatile multi-phase model because it takes into account various types of diffusion mechanisms. Due to a detailed description of intraparticle diffusion, the PSDM model is a strong candidate for simulating porous materials like granular activated carbon, where the intraparticle diffusion step is typically rate-limiting for micropollutants. The PSDM model developed by USEPA and implemented in Python is available as an open-source package and was tested in this thesis for the compounds TCE and PFHpA, without considering biofilm growth or competition between micropollutants. Its working mechanisms were studied by making use of the literature data. Model outcomes were compared with those of a real pilot study. Since the breakthrough prediction of PFHpA was accurately replicated, it provided a starting point for deeper research into the topic. The isotherm fitting tool was demonstrated separately and the USEPA fouling approach extended by implementing QSPR equations. This gave the user more control and insights into fouling. A versatile Freundlich K reduction tool was developed and implemented in the PSDM model. This allowed extra experimental data regarding fouling to be implemented. Thanks to this tool, the difference between constant and time-dependent K reduction became clear and observations revealed the weaknesses of the USEPA fouling approach. An alternative fouling approach was implemented with a fixed carbon weight reduction due to fouling from the beginning. For the pilot study case of PFHpA, it was concluded that the impact of fouling was high and approximately halved the amount of carbon available for adsorption. By comparing both fouling approaches, the main conclusion was that they are strong simplifications of the complex reality regarding fouling and have a different effect on the model outcome. Finally, scenario analysis on the Freundlich parameters showed that it is important to carefully determine such parameters from batch equilibrium experiments as they can significantly impact the breakthrough curves. Although the PSDM has high potential for simulating adsorption of micropollutants in wastewater treatment systems, further research is needed to include modelling of biofilm growth, competition between micropollutants and a more accurate representation of the fouling phenomenon.

# INTRODUCTION

As the planetary boundary for novel entities is now exceeding, it is a priority to monitor micropollutants in our aquatic environments (Persson et al., 2022). Although they are invisible, organic micropollutants (OMPs) are among the most important environmental problems in the last decades (Mohammadi et al., 2022). Moreover, with increasing pharmaceutical and cosmetical care products, the release of organic micropollutants into water bodies is expected to increase in the future. The European Union (EU) is enforcing more strict regulations on the discharge of these small but complex contaminants (Khanzada et al., 2020). There is more awareness of the importance of treatment concerning the high exposure and hazard of these OMPs.

## 1.1 Problem statement: organic micropollutants

The definition of organic micropollutants can be explained by putting the words apart: ‘organic’ substances that are commonly present in the environment in small concentrations (lower than 1 µg/L) but are still considered as ‘pollutants’ due to their biologically adverse effects at these trace concentrations (Spindola Vilela et al., 2022).

It is not surprising that micropollutants (MPs) are mainly of anthropogenic origin. They form a big group of pollutants, originating from a wide range of sources. Today, there are more than 100 000 MPs that have been used by humans and/or for animals for health care and lifestyle improvement. Typical organic micropollutants coming from industrial sources are perfluorinated compounds (per- and polyfluoroalkyl substances or PFAS), phenolic compounds and dyes. OMPs originating from agriculture are mainly pesticides. Pharmaceutical compounds discharged from the industry are of big concern too. Households are another source of micropollutants as pharmaceutics, compounds from personal care products and cleaning products end up in municipal wastewaters (Topolovec et al., 2022).

Next to health concerns, micropollutants or Contaminants of Emerging Concern (CEC) can damage the environment through persistency, biomagnification and harmful algal blooms (HABs). Because these micropollutants are very small, tracking and risk assessment may be very difficult.

In the last decades, there is more awareness that MPs are present in our industrial and household effluents. Wastewater treatment plants (WWTPs) can only partially remove these pollutants because most of them are refractory to biological treatments and very persistent. This gives them the chance to accumulate in the environment and eventually in the food-chain (Guillossou et al., 2020; Pocostales et al., 2010). Typical sources and pathways of MPs are shown in **Figure 1**. The lack of treatment in conventional activated sludge (CAS) systems for these hazardous OMPs covers the problem statement in this thesis.

It is clear that advanced treatment is needed to prevent this pollution from escalating further. Several types of advanced treatment technologies are proposed in literature. Most of them are not ready for application on large scale because of their high operational costs, high installation costs, and/or lack of knowledge on how to use them properly. The use of granular activated carbon (GAC) for the removal of OMPs has been discussed in numerous papers (Aliakbarian et al., 2015; Ma et al., 2021; Šerban et al., 2023). This mature adsorption technique has widely been applied for drinking water treatment. Further, the system is easily implemented in existing WWTPs: it can be used as a post-processing unit, also called tertiary treatment, after the conventional treatment processes.

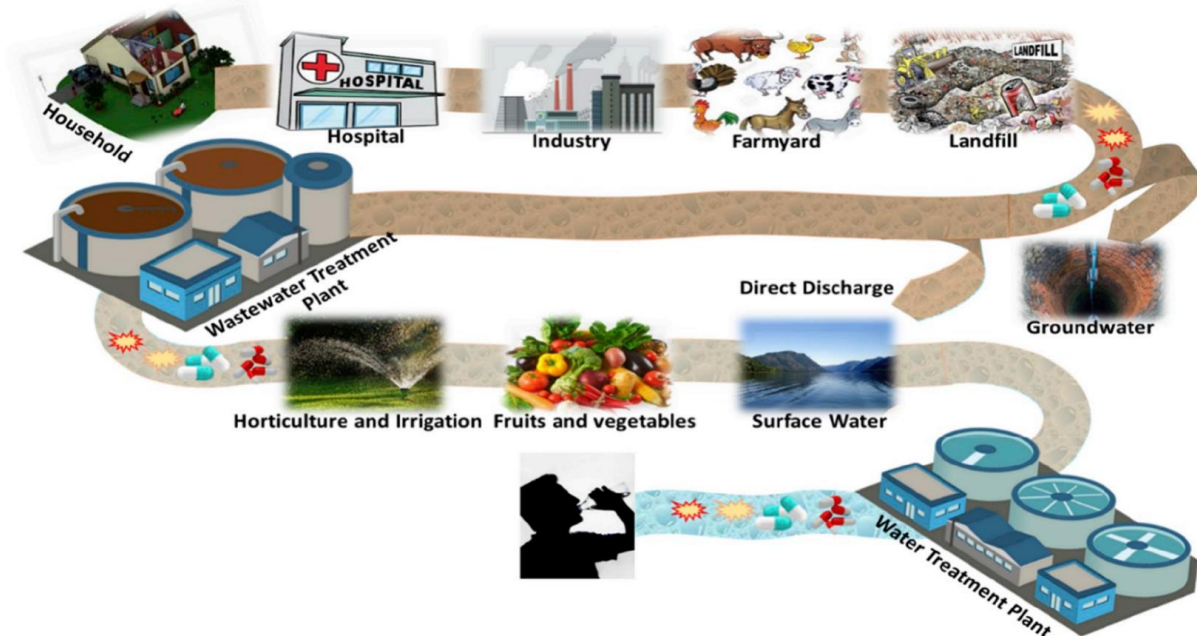


Figure 1 Sources and pathways of harmful micropollutants (Khanzada et al., 2020)

## 1.2 Modelling removal of organic micropollutants

A way to help find optimal solutions for removal of organic micropollutants, is modelling. As the first full-scale set-ups for OMPs treatment are rising, it is important to advice constructors with optimal operating conditions. These can be found by conducting pilot tests, but they are expensive and only a limited amount of conditions can be tested. Modelling can extend the amount of scenarios studied and assist in dealing with current challenges when upscaling newly purposed technologies. This way, faster decision-making is possible. As more efforts are done to measure very small concentrations of micropollutants, models can be calibrated and validated with experimental data.

## 1.3 Aim of the thesis

The aim of this thesis is to investigate existing models for adsorption of organic micropollutants through granular activated carbon, and to conduct a comparison, reliability and potential analysis for application in wastewater treatment plants. Following steps are undertaken:

- Sketch the source and fate of micropollutants in wastewater treatment plants
- Address techniques for removal of organic micropollutants
- Study the adsorption process and its variability
- Explore and compare adsorption models

An open-source model for simulation of GAC adsorption is tested in Python. Its working mechanisms are studied by making use of literature data. Model outcomes are compared with those of a real pilot study, so there is a starting point for deeper research. Small extensions are made regarding fouling. Then, a tool is developed that allows to implement more experimental fouling data. This tool is used to investigate the current fouling approach and an alternative fouling approach is developed. The latter can be used automatically and is compared with the original option.

# LITERATURE REVIEW

## 1 PRINCIPLES OF MICROPOLLUTANT REMOVAL

### **1.1 Classification of MPs**

Classification is mostly based on the source/sector or type of micropollutant. Regarding source, classes include pharmaceutical active compounds (PhACs), household personal care products (PCPs), agricultural pesticides and industrial chemicals (Khanzada et al., 2020).

Prevalent groups of OMPs within the PhACs class are antibiotics and hormones, which find their origin in hospitals. Adverse effects of antibiotics involve bacterial resistance. An example of hormones is estrogen and its adverse effects include endocrine disruption, which is why they are labelled as endocrine disrupting compounds (EDCs). Important groups of OMPs within the PCPs class are disinfectants, preservatives, insect repellents and sunscreen creams. Plastics and heavy metals are primarily inorganic micropollutants within the industrial chemicals class. Per- and polyfluoroalkyl substances (PFAS) are OMPs within the industrial chemicals class and have an important and essential application in fire retardants. Further within this class, phenolic compounds are worth mentioning as they are widely used in several industries thanks to their antioxidant, antimicrobial and anti-inflammatory properties, but are also classified as EDCs (Albuquerque et al., 2020). Finally, pesticides and herbicides are OMPs originating from the agricultural field and mostly disposed directly into water bodies.

Detailed classification in groups of MPs, together with applications and adverse effects, can be found in Das et al., (2017) and Spindola Vilela et al., (2022). Organic micropollutants are not being listed in this thesis, but a brief, summarizing overview is shown in **Figure 2**. It can be seen that the three main sources of pollution by OMPs through WWTPs are households, hospitals and industries (European Investment Bank & Bofill, 2023).

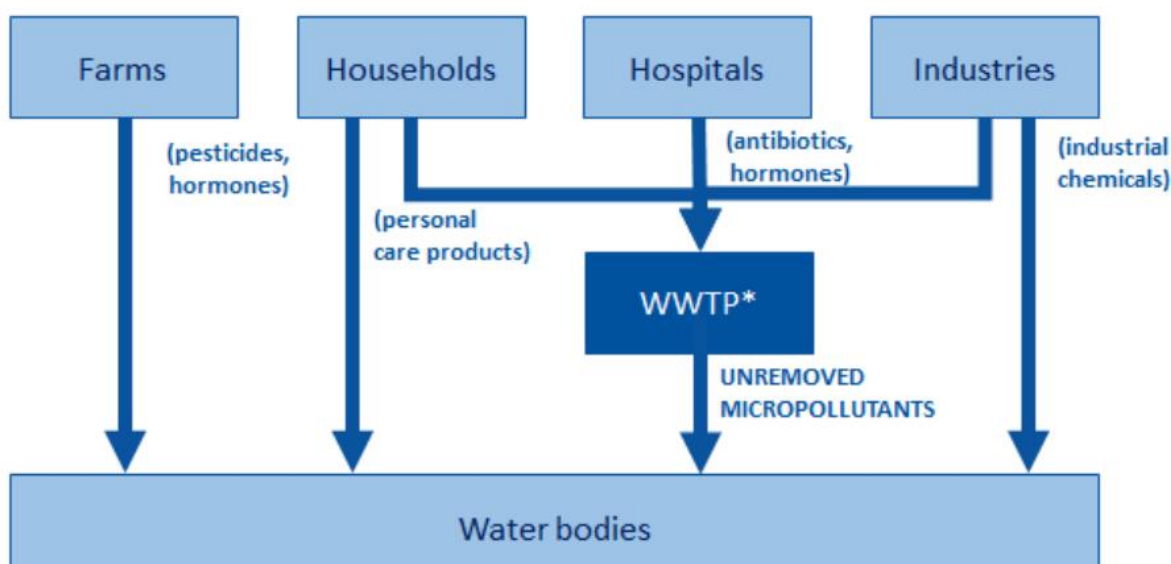


**Figure 2 Classification by source and pathways of organic micropollutants, \*wastewater treatment plant (European Investment Bank & Bofill, 2023)**

## 1.2 The fate of micropollutants in WWTPs

In typical wastewater treatment plants nowadays, there is partial removal of organic and inorganic micropollutants, through different pathways. An overview of all the relevant removal pathways in a WWTP is illustrated in **Figure 3**.

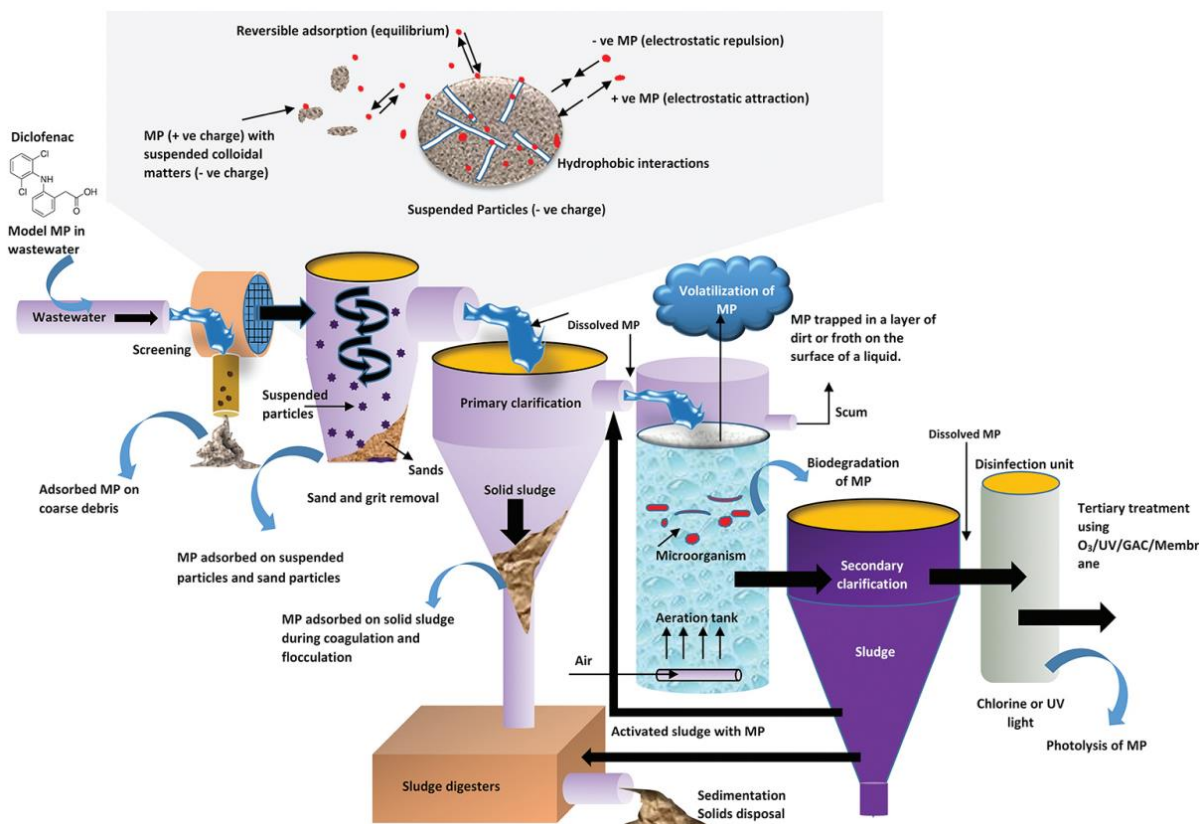


**Figure 3 Fate and removal processes of micropollutants in a WWTP (Das et al., 2017)**

Adsorption onto sediment in the primary treatment or biodegradation during the secondary treatment are the main removal mechanisms of micropollutants in conventional activated sludge (CAS) systems. Some volatile MPs have potential to be removed by volatilization. However, conventional treatment in typical WWTPs is not sufficient in the removal of organic micropollutants. As stated in the introduction, treated effluent concentrations can still be of concern. This is quantified in **Table 1**, where examples of CEC are listed per class with their respective removal efficiencies in CAS plants. It is clear that reported removal efficiencies are highly variable.

Some antibiotics such as Enrofloxacin are not impacted at all by the conventional treatment, while others, like sulfamethoxazole, can be removed to some extend. Estrogens like Enrofloxacin and Estrone (E1) can have low to high removal efficiency. The personal care product (PCP) in this table has limited removal (up to 55%). Removal of the industrial chemical compounds is again highly variable. What is remarkable is that some PFAS compounds can have negative removal efficiencies. The reference study declares that the enrichment of some PFAS may be caused by additional production via precursor degradation (Kim et al., 2012). Higher rates of formation are identified at higher HRT and temperature, due to the enhanced biological reactions (Guerra et al., 2014). Pesticides are mostly not reported in CAS systems because these are of agricultural rather than urban origin (Krzeminski et al., 2019). Concentrations in WWTP effluents are listed for many MPs in Das et al., (2017).

**Table 1 Reported CEC removal efficiencies in CAS plants (Krzeminski et al., 2019)**

Class	CEC	Removal efficiency (%)
<b>Pharmaceutical active compounds (PhACs)</b>	Sulfamethoxazole (antibiotics)	35-84
	Enrofloxacin (antibiotics)	~0
	Azithromycin (antibiotics)	11-44
	Estrone (estrogens)	58-81
	17 $\alpha$ -Ethynodiol (estrogens)	18-94
<b>Household personal care products (PCPs)</b>	2-Ethylhexyl ethoxycinnamate	30-55
<b>Industrial chemicals</b>	Butylated hydroxytoluene (phenolics)	89
	Tetrabromobisphenol A (phenolics)	10-100
	Hexabromocyclododecane	0-86
	Benzotriazole	30-91
	Perfluorobutanoic acid, PFBA (PFAS)	(-108)-65
	Perfluoropentanoic acid, PFPeA (PFAS)	(-400)-50
	Perfluorohexanoic acid, PFHxA (PFAS)	(-226)-39 (Kim et al., 2012)
	Perfluoroheptanoic acid, PFHpA (PFAS)	(-32) (Guerra et al., 2014)

Therefore, additional treatment for CES removal is required. This advanced treatment is illustrated in **Figure 3** under the name ‘Tertiary treatment’ as the last process after the secondary clarification. ‘O<sub>3</sub>’ refers to the ozonation process, which belongs to the group of advanced oxidation processes (AOP) where oxidation is applied to partially destroy micropollutants. Another type of AOPs is ‘UV’, in which ultraviolet light is used to produce oxidizing agents for degradation of the pollutants (Kumari & Kumar, 2023). ‘GAC’ and ‘Membrane’ are other types of tertiary treatment processes. With the growth of industry and emerging pollutants in the last decades, tertiary treatment is now essential before discharging the effluent in the environment. Single and combined technologies are discussed in the next section.

## 1.3 Tertiary treatment methods for MP removal in WWTPs

### 1.3.1 Single technologies for tertiary treatment

This section provides an overview of advanced treatment processes currently available to remove micropollutants in wastewater treatment plants. Here, a descriptive approach is adopted for the technology assessment. The most important treatment groups (TGs), corresponding technologies and advantages and disadvantages of the TG are listed in **Table 2**.

**Table 2 Advantages and disadvantages of different methods for OMPs removal from wastewater**

Treatment group (TG)	Advantages TG	Disadvantages TG	Reference
<b>Advanced oxidation process</b>	Organic destruction Removal of OM Rapid reaction Disinfection	Residual by-products Energy-intensive	(V. Sharma & Feng, 2017; Zahmatkesh, Amesho, et al., 2022)
- <i>UV-radiation</i>			
- <i>(Photo-)Fenton</i>			
- <i>Sonolysis</i>			
- <i>Wet Air Oxidation</i>			
- <i>Ozonation</i>			
<b>Membrane treatment</b>	Many mechanisms: size exclusion, adsorption, electrostatic repulsion FO, MD low operating costs High efficiency Ions removal Disinfection	High (re-)investment costs RO, NF energy intensive Fouling and scaling Concentrate	(Das et al., 2017; Khanzada et al., 2020; Rizzo et al., 2019; Zahmatkesh, Amesho, et al., 2022)
- <i>Reverse osmosis (RO)</i>			
- <i>Nanofiltration (NF)</i>			
- <i>Forward osmosis (FO)</i>			
- <i>Membrane distillation (MD)</i>			
<b>Biological treatment</b>	MPs degraded, transformed, mineralized (or absorbed)	High retention time Sludge generation	(Gutiérrez et al., 2021; Zahmatkesh, Amesho, et al., 2022)
- <i>MBBR*</i>			
<b>Coagulation and flocculation*</b>	Simple application	Transfer toxic compounds to solid phase	(Das et al., 2017; Zahmatkesh, Amesho, et al., 2022)
<b>Adsorption</b>	Additional DOC removal Full scale potential High efficiency Easy process Economical	Secondary pollution Need skilled labour	(Ma et al., 2021; Rizzo et al., 2019; Zahmatkesh, Amesho, et al., 2022)
- <i>Batch sorption</i>			
- <i>Continuous fixed-bed</i>			
- <i>Continuous moving bed</i>			
- <i>Continuous fluidized bed</i>			
- <i>Pulsed bed</i>			
<b>Combined treatment</b>	Minimize by-products Highest efficiencies Combine benefits MPs degraded	Complex process	(Gutiérrez et al., 2021)
- <i>MBR (+PAC)*</i>			
- <i>BAC</i>			
- <i>UV/chlorine (+GAC)</i>			
- <i>Ozonation + GAC</i>			

\*Is usually not implemented as a 'tertiary' treatment

Most common advanced oxidation processes (AOP) include UV-radiation, fenton and ozonation. What these methods have in common is that radicals are produced as a result of their mechanism. The radicals are also called reactive oxygen species (ROS), such as sulfate or hydroxyl radicals. They are strong oxidants that can rapidly react with organic pollutants (Arvaniti et al., 2022). The pollutant is transformed into smaller and more biodegradable compounds, that possibly can react again with oxidative species for mineralization to take place. The working of AOPs is schematically shown in **Figure 4**. Most common examples of AOPs are given in **Figure 5** (Trojanowicz, 2020). Some of them are discussed in the context of OMPs management.

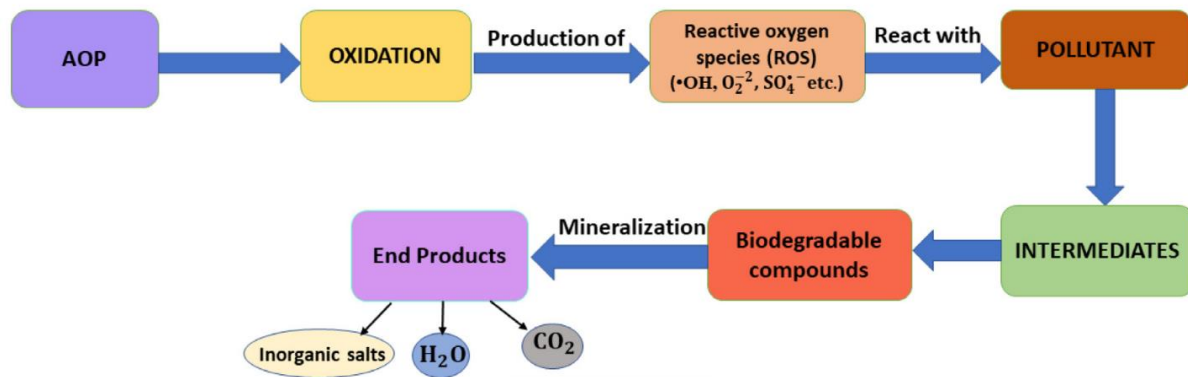


**Figure 4 Working mechanisms of the advanced oxidation process, AOP (Kumari & Kumar, 2023)**

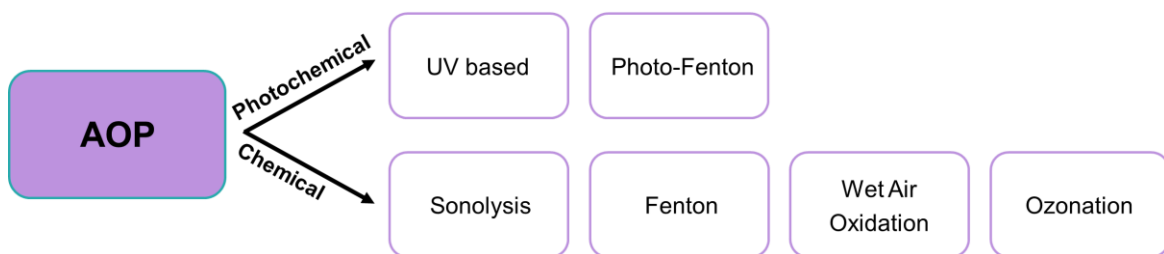


**Figure 5 Examples of AOPs subdivided into photochemical and chemical processes**

UV-radiation uses UV-light to produce highly reactive hydroxyl radicals ( $\bullet\text{OH}$ ), by which the OMPs are then oxidized. Chlorination uses chlorine, which is converted into oxidative species ( $\bullet\text{OH}$ ,  $\text{Cl}\cdot$ ,  $\text{ClO}\cdot$ ) that causes organic destruction of OMPs. UV-radiation and chlorination are not very efficient when used as a stand-alone process (up to 65% reported), unless high dosages are used. However, that would be too costly for the scope of municipal wastewater treatment. The combination of UV and chlorination is typically more efficient for removing micropollutants, and lowers the chemical and energy demand (Yin & Shang, 2020). However, the formation of toxic degradation by-products is still concerning with the combination UV-chlorine. Ozonation uses ozone, which reacts with water and produces free oxidizing hydroxyl radicals. The pollutants are then transformed into compounds called ozonation transformation products. These degradation products are smaller and more biodegradable. Next to disinfection, ozonation is also capable of reducing chemical oxygen demand (COD). It is a very effective method (>90%) for destroying OMPs but residual by-products and high operational energy costs are still some challenges to consider (Guillossou et al., 2020; Zahmatkesh, Amesho, et al., 2022; Zahmatkesh, Bokhari, et al., 2022).

Through membrane filtration, very high removal efficiencies are achievable. Reverse osmosis (RO) and nanofiltration (NF) are very efficient and widely applied for drinking water treatment, whereas microfiltration (UF) is less efficient in the removal of MPs. Next to these, forward osmosis (FO) and membrane distillation (MD) are promising technologies for the removal of OMPs due to their low operating costs and high performance. In terms of efficiency, they might be on the same level as RO and NF, but more research is needed to explore that. Drawbacks are fouling and scaling, need for expensive high-tech membranes and having the concentrate as a costly secondary pollution (Khanzada et al., 2020; Rizzo et al., 2019).

The feasibility of biological treatment for enhanced degradation of MPs in WWTPs has been recently explored (Gutiérrez et al., 2021). A moving bed biofilm reactor (MBBR) is a reactor where a biofilm grows on plastic carriers. The working principle of 'micropollutants removal' by MBBR is depicted in **Figure 6**. The different processes, i.e., nitrification/denitrification and organic carbon (OC) removal, occur all together within the biofilm. Because these processes occur simultaneous in one reactor, it is also called a 'hybrid' reactor (Mohammadi et al., 2022). Compared to CAS, higher MP removal rates are possible thanks to the high diversity of microorganisms on the carriers (Ahmadi et al., 2023). MBBR is usually not a tertiary treatment but an upgrade to the CAS system. MBBR can be recommended when existing wastewater treatment processes need to be improved or when designing new installations. This technology is more recent and more advanced for secondary treatment. MBBR has also been investigated as a tertiary treatment after CAS. In this case it is called 'tertiary MBBR' and it showed to be an improved addition to the system in the context of CEC removal and degradation (Edefell et al., 2021).

Coagulation and flocculation are processes that are more part of the primary treatment. This group received less interest for CEC removal as MPs adsorbed to the solid sludge are a secondary waste. The sediment is then a pollution concern unless MPs could be purified, which again would be a challenging task (Zahmatkesh, Amesho, et al., 2022).

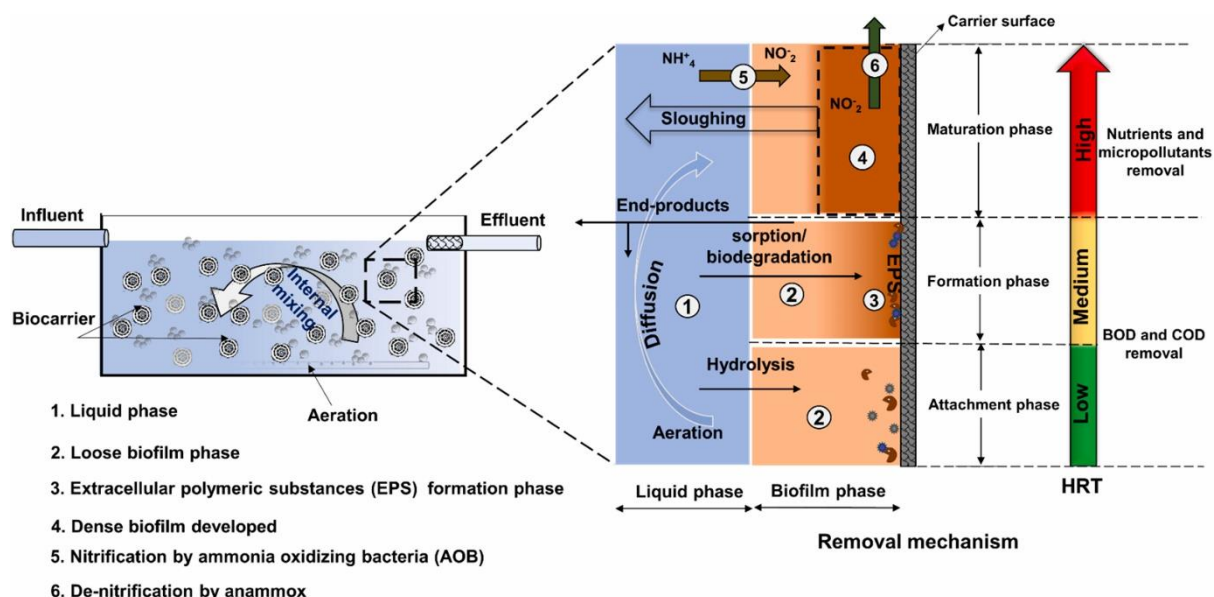


**Figure 6 Working principle of a moving bed biofilm reactor (MBBR) (Saidulu et al., 2021)**

Adsorption is one of the promising treatment groups for CEC removal in **Table 2**. It features very high efficiencies, with low energy and chemical demands, and is easy to install. Economically, the adsorption method is attracting as installation and operation costs are rather low. Another benefit is the effective, additional removal of heavy metals (HM) and some dissolved organic matter (DOC). Moreover, full-scale installations at drinking water facilities can be transferred to wastewater facilities. Compared to membrane treatment, adsorption has several advantages. First, sorbents can be very abundant when agricultural, food, or industrial wastes are used (Issabayeva et al., 2017), while membranes are products manufactured by complex processes. Another advantage is that activated carbon (AC) has perfect adsorption ability for relatively low molecular mass organic pollutants, making it ideal for tackling micropollutants removal (Aliakbarian et al., 2015). A downside of adsorption is the regeneration process. Through regeneration, the concentrated stream of MPs can be removed, but not always recovered. These waste streams are most frequently managed as hazardous waste and then the problem is rather 'relocated' than solved. Moreover, regeneration can sometimes be associated with high energy demands (Ma et al., 2021; Rizzo et al., 2019).

Combining some of the above treatment groups can offer many benefits and often results in highest abatements. Examples of how treatment groups from **Table 2** can be combined are discussed in the next section.

### 1.3.2 Combined technologies for tertiary treatment

A membrane bioreactor (MBR) is an advanced and alternative technology for CAS systems. The combination of biological and membrane treatment provides better-quality effluent with low micropollutant concentrations. It is already widely implemented for water reuse applications. The working principle of MPR is shown in **Figure 7**, where OMPs are represented under the name 'POPs' or persistent organic pollutants. Fouling is still an issue for this method (Zahmatkesh, Amesho, et al., 2022). Also, a MBR is not a tertiary treatment but rather a more effective substitution for the secondary sedimentation process. MBR is recommended for new installations.

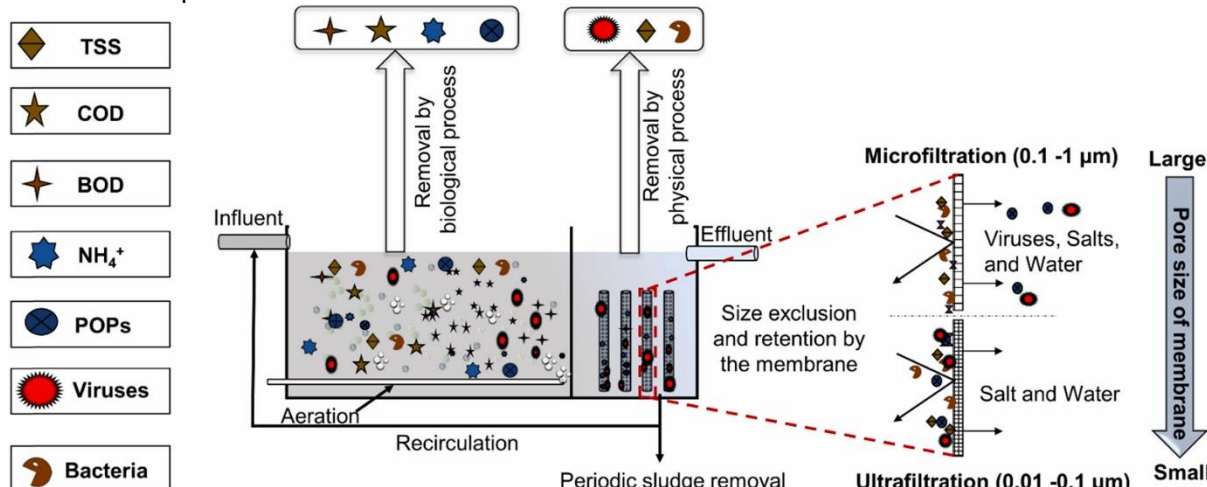


**Figure 7 Working principle of a membrane bioreactor, MBR (Saidulu et al., 2021)**

Yet another, interesting point is the addition of AC to MBRs. Research has been done to test the addition of powdered activated carbon (PAC) inside the MBR, or GAC as a post-treatment to the MBR. It showed that in either of the technologies, AC effectively enhances the removal of many MPs and at the same time improves the MBR performance (Gutiérrez et al., 2021).

When biological treatment is combined with adsorption, it is called biological activated carbon (BAC). A thin biofilm forms on top of the surface of the activated carbon and allows for the MPs to be also biodegraded. This way, activated carbon can be partially regenerated by the microorganisms while the carbon bed is in operation (Xiaojian et al., 1991). There is no controllable distinction between non-biological and biological AC. However, it is found that pre-ozonation significantly enhances the biological activity on GAC (The BAC Process for Water Purification, 2000). A schematic representation of GAC and BAC is shown in **Figure 8**.

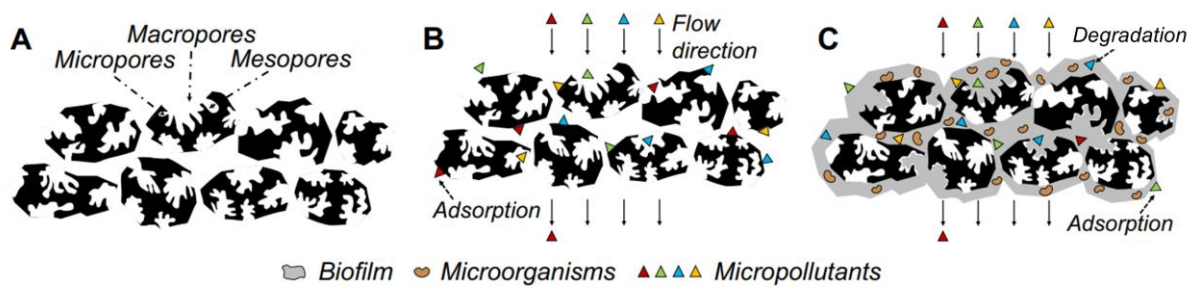


**Figure 8 Schematic representation of A: structure of GAC, B: MPs adsorption on GAC, C: BAC (Gutiérrez et al., 2021)**

Combinations between advanced oxidation processes and activated carbon have also been investigated, like UV/chlorine – GAC. Degradation by-products were eliminated by the post-adsorption. MPs adsorption rates increased by a factor of 2-3 thanks to the UV/chlorine (Yin & Shang, 2020).

A combination of ozonation and GAC is getting interest for designing full-scale advanced treatment (Cantoni et al., 2024). Hence, it is considered for implementation in Belgium. It can be easily implemented at the end of the conventional wastewater process train without a need for redesign. Ozonation is beneficial in degrading and transforming micropollutants. It also removes compounds that are refractory to adsorption. However, a single ozonation unit demands high energy and can produce toxic by-products. Bromate ( $\text{BrO}_3^-$ ) and N-nitrosodimethylamine (NDMA) are typical by-products created by ozonation. These are potentially carcinogenic, although this is not proven yet. Post-adsorption by GAC allows using a lower dose of ozone because not all the removal work needs to be done by this process. This lowers the energy consumption for ozone generation and lowers the by-products. Left-over by-products are adsorbed onto the carbon. Another advantage is that competition for adsorption reduces. Specifically, dissolved organic carbon (DOC) normally competes with OMPs for the adsorption sites and also causes pore blockage. Ozonation already oxidizes part of the DOM, resulting in less competition from it. Finally, pre-ozonation enhances BAC formation, stimulating biodegradation onto the GAC. Regeneration will be needed less frequently (Aquafin, 2023; Guilloussou et al., 2020). On top of these benefits, it is true that the range of removed MPs is wider thanks to the combined two treatment mechanisms. This can be nuanced with partitioning coefficients  $\text{LogK}_{\text{ow}}$  and  $\text{LogK}_{\text{o3}}$ .  $\text{LogK}_{\text{ow}}$  indicates the hydrophobicity and therefore affinity of the compound towards AC.  $\text{LogK}_{\text{o3}}$  indicates its reactivity with ozone. Values for compound-specific coefficients are shown in **Table 3**. Highest removals are observed for compounds with high  $\text{LogK}_{\text{ow}}$  and/or high  $\text{LogK}_{\text{o3}}$  (Cantoni et al., 2024). This is an interesting way to quantify affinity towards one of the two processes.

**Table 3 Examples of CEC characteristics for affinity towards AC and ozone (Cantoni et al., 2024)**

CEC	$\text{LogK}_{\text{ow}}$	$\text{LogK}_{\text{o3}}$	Function CEC
<b>Acesulfame (ACS)</b>	-0.55	1.94	Sweetener
<b>Benzotriazole (BNZ)</b>	1.3	2.38	UV-filter
<b>Diclofenac (DCF)</b>	4.51	6.20	Anti-inflammatory

## 1.4 The adsorption process

Adsorption is a physiochemical interface mass-transfer phenomenon (Ngeno et al., 2022). This definition already gives a hint of its complexity for modelling. Namely, it can be a physical process, a chemical process, or both. The pollutant, also called the adsorbate or solute, is accumulated between liquid and solid phases. It needs to be clear that the pollutant itself doesn't change its phase but there are two phases involved in the sorption process. In the liquid phase, the pollutant is dissolved. When the pollutant is in the solid phase, also known as the sludge phase, it means that the pollutant is adsorbed onto the solid (Mohammadi et al., 2022). The adsorbent, e.g. activated carbon, is a porous material with both outer and inner surfaces that are exposed to the adsorbates. On the surface, the active sites are the places where the solute can directly adsorb onto. However, the pollutant first needs to travel a pathway from the aqueous media (liquid phase) to the active sites (solid phase). In this pathway, different mass transfer and diffusion mechanisms take place. Diffusion is defined by the movement of particles due to a concentration gradient. Once the active site is reached, different adsorption mechanisms are possible: chemisorption, physisorption or both. Chemisorption include ionic interactions or the formation of chemical bonds between the sorbate and sorbent molecules. Physisorption include Van der Waals or  $\pi$ - $\pi$  interactions. These adsorption mechanisms influence the way the pollutants are structured onto the surface: monolayered or multilayered. Physisorption, such as Van der Waals interaction, mainly contributes to multilayer adsorption. Chemisorption, such as hydrogen bonding or the formation of strong bonds, mainly contributes to monolayer adsorption. It is the result of interaction between the adsorbate and functional groups on the adsorbent surface (Aliakbarian et al., 2015; Ngeno et al., 2022; Wang & Guo, 2023). An illustration of the adsorption process is shown in **Figure 9**.

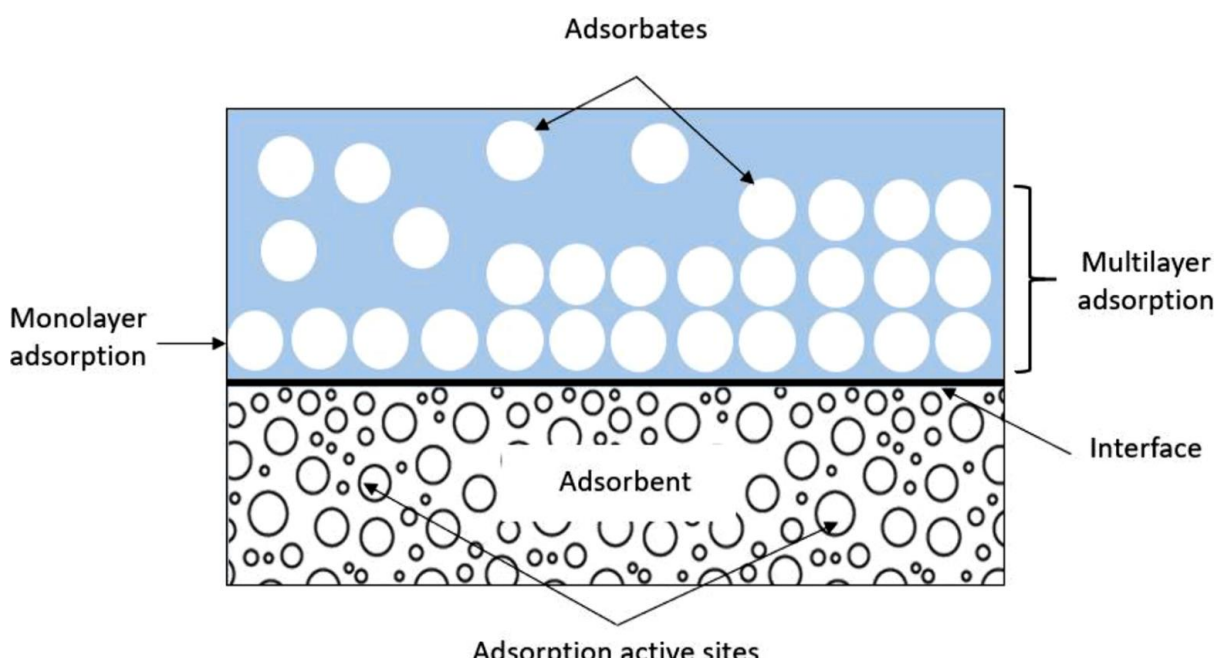


Figure 9 Illustration of the adsorption process (Ngeno et al., 2022)

## 1.5 Types of adsorbents

An overview of different adsorbent groups, distinguished based on their origin or nature, is shown in **Table 4**. Each group is provided with some of the most important adsorbents and their adsorption capacity for phenol. Phenol was taken as the standard compound to enable comparison. The values for phenol are extracted from the review paper of Issabayeva et al., (2017). It should be noted that, next to organic micropollutants such as phenols, there are many others. Also, relative values for adsorption capacity can differ depending on the environmental conditions. The range of influent concentrations is also a factor that determines which adsorbent suits the best for specific influent wastewater streams (Issabayeva et al., 2017). Adsorption onto granular activated carbon (GAC) was chosen by the United States Environmental Protection Agency (US-EPA) as the best available technology for the treatment of many regulated organic pollutants (Westerhoff et al., 2005). Thanks to its good properties, GAC is still one of the most widespread technologies in drinking water treatment (Piazzoli & Antonelli, 2018). However, there exist many other possibilities next to GAC, each having its own pros and cons.

**Table 4 Overview of adsorbent groups with some of the most important adsorbents listed. The values for adsorption capacity are given for phenol as the adsorbate compound (Issabayeva et al., 2017)**

Adsorbent		Capacity (mg/g)
<i>Carbonaceous adsorbents</i>	<b>Commercial AC</b>	
	GAC	350
	PAC	303
	<b>Agricultural waste-based AC</b>	
	Coconut shell AC	206-240
	Sugar cane bagasse	33
	Tea leaves	9.49
	Rice husk (ash)	0.0022-14.38
	<b>Food waste-based AC</b>	
	Corn cob AC	232-340
<i>Clay and mineral-based adsorbents</i>	Corn cob	177.6
	Chitosan (seafood waste)	59.74
	<b>Industry waste-based AC</b>	
	PET	162-278
	Coal slug	63.78
	Modified bentonite	333
<i>Polymer-based adsorbents</i>	Red mud	59.2
	Surface modified zeolite	37.92
	Natural zeolite	34.5
	Natural clay	15
<i>Novel adsorbents</i>	PCH	14.5
	BMS	1000
	XAD-16	141.17
	NJ-8	136.9
	MAA-coated NPs	950
	Nanoparticles (NPs)	550
	HMCSSs	207.8
	Nanotubes	1.1-64.6

Four groups are separated based on their origin or nature and will be shortly discussed. It also must be noted that adsorbents can be modified (e.g. by acid or alkali modification) to improve their properties. The more they are modified, the better their adsorption capacity would be but also the higher their price. The following distinction according to the level of modification can be made (Patel, 2019):

- Semi-synthetic adsorbents: natural materials undergo chemical and physical activation to develop a highly porous structure. This group includes activated carbon and seems to find a very good balance between costs and efficiency.
- Natural adsorbents such as unmodified clay and mineral-based adsorbents form the second and most economical group. It is a sustainable option as no modification is needed and there is high abundance of them in nature. However, they typically come with low adsorption capacity.
- Synthetic adsorbents undergo advanced laboratory processes to improve adsorption capacity, but the price and sustainability of this group are the main concerns. Manufacturing is relatively costly. Polymer-based and novel adsorbents belong to this group.

Carbonaceous adsorbents are carbon-based adsorbents and include activated carbon (AC in **Table 4**). AC is well-known for its good adsorption ability for relative low molecular mass organic compounds, its good physical and chemical properties, porous structure, large specific area and availability of surface functional groups for binding (Aliakbarian et al., 2015; Issabayeva et al., 2017; Serban et al., 2023). The activation process and different sources for AC are further discussed below.

Activation can be done physically or chemically and is typically done through pyrolysis. In this process, organic material is decomposed by heating in the absence of oxygen. This way, the material is converted to carbon. Two important variables in this process are heating rate and duration. Chemical activation requires the addition of a chemical to the material that will ultimately modify the surface groups. These surface functional groups will help improve the adsorption characteristics of the material. Chemical activation requires less energy compared to the physical activation. Also, short reaction times are possible. A drawback of it is that the used chemicals can be environmentally hazardous. Physical activation includes the addition of oxidizing agents like steam, carbon dioxide ( $\text{CO}_2$ ) and air. The activator used is more environmentally friendly, but the yield might be lower (Ngeno et al., 2022).

Commercial AC is a term that refers to AC gained from conventional, fossil sources. By far the oldest adsorbent ever used is charcoal. It has been applied widely in drinking water facilities. In the past, the aim was to get more clean drinking water, since there was not yet an incentive for sustainable designs. Charcoal and later petroleum coke and lignite are products originated from fossil sources and are not the most eco-friendly adsorbents. Adsorption capacities for phenol on commercial granular and powdered activated carbon are 350 and 303 mg/g respectively (Issabayeva et al., 2017).

The differentiation between granular activated carbon (GAC) and powdered activated carbon (PAC) is made based on its particle size. They can be both created from conventional or unconventional carbon-based sources, but PAC is the more refined version (particles  $< 50\mu\text{m}$ ). GAC has larger particle size (0.4 - 2 mm) and smaller external surface. However, it can be easily reactivated through regeneration. Another advantage is the high porosity of the granules, which enhances mass transfer of MPs significantly. PAC has finer particles and is mainly used in batch reactors, where it can flexibly be dosed. The capital cost of PAC is two times lower than GAC. However, its regeneration is cost and energy intensive and therefore it is usually not carried out. Consequently, regular replacement of PAC will lead to higher operational costs. Another disadvantage of PAC is that it causes sludge to accumulate and leak through treatment filters (Brandt et al., 2017, p. 10; Issabayeva et al., 2017).

As said, activated carbon can also be generated from unconventional sources which can be more renewable. Agricultural, food and industrial wastes are very abundant and can be converted into effective AC. Adsorption capacities for phenol are listed in **Table 4**. Although their efficiency is not very stable, some can reach almost the same efficiency as the commercial activated carbons. Big advantages compared to commercial AC is their high and local abundance and low production costs. This can give these semi-synthetic adsorbents a very good balance between sustainability and efficiency. Corn, being a globally produced crop, is a good example of a sustainable precursor. Corn cob is widely abundant and, when activated, reaches adsorption capacities up to 340 mg/g. Coconut shells AC also have significant adsorption capacity, up to 240 mg/g, and can be a sustainable option. Also industrial carbon-based wastes such as polyethylene terephthalate (PET) can be considered. Plastic waste is clearly a major global environmental problem and PET seems to have high carbon content. PET waste can be converted into activated carbon through a chemical, physical or other combined activation processes. For the adsorption of phenol, a maximum adsorption capacity of 278 mg/g has been reported (Issabayeva et al., 2017; Sharifian & Asasian-Kolur, 2022).

Clay and mineral-based adsorbents form the most natural group of adsorbents as they are directly available in nature. However, these adsorbents can also be modified to improve their adsorption properties. These adsorbents are not carbon-based. Zeolite is a mineral with medium capacity for phenol, but is getting more interest thanks to its easy regeneration. Regeneration also plays a significant role in determining the strengths of an adsorbent choice. Bentonite is a clay-containing sorbent with exchangeable cations. Naturally, its adsorption capacity is low but if it is treated and activated, up to 333 mg phenols/g can be adsorbed onto it, which is close to the 350 mg/g achieved with GAC (Issabayeva et al., 2017).

Polymer-based adsorbents are non-carbonaceous, economically promising adsorbents that show good properties for the removal of organic micropollutants. The main concern is the harm of these materials to the environment and the harm of the polymerization process. The polymers can show outstanding (up to 1000 mg/g) adsorption capacity for phenol. They have a specific, small pore size distribution and can easily be regenerated (Issabayeva et al., 2017).

A fourth group is the group of novel adsorbents. Here, novel materials and techniques are used to obtain optimal adsorption capacities. They undergo a variety of thermal and chemical modifications mostly on lab-scale. Just as polymer-based, these synthetic adsorbents can have a high cost of production, disposal and potential pollution to the environment. An example is the manufacture of nanotubes with an adsorption capacity for phenol around 64,6 mg/g. This can be a novel continuation or the process where PET waste is activated. Other novel processes are the synthesis of nanoparticles (NPs) and their coating, which again leads to outstanding adsorption capacities, up to 950 mg phenol/g of adsorbent (Issabayeva et al., 2017; Sharifian & Asasian-Kolur, 2022).

A last division of adsorbents can be done based on their polarity (Ngeno et al., 2022). Polar adsorbents are hydrophilic and typically show a higher affinity to polar substances such as alcohols. Clay and mineral-based adsorbents such as zeolite and bentonite typically are polar adsorbents. Non-polar adsorbents on the other hand are hydrophobic and show a higher affinity to non-polar substances such as oil and hydrocarbons. Carbonaceous and polymer-based adsorbents can be examples of non-polar adsorbents.

## 1.6 Types of adsorption set-ups

Various adsorption systems exist. A summary of different systems, with their advantages and disadvantages are listed in **Table 5** that is derived from the study of Patel, (2019). The differences are mainly based on the flow of the adsorbent and adsorbate. Batch adsorption is a non-continuous process in which adsorbent and adsorbate are mixed, and after equilibrium the adsorbent is removed by drawing off. It is only possible with low amount of adsorbent and low pollution load. Therefore, this technique refrains from industrial-scale applications. The same is true for pulsed bed adsorption, in which the exhausted adsorbent is periodically removed from the bottom while new or regenerated adsorbent is added on top (Sookkumnerd, 2019). The other sorption processes are called continuous because the influent flow can be fed continuously through the bed. The term continuous gives no indication about the regeneration, this can be periodically. Typically, also larger amounts of adsorbent are used here. Continuous sorption processes can be used for higher amount of wastewater with higher pollution loads and are therefore more interesting in the application of municipal wastewater treatment. Among them, continuous fixed-bed adsorption is depicted as a suitable technique. It doesn't require large physical investment or large area but can be implemented at large scale (Patel, 2019, 2022).

**Table 5 Various adsorption systems with their corresponding pros and cons (Patel, 2019)**

Adsorption system	Introduction	Pros +	Cons -
<b>Batch sorption</b>	Adsorbent and adsorbate are mixed in diluted solution at constant volume	Easy and cheap Desired for research	Non-continuous For small quantity of wastewater and minimum pollution load Usually not industrialized Adsorbent removed by simple filtration
<b>Continuous fixed-bed sorption</b>	Adsorbate continuously flows through the adsorbent bed at constant rate	Easy and cheap Continuous For higher quantity of wastewater and higher pollution load Widely used for industrial application	Attrition (wear particles) Feed channelling Dead zones
<b>Continuous moving bed sorption</b>	Continuously flowing adsorbate and also adsorbent are in motion	Continuous good contact with fresh adsorbent	Complicated & expensive Large amount of adsorbent required Continuous regeneration of adsorbent essential
<b>Continuous fluidized bed sorption</b>	Adsorbate is in contact with fluidized bed of adsorbent	Continuous For higher quantity of wastewater and higher pollution load Automatically controllable Industrial scale	Complicated & expensive Rapid mixing leads to non-uniform residence time
<b>Pulsed bed sorption</b>	Adsorbate is in contact with the same piece of adsorbent in bed, until effluent quality exceeds limit	Easy and cheap Automatically controllable Low adsorbent dosage required Optimal regeneration time	For small quantity of wastewater and minimum pollution load

## 1.7 Adsorption equilibrium

As explained in **section 1.4**, adsorption is a process where the solute or adsorbate accumulates between two phases; the liquid phase and the solid phase. The adsorbate is adsorbed onto the active sites of the solid surface, i.e. any external or internal surface of the GAC. As the amount of activated carbon in the bed is limited, the number of active sites is limited as a consequence. Not all pollutants are removed but an equilibrium is obtained. The adsorption process involves both sorption and desorption. Equilibrium is reached between concentrations in the liquid phase and in the solid phase.

Equilibrium behaviour of a solute in GAC is described through the adsorption isotherm. The isotherm is determined by conducting a conventional static method in a closed system. A prior determined amount of carbon is added in a beaker together with polluted water. The water contains single-solute pollution with a known initial concentration. Equilibrium is reached when the micropollutant is long enough in contact with the adsorbent. The adsorption and desorption are now equal in rates. Solute concentration is carefully measured after equilibrium. The two important equilibrium values are:

- $q_e$  = [pollutant] in solid phase at equilibrium (mg/g AC), also called adsorption capacity
- $C_e$  = [pollutant] in liquid phase at equilibrium (mg/L bulk liquid)

These values are determined for different initial solute concentrations, and the relationship is plotted. The relationship is called the equilibrium isotherm and examples of it can be seen in **Figure 10**. Due to complexity of adsorbate – adsorbent interactions, diverse shapes of isotherms exist for diverse adsorption systems (**Figure 10(a)**). This is why, for the respective micropollutant and GAC, it is desired to determine equilibrium behaviour experimentally. Examples of L-shape isotherms are schematically shown in **Figure 10(b)**. Differences can be attributed to various micropollutants, for example. The red isotherm seems to be superior because adsorption capacity is highest at any dosage.

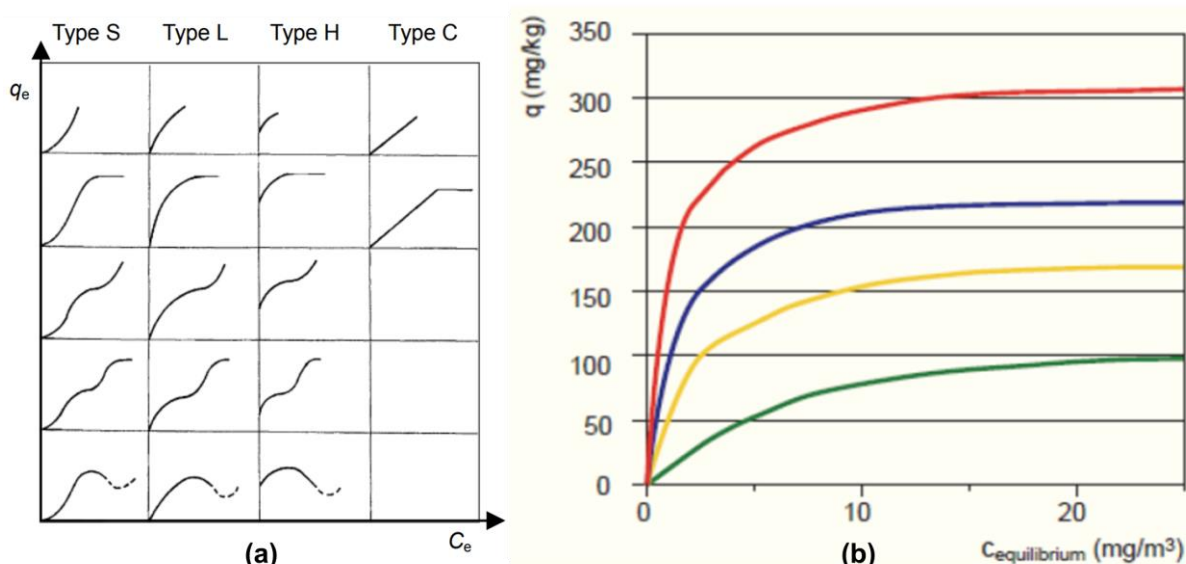


**Figure 10 Equilibrium isotherms: (a) classification according to shape, (b) shape L examples, each colour is a different sorption system  
(Vanoppen, 2023; Xu et al., 2013)**

It is assumed that at the surface of the adsorbent, the solid-phase solute concentration (amount of solute adsorbed) is in equilibrium with the liquid-phase solute concentration (Jarvie et al., 2005).

## 1.8 Adsorption kinetics

The adsorption kinetics describe the whole movement process of the solute inside the fixed-bed adsorption column. Only considering adsorption onto the active sites is not sufficient when modelling GAC columns. There is a sequence of steps preceding adsorption, from which duration of each step can be relevant to take into consideration. Different steps, next to the adsorption itself, are schematically represented in **Figure 11**.

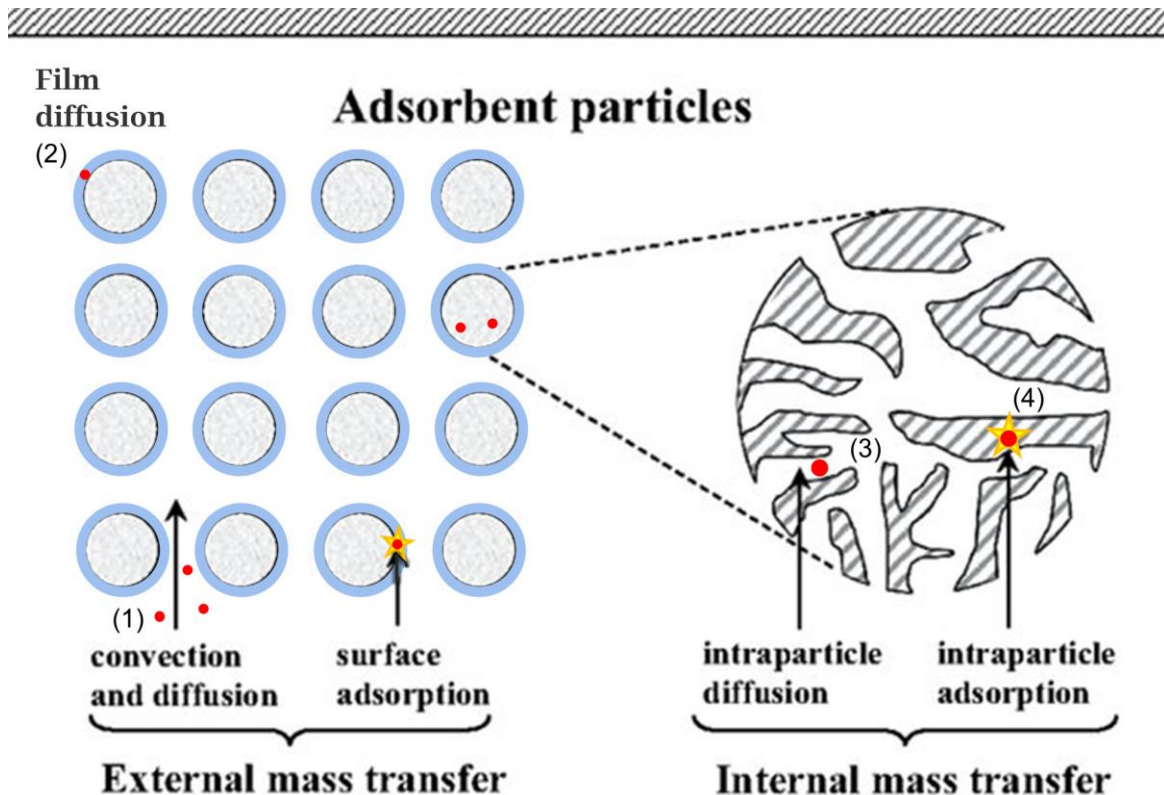


Figure 11 Different steps for adsorption kinetics (1) (2) (3) and reaction (4) occurring during fixed-bed adsorption (Zhou et al., 2016). Edit for liquid instead of gas.  
Blue = particle film

The following are basic mechanisms that are important in an adsorption column (**Figure 11**). There are four steps the solute undergoes when removed by adsorption and any of them can be rate-limiting (Xu et al., 2013).

- (1) **Liquid phase mass transfer** including convective mass transfer and molecular diffusion.
- (2) **External film diffusion** between liquid phase and exterior surface of the adsorbent. This mass transfer occurs in the 'boundary layer', which is the surrounding of every adsorbent particle inside the GAC bed.
- (3) **Intraparticle diffusion** which consist of pore diffusion and surface diffusion. Pore diffusion is the mass transfer of the solute in the pore volumes of the GAC particle. More specifically, it is a general name for molecular and/or Knudsen diffusion. Molecular diffusion mainly takes place in macropores and results from collisions between molecules. Knudsen diffusion dominates in micropores resulting from collisions between molecules and the pore wall. Surface diffusion is

the movement of the solute that hops between adsorption sites. Intraparticle diffusion strongly depends on concentration and size of the pollutant (S. Sharma et al., 2023).

It is assumed that, at the adsorbent surface, the solid-phase solute concentration is in equilibrium with the liquid-phase solute concentration (Jarvie et al., 2005). Locally, the liquid-phase concentration at the adsorbent particle surface is related to the adsorption capacity at the particle surface by the equilibrium relationship (Inglezakis et al., 2019). Therefore, the isotherm is a relevant aspect here. It gives information about the amount of solute that can be adsorbed when the concentrated stream is near to the surface and it is compound-specific.

- (4) **The adsorption- desorption reaction** on the active site (chemical, monolayered) or onto other particles (physical, multilayered). The adsorption itself can take place directly onto the external surface of an AC granule, or after intraparticle mass transfer onto the internal surface of an AC granule. This is also illustrated with a yellow star in **Figure 11**.

**Figure 12** demonstrates the intraparticle diffusion mechanisms more in detail.

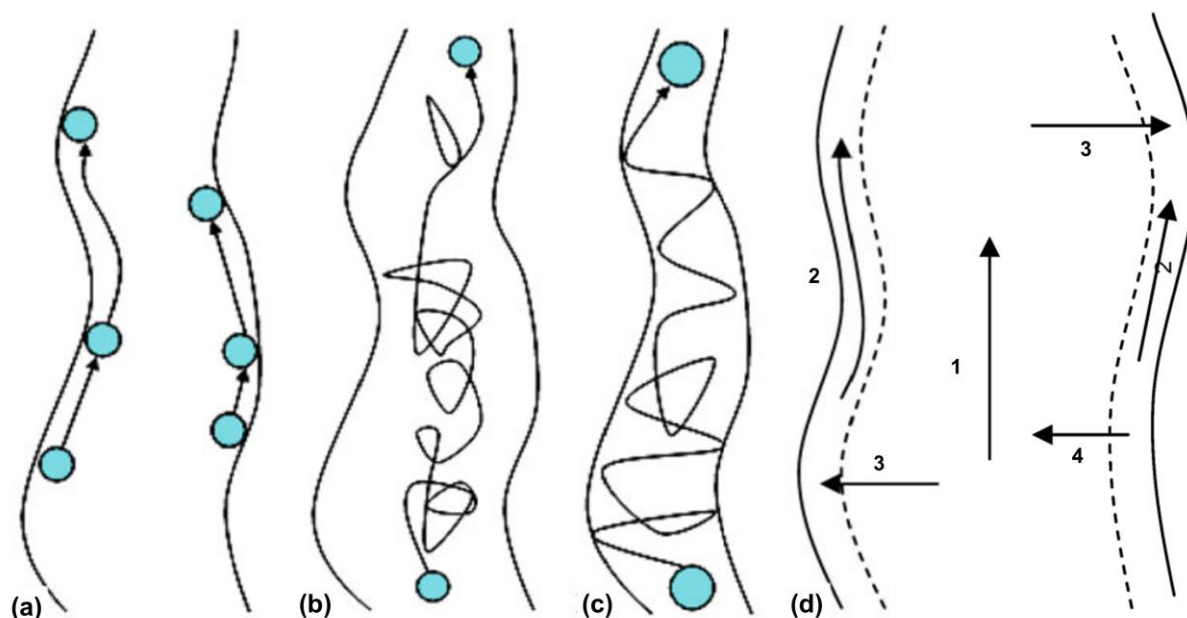


**Figure 12 Intraparticle diffusion mechanisms:** (a) surface diffusion, (b) pore diffusion, (c) pore diffusion with significant Knudsen diffusion, (d) combination of 1 pore diffusion, 2 surface diffusion, 3 adsorption, 4 desorption (Xu et al., 2013)

## 1.9 The breakthrough curve

The sequence of adsorption in a continuous fixed-bed adsorption column is illustrated in **Figure 13**. Adsorption, i.e. mass transfer, does not occur in the entire column simultaneously. If the influent is coming from above, the activated carbon in the top layer of the fixed-bed column will initially adsorb all the micropollutants. Meanwhile, the bottom of the column receives already well treated influent with low concentration of OMPs, leading to a very low mass transfer.

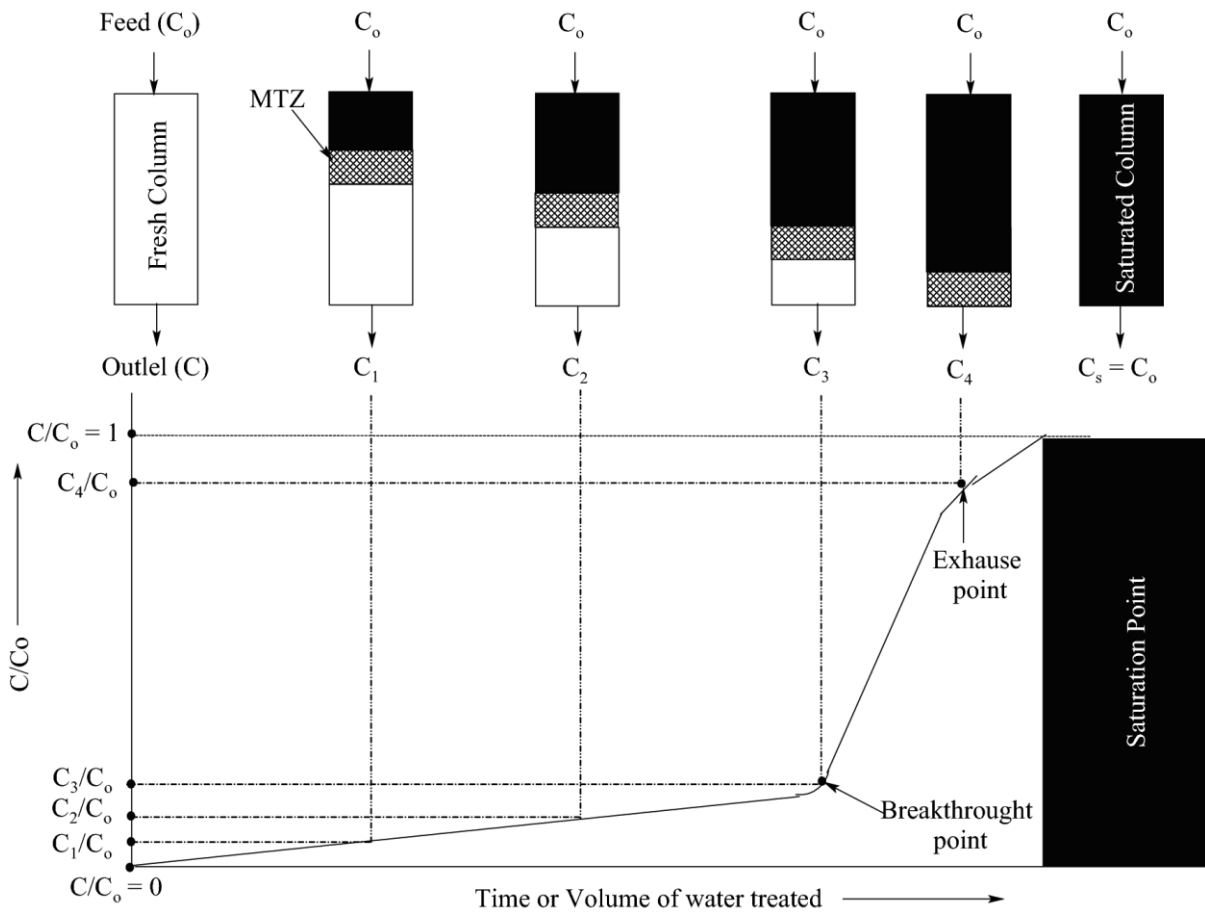


**Figure 13 Representation of adsorption in a fixed-bed column and the link with breakthrough curve (Patel, 2019)**

As said, initially, there is fresh carbon on top that is in contact with non-treated effluent and causes the driving force ( $C_0 - C_e$ ) to be highest on top of the column.  $C_0$  is the concentration of pollutant in the influent. At the inlet, no adsorption has already been done and  $C = C_0$ . At the bottom, initially there is no driving force because the influent is already treated by the upper part and doesn't contain pollutants anymore. However, the above part gets saturated after some time and the zone with highest driving force will move downwards. The region where mass transfer occurs depends on time and space and is called the mass transfer zone (MTZ). It is illustrated as the dotted area in **Figure 13** and is preceded by a saturated carbon zone (black area) and followed by fresh carbon (white area).

A breakthrough curve (BTC) is a plot of the fixed-bed column effluent concentration as function of time or volume of water treated. Initially, with a fully fresh column, the effluent concentration is perfectly treated and ideally contains zero pollutants. After a while, due to saturation, the effluent concentration increases. Above the breakthrough point, the effluent concentration is considered too high for a successful removal. This can be around 5% of the influent concentration, dependent on the desired effluent quality. From then, typically concentrations increase more rapidly and at the point of exhaustion, the bed is considered exhausted. The effluent concentration is only 5% lower than the highly concentrated influent. At perfect saturation, there is absolutely no adsorption happening anymore (Sabri & Abbood, 2019).

## **2 ADSORPTION ON ACTIVATED CARBON: BREAKTHROUGH CURVE MODELS**

This chapter explains what breakthrough curve models are and what opportunities they can deliver. It goes through why different models exist and which ones are appropriate for modelling tertiary GAC treatment in WWTPs. The scope of this section is limited to single-solute adsorption onto non-biological GAC in fixed-bed columns.

### **2.1 Opportunities and challenges**

A breakthrough curve (BTC) is a crucial piece of information for the design and operation of real-life adsorption systems tackling OMPs in municipal wastewater treatment systems. With the BTC, one can make conclusions about the adsorption performance, the time required before regeneration is needed, the removal efficiency at any time, etc. However, making BTCs for a variety of compounds in a variety of conditions is a costly operation. Applying for municipal wastewater, this requires many pilot-scale experiments. Models that could trustfully predict BTCs for all these different scenarios could save a lot of time and money. It would help to predict in which scenarios one gets maximum removal efficiency, adsorption capacity, and to predict bed replacement intervals. This facilitates to figure out if GAC is a viable technology for full-scale advanced wastewater treatment. Hence, there is opportunity to meet discharge limits for micropollutants in the future. In the coming years, the need for optimised treatment systems will only increase as legislation around MPs will get stricter (Burkhardt et al., 2022a).

A first challenge is related to the complexity of the municipal WWTP's influent. It is a complex stream containing many different MPs in highly varying concentrations. It is not only the concentration of MPs itself that vary over time. The WWTP's influent composition is uncertain and variable. For example, dissolved organic matter (DOM) is important to address as it competes with MPs, but it is variable and hard to quantify. Environmental and operating conditions can also be variable. Moreover, the flow rate of the incoming stream and weather conditions change unpredictably over time (Inglezakis et al., 2019).

A second challenge can be seen as a consequence of the first one. Because adsorption systems for MPs are relatively new and complicated, there is an information gap in literature. Existing models are rarely used for simulating full-scale fixed-bed GAC columns treating municipal wastewater. Nevertheless, most are limited in scope and complexity. An example could be modelling the adsorption of phenolic compounds from olive mill wastewater (Aliakbarian et al., 2015). Here a specific influent composition is considered. An empirical model with limited amount of equations could work but can fail in describing other polluted streams where for example other adsorption mechanisms apply, such as multilayer adsorption (Xu et al., 2013). Another reason why research is limited for this topic is the lack of experimental data on MPs in wastewater. Measuring trace concentrations is time-consuming and costly. Also, it is only recently that measuring becomes more relevant as regulatory limits evolve.

The model quickly becomes complex when considering all variabilities in the context of municipal wastewater. The more complex, also the more equations and parameters that are needed. However, calibrating a model with too many parameters can be challenging and it may require significant effort to determine or calculate them. Also, the sum of uncertainties for all these parameters would be too high. It is said that applicability of large adsorption models is restricted due to the low availability of internal transport parameters (Worch, 2008). A balance need to be found between accuracy of the process description and reliability of the model results.

## 2.2 Components of fixed-bed BTC models

A breakthrough curve (BTC) model is a model containing a set of partial differential equations, and usually consists of three components (Worch, 2008; Xu et al., 2013):

- The differential mass balance equation
- The differential uptake rate equation(s) describing adsorption kinetics
- The isotherm equation describing equilibrium (in this scope for single-solute)

This division is necessary to fully describe the four steps the micropollutant undergoes in a fixed-bed adsorption column, as explained by **Figure 11**. The uptake rate depends on how fast mass transfer and diffusion occurs in the pathway to the adsorption sites. The isotherm is useful at the adsorbent surface, where solid- and liquid-phase concentrations are assumed to be in equilibrium (Jarvie et al., 2005).

## 2.3 Equilibrium relationship: isotherm equations

This section presents an overview of (common) isotherm equations that can be used in fixed-bed BTC models. The purpose here is to simulate equilibrium behaviour as good as possible. As said, it is desired that equilibrium is studied experimentally, if not done before, because every solute-sorbent interaction is different. In the model, equilibrium is represented by an isotherm equation. This is a simple function with two or more isotherm parameters. When reliable experimental equilibrium data is available, the isotherm equation can be fitted to this dataset. Numerous isotherm equations have been developed in the past to mimic the diverse shapes that exist in practice. The Freundlich and Langmuir equations are simple and most frequently applied for single-solute equilibrium simulation (Aliakbarian et al., 2015).

Some isotherm equations are based on monolayer (chemical) adsorption, other on multilayer (physical) adsorption. When Van der Waals interaction dominates the mechanism, the adsorption is mainly a multilayered process as solutes can also physically attract each other. When the mechanism is mainly dominated by hydrogen / strong bonding with functional groups on the surface, adsorption is monolayered (Wang & Guo, 2023). The two adsorption mechanisms are illustrated in **Figure 14**. Names of common isotherm equations for heavy metals are shown in **Figure 15**.

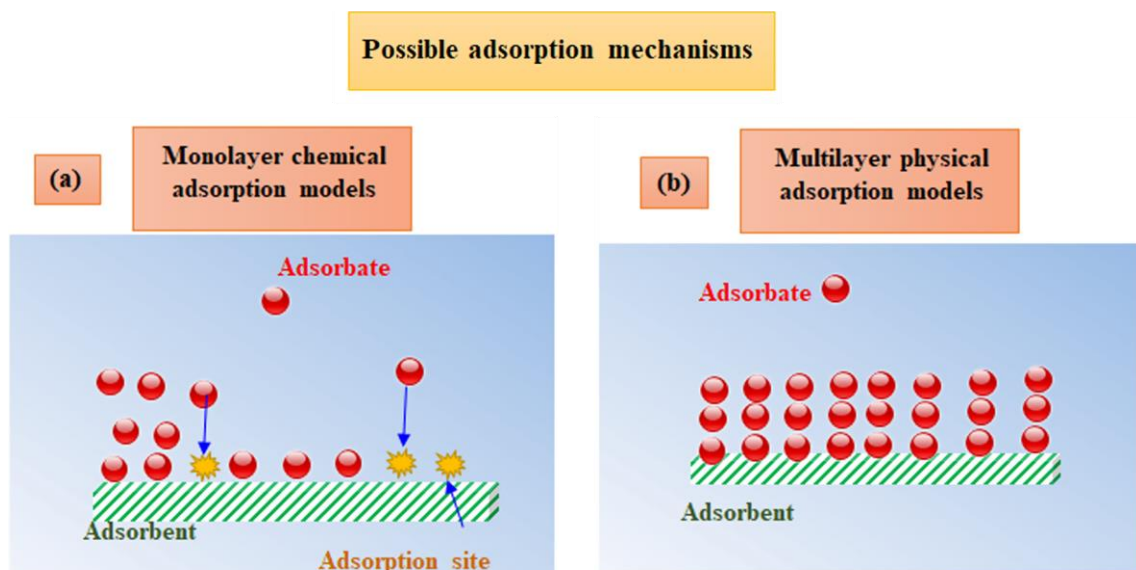


Figure 14 Theoretical adsorption mechanisms on the adsorbent surface (Saleh, 2022)

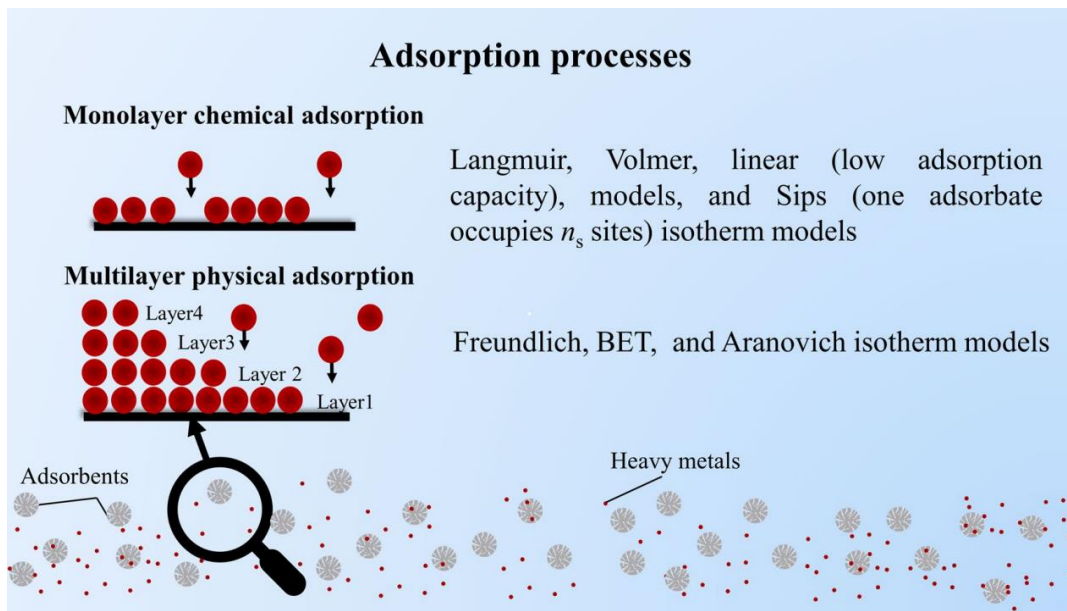


Figure 15 Adsorption mechanisms and corresponding adsorption isotherm models (Wang & Guo, 2023)

### 2.3.1 Freundlich isotherm equation

The nonlinear Freundlich equation is one of the most widely used models for describing equilibrium. It covers both multilayer and monolayer adsorption with 50 % active site occupation (Wang & Guo, 2023). The isotherm assumes the following:

- The surface is heterogeneous: adsorption energy varies as a function of the surface coverage due to variation in adsorption heat. On the heterogeneous surface, affinities between adsorbent and adsorbate show an unstable distribution (Aliakbarian et al., 2015; Šerban et al., 2023)

The equilibrium parameters follow a relationship that is mathematically described in equation (1) or linearized in equation (2) (Aliakbarian et al., 2015; Šerban et al., 2023; Vanoppen, 2023).

$$q_e = K_F * C_e^{1/n} \quad (1)$$

$$\ln(q_e) = \ln(K_F) + \frac{1}{n} \ln(C_e) \quad (2)$$

Where:

- $q_e$  = equilibrium solid-phase mass of solute per mass of sorbent (mg<sub>solute</sub>/g<sub>carbon</sub>)
- $C_e$  = equilibrium solute concentration in bulk liquid (mg<sub>solute</sub>/L)
- $K_F$  = Freundlich coefficient ((mg/g)\*(L/mg)<sup>n</sup>)
- $1/n$  = Freundlich exponent (-)

$K_F$  is a constant for a given sorbate related to the sorption capacity and  $1/n$  is a constant for a given sorbent related to the sorption intensity (Aliakbarian et al., 2015; Vanoppen, 2023). The Freundlich exponent accounts for adsorption site energy distribution (Jarvie et al., 2005). The Freundlich isotherm is an empirical equation and critics claim that it lacks a physical meaning (Saleh, 2022).

### 2.3.2 Langmuir isotherm equation

The Langmuir equation is also popular in isotherm studies and falls under the class of chemical isotherms. Chemical isotherms consider monolayer adsorption, which means that all molecules are localised in the adsorption sites. The equation is not empirical but theoretical and therefore it has more physical meaning for this context (Wang & Guo, 2020). Assumptions for this model are:

- The surface is homogeneous: all adsorption sites are energetically identical. The surface's adsorption sites have uniform energies of adsorption without transmigration of adsorbate in the pores of the adsorbent surface (Aliakbarian et al., 2015; S. Sharma et al., 2023)
- There are no lateral interactions between adsorbed molecules: interaction between solutes is ignored (S. Sharma et al., 2023; Wang & Guo, 2023)

These assumptions are thus true for chemical adsorption, also called chemisorption (S. Sharma et al., 2023). The equilibrium parameters follow a relationship that is mathematically described in equation (3) (Aliakbarian et al., 2015; Wang & Guo, 2020, 2023)

$$q_e = \frac{q_m K_L C_e}{1 + K_L C_e} \quad (3)$$

Where:

- $q_e$  = equilibrium solid-phase mass of solute per mass of sorbent (mg<sub>solute</sub>/g<sub>carbon</sub>)
- $C_e$  = equilibrium solute concentration in bulk liquid (mg<sub>solute</sub>/L)
- $K_L$  = Langmuir constant, ratio adsorption and desorption rates (L/mg)
- $q_m$  = maximum adsorption capacity (mg<sub>solute</sub>/g<sub>carbon</sub>)

When this model is applied, an indicator is used to evaluate if the adsorption can be considered favourable. It is favourable if the Langmuir separation factor ( $R_L$ ) is situated between 0 and 1. This constant can be calculated by equation (4) (Şerban et al., 2023; Wang & Guo, 2023).

$$R_L = \frac{1}{1 + K_L C_0} \quad (4)$$

Where:

- $R_L$  = separation factor (-)
- $C_0$  = initial solute concentration in bulk liquid (mg<sub>solute</sub>/L)
- $K_L$  = Langmuir constant (L/mg)

Other isotherm models in **Figure 15** are well explained by Wang & Guo, (2020) and Saleh, (2022, p. 4). A summary and general classification of adsorption isotherms are represented in **Figure 16**.

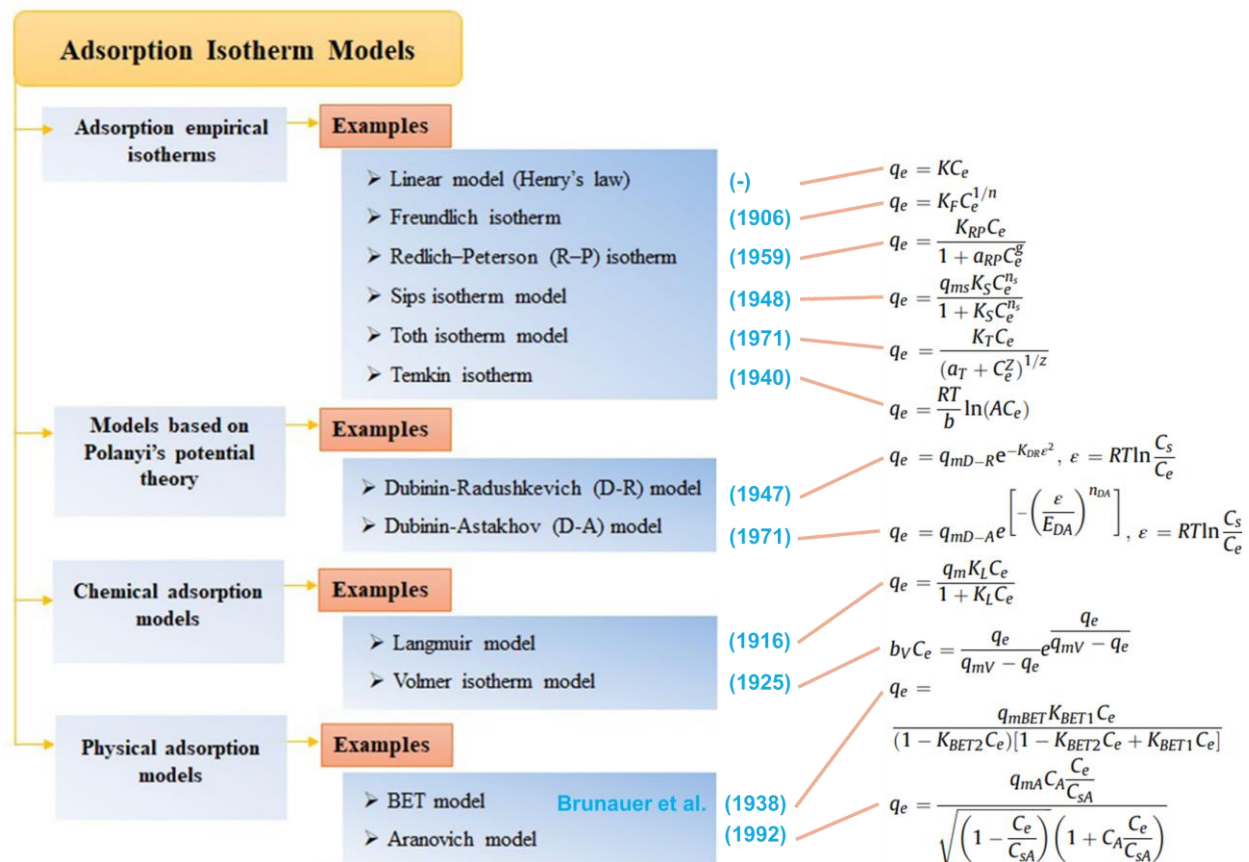


Figure 16 Classification, reference and equation of adsorption isotherm models  
(Saleh, 2022; Wang & Guo, 2020)

## 2.4 Fixed-bed BTC models

### 2.4.1 Pore and Surface Diffusion Model (PSDM)

The pore and surface diffusion model (PSDM) is a comprehensive diffusion-based model (Xu et al., 2013). It is also called a 'general rate' model and classified as a mass transfer model. It is able to describe mass transfer very well and assumes that the adsorption surface reaction is instant and not the rate controlling step. Also, an isotherm is included. It is true that in porous materials like GAC, the adsorption of micropollutants is typically rate-limited by the intraparticle diffusion step and not by the adsorption reaction step. The fact that the PSDM includes a combination of all mass transfer resistances (external, fluid film, pore (macropore) and surface (micropore) diffusion) makes the model very interesting for adsorption of various micropollutants onto GAC (Inglezakis et al., 2019). From the earlier discussion on four possibly rate-limiting steps in an adsorption column, the ones that are included in the model are marked below in green. It is called a multi-phase model because it takes into account multiple types of diffusion which are film, pore and surface diffusions (S. Sharma et al., 2023).

- (1) Liquid phase mass transfer
- (2) External film diffusion
- (3) Intraparticle diffusion: Pore diffusion and Surface diffusion  
The isotherm
- (4) The adsorption- desorption reaction

(1) In liquid phase mass transfer, solutes can move through the column in axial or radial direction. However, as the length of the column is typically larger and radial velocities are rather small, only axial movement can be considered in the model. It is then assumed that the cross-sections are homogeneous. A macroscopic mass conservation equation is required to include variations in the column in z-direction. These variables are: concentration of adsorbed adsorbate  $q$ , concentration of the bulk solution  $C$ , distance to inlet  $z$ , superficial velocity  $u$  and the axial dispersion coefficient  $D_z$  (Xu et al., 2013). The variables are included in the differential mass balance equation (5).

$$\varepsilon_b \frac{\partial C}{\partial t} + u \frac{\partial C}{\partial z} + (1 - \varepsilon_b) \rho_b \frac{\partial q}{\partial t} = D_z \frac{\partial^2 C}{\partial z^2} \quad (5)$$

Where (Jarvie et al., 2005):

- $\varepsilon_b$  = bed porosity or bed void fraction (-)
- $\rho_b$  = bed (adsorbent) density ( $\text{g}/\text{cm}^3$ )

Usually, axial dispersion is ignored so the right-hand side of the equation becomes zero. Mass conservation in the column with the components of the differential mass balance equation is shown in **Figure 17**. Mass balances are necessary to simulate the movement of the mass transfer zone as seen in **Figure 13**. The mass balance equation is generally applied in fixed-bed BTC models (Xu et al., 2013).

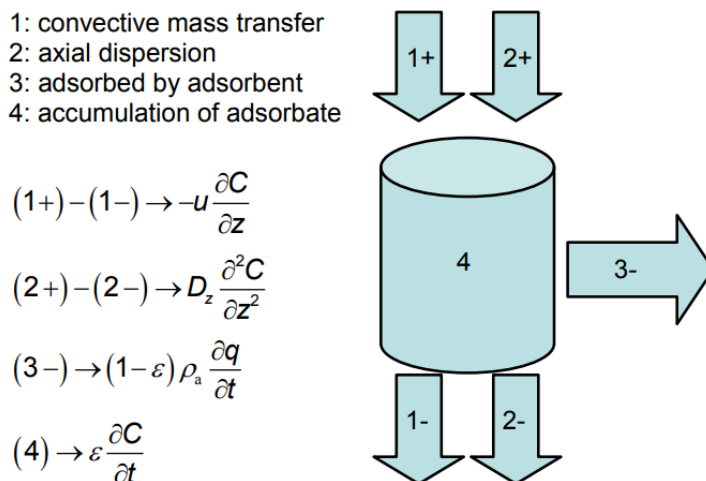


**Figure 17 Schematic representation of mass conservation in the column with components of the differential mass balance equation (Xu et al., 2013)**

There are some assumptions for this mass balance equation. The packing material is assumed to be made of spherical and uniform porous particles. The bed is considered homogenous and the concentration gradient in the radial direction of the bed is negligible. The flow rate is constant and does not vary within the column (Xu et al., 2013).

The PSDM simulates mass transfer in the bulk liquid via the liquid diffusion coefficient  $D_l$  ( $\text{cm}^2/\text{s}$ ), which is compound-specific. This parameter can be estimated from equation (6).  $V_b$  ( $\text{cm}^3/\text{mol}$ ) is the molar volume of the synthetic organic compound (SOC) at the boiling point temperature and  $\mu_l$  (centipoise) the liquid viscosity (Jarvie et al., 2005).

$$D_l = \frac{13.26 * 10^{-5}}{\mu_l^{1.14} V_b^{0.589}} \quad (6)$$

(2) External film diffusion is also included in the PSDM model. External film diffusion occurs within the film surrounded by every particle, also called the ‘boundary layer’. This layer is located at the interface between the exterior surface of the adsorbent particle, and the bulk solution. In some cases, film diffusion can predominate and thus be the rate-controlling step within the general rate model. At the adsorbent surface, the solute/ sorbent concentrations are assumed to be in equilibrium. In the bulk liquid, concentration of pollutants are higher. Thus, the driving force for film diffusion is the concentration gradient (Xu et al., 2013). External diffusion is modelled by equation: (7), (Worch, 2008).

$$\frac{dq}{dt} = \frac{k_F a_V}{\rho_b} (C - C_s) \quad (7)$$

Where

$$a_V = \frac{3}{r_p} (1 - \varepsilon_b) \quad (8)$$

and:

- $k_F a_V$  = volumetric film diffusion mass transfer coefficient (1/s)
- $\rho_b$  = bed density (g/cm<sup>3</sup>)
- $C$  = concentration in the bulk liquid (mg<sub>solute</sub>/L)
- $C_s$  = concentration at the external particle surface (mg<sub>solute</sub>/L)
- $a_V$  = area available for mass transfer per reactor volume (cm<sup>2</sup>/cm<sup>3</sup>)
- $r_p$  = radius adsorbent particle (cm)

$k_f$  (cm/s) is the external mass transfer coefficient and can be estimated from the correlation of Gnielinski, 1978. This can be seen in equation (9), (Jarvie et al., 2005). It is clear that  $k_f$  depends on the adsorbent particle and liquid properties.

$$k_f = \frac{(1 + 1.5(1 - \varepsilon_b))\phi D_l}{2r_p} [2 + 0.644 Re^{1/2} Sc^{1/3}] \quad (9)$$

The parameters Reynolds ( $Re$ ) and Schmidt ( $Sc$ ) dimensionless numbers are then estimated by equations (10) and (11) (Jarvie et al., 2005)

$$Re = \frac{2\rho_l r_p V}{\varepsilon_b \mu_l} \quad (10)$$

$$Sc = \frac{\mu_l}{\rho_l D_l} \quad (11)$$

Where:

- $\phi$  = adsorbent particle shape correction factor (-)
- $Re$  = Reynolds number (-)
- $Sc$  = Schmidt number (-)
- $\rho_l$  = density of the water (g/cm<sup>3</sup>)
- $V$  = superficial loading velocity (cm/s)

(3) Intraparticle diffusion is well-covered by the PSDM as it both includes surface and pore diffusion, which are represented by the intraparticle mass transfer coefficients, respectively  $D_s$  and  $D_p$ . These parameters can be estimated from the correlations of Crittenden, 1987 (equation (12)) and Zimmer, 1988 (equation (13)) which are reported in the 'fixed-bed model parameter estimation' review by Jarvie et al., (2005).

$$D_s = SPDFR * \left[ \frac{D_l \varepsilon_p C_0}{\tau_p K C_0^{1/n} \rho_a} \right] \quad (12)$$

$$D_p = \frac{D_l}{\tau_p} \quad (13)$$

- $SPDFR$  = surface to pore diffusion ratio (-)
- $\varepsilon_p$  = adsorbent particle void fraction (-)
- $C_0$  = average influent liquid-phase concentration ( $\mu\text{mole/L}$ )
- $\tau_p$  = tortuosity of diffusion path length within particle (-)
- $\rho_a$  = Apparent adsorbent particle density ( $\text{g/cm}^3$ )
- $D_s$  = surface diffusion coefficient ( $\text{cm}^2/\text{s}$ )
- $D_p$  = pore diffusion coefficient ( $\text{cm}^2/\text{s}$ )

Because both pore and surface diffusions are considered, the model is called heterogeneous. The partial differential equation to be numerically solved is given by equation (14) (S. Sharma et al., 2023). The mass transfer uptake rate in the GAC granule is described using Fick's law (Xu et al., 2013).

$$\frac{\partial q}{\partial t} = D_s \left( \frac{\partial^2 q}{\partial r^2} + \frac{2}{r} \frac{\partial q}{\partial r} \right) + \frac{D_p}{\rho_p} \left( \frac{\partial^2 C_p}{\partial r^2} + \frac{2}{r} \frac{\partial C_p}{\partial r} \right) \quad (14)$$

The uptake rate  $\frac{\partial q}{\partial t}$  depends on both surface and pore diffusions.  $r$  (cm) is the radial coordinate and is zero at the centre of the adsorbent particle. Thus, the deeper in the pores of the particle, the higher the uptake rate.  $\rho_p$  is the adsorbent particle density ( $\text{g/cm}^3$ ) and  $C_p$  the concentration inside the pores ( $\mu\text{g/L}$ ).

Locally, the fluid phase concentration at the adsorbent particle surface  $C_s$  is a function of the adsorption capacity at the particle surface  $q_s$  using an equilibrium relationship (equation (15)), which is often the Freundlich isotherm (Inglezakis et al., 2019).

$$q_s = f(C_s) \quad (15)$$

As said before, the adsorption reaction is not rate-limiting but assumed to be instant. An overview of the PSDM model is seen in **Figure 18**. On the left-hand side, the external mass transfer in the fluid film is illustrated, with the concentration gradient being the linear driving force. Equations are written in the form of a mass flux instead of an uptake rate. Once at the adsorbent surface, equilibrium is obtained. Here, the Freundlich single-solute isotherm is used to calculate the amount of mass adsorbed  $q$  ( $\text{mg}_{\text{solute}}/\text{g}_{\text{carbon}}$ ). The solute can also first diffuse inside the particle with a mass flux shown at the right-hand side of the figure. Diffusion mechanisms are simplified using two diffusion coefficients for pore and surface diffusions (Jarvie et al., 2005; S. Sharma et al., 2023).

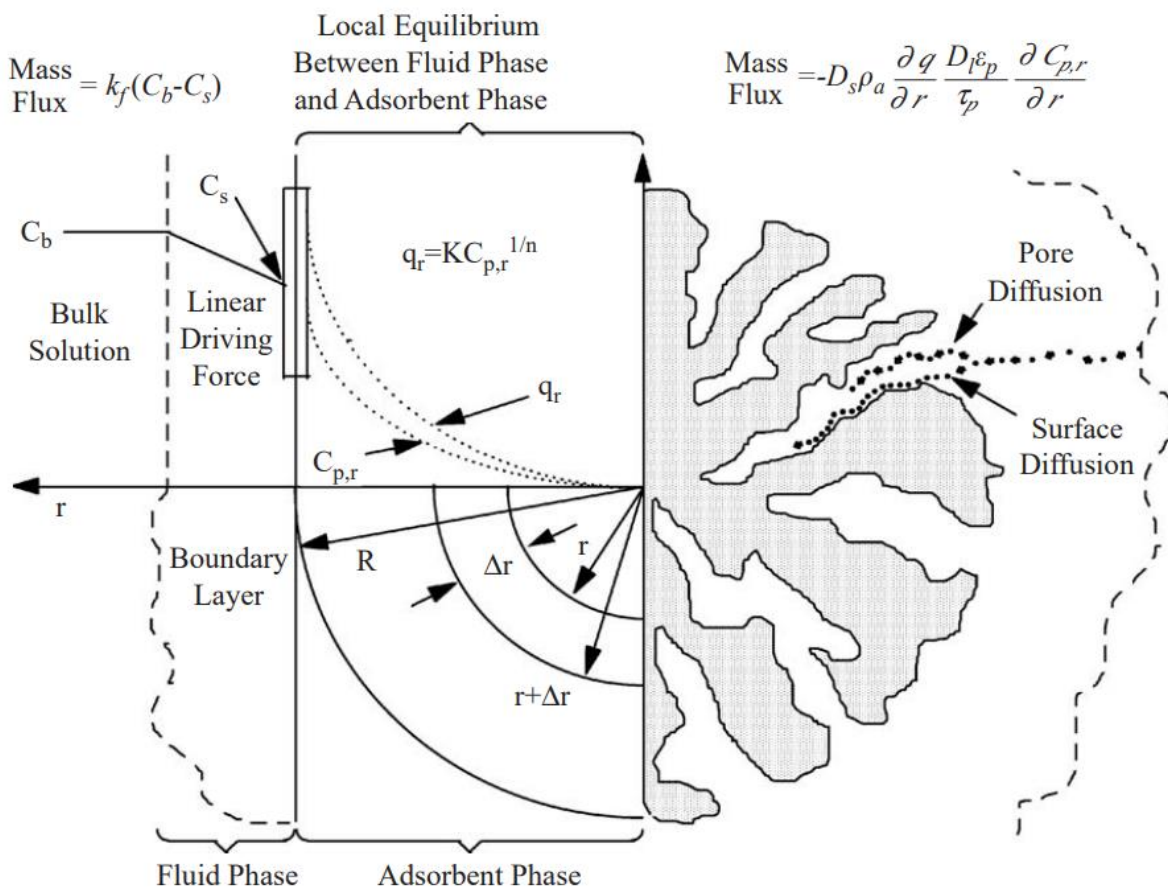


**Figure 18 Schematic overview of the pore surface diffusion model (PSDM) and the mechanisms that are included in its partial differential equations (Jarvie et al., 2005)**

#### 2.4.2 Homogeneous Surface Diffusion Model (HSDM)

The homogeneous surface diffusion model is also a diffusion-based, mass transfer model which assumes that surface diffusion is predominant and pore diffusion is negligible, leading to a homogeneous adsorbent particle. This 'general rate' model is originally based on Fick's law with the PSDM being an extension of it. HSDM is a simpler and more popular model, with a simplified differential equation (16) for the uptake rate which is related to the surface diffusion. Equation (7) is still valid for external film diffusion and the equilibrium relationship involves the same calculation by equation (15) (Inglezakis et al., 2019). The steps related to fixed-bed adsorption that are included in the HSDM are marked below in green. It is called a two-phase model as it considers two diffusion types: intraparticle surface and external film diffusion (S. Sharma et al., 2023).

- (1) Liquid phase mass transfer
- (2) External film diffusion
- (3) Intraparticle diffusion: Pore diffusion and Surface diffusion  
The isotherm
- (4) The adsorption- desorption reaction

$$\frac{\partial q}{\partial t} = D_s \left( \frac{\partial^2 q}{\partial r^2} + \frac{2}{r} \frac{\partial q}{\partial r} \right) \quad (16)$$

### 2.4.3 Pore Diffusion Model (PDM)

The pore diffusion model is also a variant of the complete PSDM which assumes that pore diffusion is predominant and surface diffusion is negligible. It is less common than the HSDM but it is represented by partial differential equation (17). From the four possibly rate-limiting steps in an adsorption column, the ones that are included in the model are marked below in green. Mass balance and diffusion equations are again similar as in the previously described PSDM, except for the surface diffusion. It is also called a two-phase model as it considers two diffusion types: intraparticle pore and external film diffusion (S. Sharma et al., 2023).

- (1) Liquid phase mass transfer
- (2) External film diffusion
- (3) Intraparticle diffusion: Pore diffusion and Surface diffusion  
The isotherm
- (4) The adsorption- desorption reaction

$$\frac{\partial q}{\partial t} = \frac{D_P}{\rho_P} \left( \frac{\partial^2 C_p}{\partial r^2} + \frac{2}{r} \frac{\partial C_p}{\partial r} \right) \quad (17)$$

### 2.4.4 Linear Driving Force (LDF) model

The linear driving force (LDF) model is a diffusion-based model and an approximation to the more accurate but also more complicated PSDM. The model is based on a simplified mass transfer equation (18) with an all-in-one or 'lumped' intraparticle mass transfer coefficient  $k$  (S. Sharma et al., 2023; Xu et al., 2013). It states that the rate of adsorption is proportional to the amount of adsorbate still required to achieve the equilibrium, which is covered by the driving force factor ( $q_s - q_a$ ).  $q_s$  is the equilibrium adsorption amount at the external particle surface and is related to  $C_s$  by an appropriate adsorption isotherm (equation (15)).  $q_a$  is the mean loading in the particle. The uptake rate  $\frac{dq}{dt}$  (here an ordinary differential equation in contrast to the previous models) depends on the linear difference between  $q_s$  and  $q_a$ . External diffusion can be considered by including equation (7) (S. Sharma et al., 2023; Worch, 2008). The steps included in the LDF model are marked below in green. It is called a two-phase model as it considers both intraparticle and external film diffusion (S. Sharma et al., 2023).

- (1) Liquid phase mass transfer
- (2) External film diffusion
- (3) Intraparticle diffusion: lumped mass transfer coefficient  
The isotherm
- (4) The adsorption- desorption reaction

$$\frac{dq}{dt} = k(q_s - q_a) \quad (18)$$

A comparison of the PSDM model and LDF model is depicted in **Figure 19**. It can be seen that for the LDF model, an average  $q_a$  of the adsorption capacity is used for calculating the linear driving force and thus uptake rate. Namely, the solid pink line represents the average of the dashed pink line and increases over time. At each point in time, the sloped black arrow represents the linear difference ( $q_s - q_a$ ). The uptake rate becomes smaller as the linear difference becomes smaller. In the end, there is no difference between them anymore (horizontal black arrow). In both cases, after some time the particle loading is maximized, i.e. equal to equilibrium loading, as the granule is fully saturated.

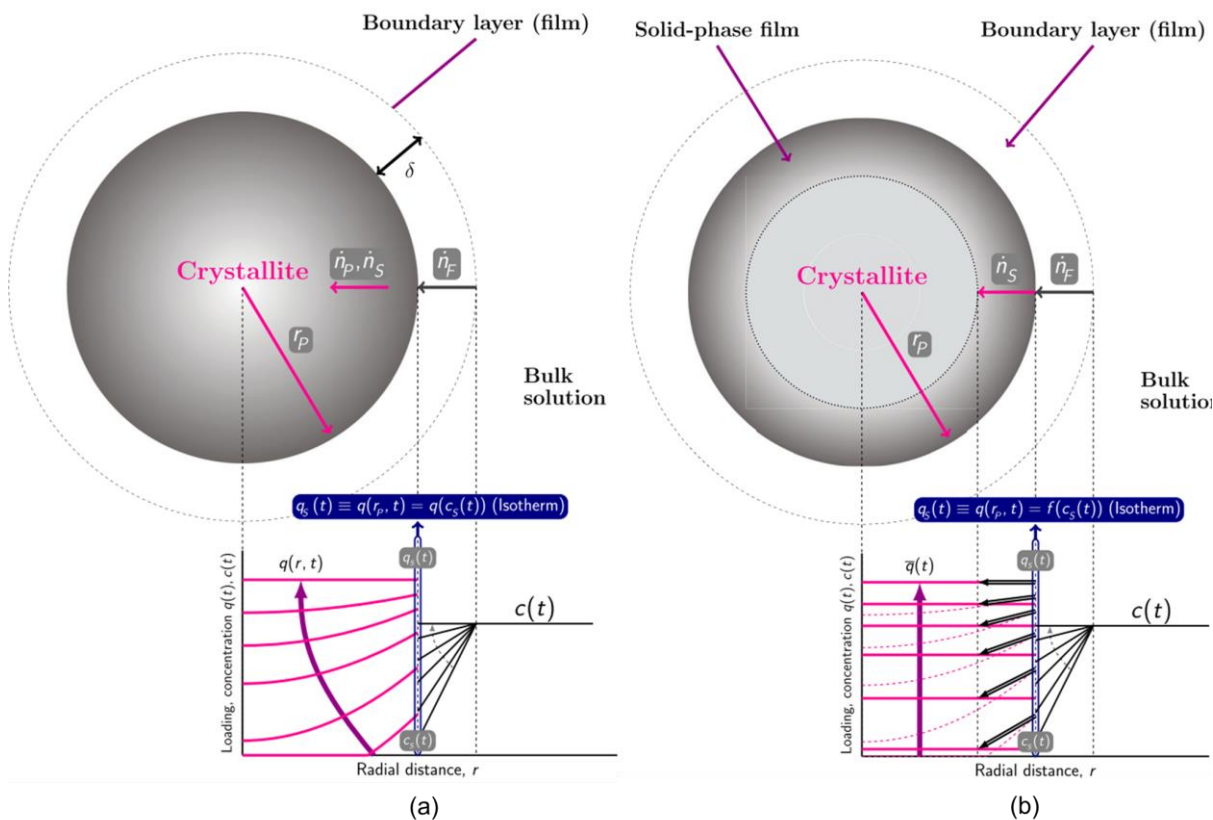


**Figure 19** loading and concentration profiles of the (a) PSDM model with  $\dot{n}_p$  and  $\dot{n}_s$  respectively the flux by pore and surface diffusion, (b) LDF model with  $\dot{n}_s$  the solid flux driven by the linear driving force ( $q_s - q_a$ ), black arrows. For both,  $\dot{n}_F$  is the film flux (i.e. external film diffusion) driven by the concentration gradient ( $C - C_s$ ). The surface is considered to be in equilibrium and the adsorbent loading is calculated from the isotherm  $q_s = f(c_s)$  (S. Sharma et al., 2023)

## 2.4.5 The Thomas model (TM) and Clark model (CM)

The Thomas and Clark models are only suitable where external and internal diffusion resistances are extremely small (Xu et al., 2013). These models neglect intraparticle diffusion and are also called ‘chemical kinetic models’. Mass transfer rate is assumed to be the difference between two opposing second-order reactions with different rate constants. It is assumed that there is local equilibrium in any cross-section along the bed. The Thomas model uses the Langmuir isotherm. The Clark model describes mass transfer in combination with the Freundlich isotherm. From the earlier discussed four possibly rate-limiting steps in an adsorption column, only the isotherm and the adsorption-desorption reaction are included here (marked in green below). The Thomas and Clark model are examples of one-phase models because they take into account only chemical kinetic mass transfer and the isotherm. Other one-phase models include the Bohart-Adams model and the Yoon-Nelson model (S. Sharma et al., 2023). The equations of these models can be found in the comprehensive review of fixed-bed column adsorption reported in Patel, (2019).

- (1) Liquid phase mass transfer
- (2) External film diffusion
- (3) Intraparticle diffusion: Pore diffusion and Surface diffusion  
**The isotherm**
- (4) **The adsorption- desorption reaction**

## 2.4.6 Pseudo-First-Order (PFO) model

The pseudo-first-order (PFO) model by Lagergren, 1898, is not diffusion-based but is an ‘adsorption reaction model’. It is only valid when the adsorption reaction itself (particularly chemisorption) is rate-limiting, without any concern about the diffusion mechanism. The model describes conditions where the number of active sites is significantly lower than the number of adsorbates (Wang & Guo, 2023). The focus is on the adsorption reaction near the active sites and diffusion or mass transfer is fast enough to be neglected (Silva et al., 2021). Moreover, the model does not include any isotherms (Inglezakis et al., 2019). The steps related to fixed-bed adsorption that are included in the PFO model are marked green here. It is called a zero-phase model because the model ignores mass transfer and assumes instantaneous equilibrium (S. Sharma et al., 2023).

- (1) Liquid phase mass transfer
- (2) External film diffusion
- (3) Intraparticle diffusion  
The isotherm
- (4) **The adsorption reaction: chemisorption**

The mathematical description of the PFO model is seen in equation (19) (Wang & Guo, 2023).

$$\frac{dq_t}{dt} = k_1(q_e - q_t) \quad (19)$$

Where:

- $q_t$  = adsorption capacity at time t (mg<sub>solute</sub>/g<sub>carbon</sub>)
- $q_e$  = equilibrium adsorption capacity (mg<sub>solute</sub>/g<sub>carbon</sub>)
- $k_1$  = PFO rate constant (1/h)

$k_1$  is then the reaction rate constant with chemical reaction being the controlling step. The PFO model has the same mathematical form as the LDF model but it is not diffusion-based and no isotherm is included. Lagergren’s model is criticized for being theoretically inconsistent (Inglezakis et al., 2019). However, it is mentioned here because, just as the PSO model, it has been extensively used in the literature (Ramos et al., 2014; Serban et al., 2023). It is a highly simplified empirical equation with absence of physical significance if underlying assumptions are not observed. The flexible mathematical form is a descriptive tool rather than a predictive tool. Therefore, The reaction-based models are not considered for higher scale predictions (Inglezakis et al., 2019).

## 2.4.7 Pseudo-Second-Order (PSO) model

Next to the PFO model, the pseudo-second-order (PSO) kinetics model is also popular due to its simplicity. The model describes conditions where the number of active sites has the same order of magnitude as the number of adsorbates (Wang & Guo, 2023). Theoretically, PSO assumes that the rate-limiting step is most likely the chemical, strong covalent bonding, so again chemisorption (Inglezakis et al., 2019). It is together with the PFO categorized under the group of reaction kinetics-based models (Inglezakis et al., 2019). The mathematical description of the PSO is seen in equation (20) or integrated in equation (21). Plotting  $\frac{t}{q_t}$  against time (equation (22)) at different activated carbon quantities can be used to estimate the second-order-rate constant of sorption  $k_2$  (Aliakbarian et al., 2015). The steps related to fixed-bed adsorption that are included in the PSO model are the same as the PFO model (marked in green).

It is called a zero-phase model because the model ignores mass transfer and assumes instantaneous equilibrium (S. Sharma et al., 2023).

(1) Liquid phase mass transfer

(2) External film diffusion

(3) Intraparticle diffusion

The isotherm

(4) **The adsorption reaction: chemisorption**

$$\frac{dq_t}{dt} = k_2(q_e - q_t)^2 \quad (20)$$

$$q_t = \frac{q_e^2 k_2 t}{1 + q_e k_2 t} \quad (21)$$

$$\frac{t}{q_t} = \frac{1}{k_2 q_e^2} + \frac{t}{q_e} \quad (22)$$

Where:

- $q_t$  = adsorption capacity at time t (mg<sub>solute</sub>/g<sub>carbon</sub>)
- $q_e$  = equilibrium adsorption capacity (mg<sub>solute</sub>/g<sub>carbon</sub>)
- $k_2$  = PSO rate constant (g/(h\*mg))

Being a purely empirical fitting exercise lacking physical significance, this model is also not ideal in varying conditions. This makes it unreliable for modelling urban wastewater treatment processes. Unfortunately, many researchers evaluated its applicability only on the quality of the fit with the experimental data and not on the underlying theory, which is clearly a misperception (Inglezakis et al., 2019; Yao & Zhu, 2021).

## 2.5 Conclusion BTC models

Zero-phase models such as the PFO or PSO model lack physical significance, are empirical and therefore more suitable as descriptive tools. One-phase models such as the Thomas or Clark model consider chemical mass transfer but neglect the intraparticle diffusion. This is a drawback because in porous materials like GAC, the adsorption of micropollutants is typically rate-limited by intraparticle diffusion (Inglezakis et al., 2019). Two-phase models are then a better approximation and more accurate than one-phase models, but they require numerical solvers. Some intraparticle and external diffusions are considered in such models. The HSDM, PDM and LDF are therefore realistic candidates for modelling the removal of micropollutants to some extent. Multi-phase models like the PSDM model are very complex but this complexity can be worth including when modelling adsorption of variable-size micropollutants under the highly variable conditions present in municipal wastewater treatment. With detailed modelling of intraparticle diffusion (pore and surface), the PSDM is a strong candidate for simulating GAC in wastewater treatment plants. It is still worth mentioning that dynamic adsorption is a very complicated process and even multi-phase models are still simplified compared to reality. These simplifications include fast adsorption reaction rate, adsorbent granules of equal size in the column and no wall effect, to name a few. Also, as previously said more effort is needed to determine the model parameters and numerical solvers are required to obtain a solution for them (S. Sharma et al., 2023; Xu et al., 2013).

## MATERIALS AND METHODS

The tool that is used for simulation of GAC adsorption is the PSDM model implemented in Python by USEPA (Burkhardt, 2020). Additional plots, edits of the PSDM USEPA code and extensions can be found in the thesis's GitHub repository (<https://github.com/matcoghe/Thesis-Modelling-activated-carbon.git>), where folders are organized according to the chapters and structure of the thesis as the following:

- 5.1 Isotherm fitting tool
- 5.2 Example modelling of compound TCE
- 5.3 Pilot modelling of compound PFHpA
- 5.4 USEPA fouling approach
- 6.1 Extending the USEPA fouling approach
- 6.2 Alternative fouling approach
- 6.3 Scenario analysis on the Freundlich parameters

The PSDM model was executed from a *notebook (.ipynb)*, that also shares the name of the respective section in this document. It uses the scripts PSMD.py, PSDM\_extra.py, PSDM\_functions.py and PSDM\_tools.py. Edits or extensions are highlighted with a “//Mathieu” comment line at the beginning. Language and grammar of the thesis text is optimized with help of ChatGPT. Paragraphs were written by the author, only sentences or words were adjusted with advice of artificial intelligence.

### 3 PSDM BY USEPA MODEL

The United States Environmental Protection Agency (USEPA) implemented the Pore and Surface Diffusion Model (PSDM) into Python and made it publicly available as an open-source code on GitHub [https://github.com/USEPA/Water\\_Treatment\\_Models/tree/master/PSDM](https://github.com/USEPA/Water_Treatment_Models/tree/master/PSDM) (Burkhardt, 2020). The model was derived from an earlier AdDesignS™ version from Michigan Technological University. These software packages were originally developed for cleaning up contamination sites all over the United States. The objective was to estimate how effective adsorption was in the removal of fuel from contaminated water that was coming from leaking storage tanks in California (Hokanson et al., 1999).

As explained in Chapter 2, the PSDM is a good BTC model for simulating the adsorption of micropollutants by GAC in full-scale wastewater systems. The diffusion-based, multi-phase model describes intraparticle diffusion very well, at both pore and surface level. This is necessary as intraparticle diffusion is typically rate-limiting for porous materials like GAC, and very variable (Inglezakis et al., 2019). This can be seen in **Figure 12**, where the diffusion type depends on the size of the pollutant and diameter of the pores. There is an automated parameter-fitting and parameter-estimation tool included in the USEPA model. Further, it is possible to consider the fouling phenomenon, i.e. competition of dissolved organic carbon (DOC) with micropollutants for the adsorption sites. Fouling is often also referred to as preloading by natural organic matter (NOM) (Burkhardt et al., 2022a). To understand how the PSDM model works, one can refer to **section 2.4.1**, where the equations are presented in the sequence of steps that the solute undergoes in a fixed-bed column. A summarizing overview of the PSDM mechanisms for one GAC granule is presented also in **Figure 18**. These granules are assumed to have the same size and be equally distributed in the column. Equations are shown in **Table 6** next to the ones of the USEPA model.

Relevant parameters of the USEPA PSDM model are listed in **Table 7**. It can be noticed that the bed has two dimensions; length and diameter. Thus, the PSDM model by USEPA assumes a cylindrical fixed-bed column. The apparent particle density ( $\rho_a$ ) is the mass of the AC granule (particle) divided by the apparent (solid) particle volume (Webb, 2001). Tortuosity of the particle ( $\tau_p$ ) is the ratio of the actual diffusion path length ( $L_e$ ) to the shortest, straight path length ( $L$ ) of a flow in the GAC particle (Mudhoo et al., 2024). Partial differential equations are solved with the orthogonal collocation numerical solver (`solve_ivp` from `scipy.integrate` (SciPy -, n.d.)) (Burkhardt et al., 2022a). The number of radial and axial collocation points represent the number of nodes in the radial and axial direction in the column respectively. The problem is simplified to a 2D problem. For every node location, concentrations are calculated using the partial differential equations. Axial collocation points are usually the most significant in a long cylinder. Equations (23) and (24) are used to calculate bed porosity ( $\varepsilon_b$ ) and empty bed contact time ( $EBCT$ ) (Burkhardt, 2020).

$$\varepsilon_b = 1 - \frac{\text{Weight bed (wt)}}{\text{Volume bed} * \text{Particle density } (\rho_p)} \quad (23)$$

$$EBCT = \frac{\text{Area} * L \text{ (= volume column)}}{\text{Flow rate (flrt)}} \quad (24)$$

**Table 6 Model equations of the PSDM model by USEPA in Python language**

Mathematical equations (Jarvie et al., 2005)	Equations USEPA code (Burkhardt, 2020)
<b>Mass balance differential equation</b>	
$\varepsilon_b \frac{\partial C}{\partial t} + u \frac{\partial C}{\partial z} + (1 - \varepsilon_b) \rho_b \frac{\partial q}{\partial t} = D_z \frac{\partial^2 C}{\partial z^2}$	<b>Mass balance</b>
<b>Uptake rate differential equations</b>	
$\frac{dq}{dt} = \frac{k_F a_V}{\rho_b} (C - C_s)$	<b>External film</b>
$\frac{\partial q}{\partial t} = D_s \left( \frac{\partial^2 q}{\partial r^2} + \frac{2}{r} \frac{\partial q}{\partial r} \right) + \frac{D_p}{\rho_p} \left( \frac{\partial^2 C_p}{\partial r^2} + \frac{2}{r} \frac{\partial C_p}{\partial r} \right)$	<b>Granule</b>
<b>Isotherm equation (Freundlich)</b>	
$q_e = K_F * C_e^{1/n}$	<code>def freundlich(c, k, invN):     return k * c**invN</code>
<b>Parameter estimation equations</b>	
$D_l = \frac{13.26 * 10^{-5}}{\mu_l^{1.14} V_b^{0.589}}$	$difl = 13.26e-5 / (((vw * 100.)**1.14)*(mol_vol**0.589))$
$k_f = \frac{(1 + 1.5(1 - \varepsilon_b)) \phi D_l}{2r_p} [2 + 0.644 Re^{1/2} Sc^{1/3}]$	$kf_v = multi_p*(1+1.5*(1-ebed))*(2+0.644*(re**0.5)*(sc**(1./3.)))$
$D_s = SPDFR * \left[ \frac{D_l \varepsilon_p C_0}{\tau_p K C_0^{1/n} \rho_a} \right]$	$ds_v = epor*difl*cb0*psdfr/(1e3*rhop*molar_k*cb0**xn_v)$
$D_p = \frac{D_l}{\tau_p}$	$dp_v = (difl/(tortu))$

**Table 7 Model parameters of the PSDM model by USEPA: input, state and output parameters (Burkhardt, 2020)**

Parameter		Model name	Default	Unit	Type*
<b>Input parameters</b>					
<i>Compound properties</i>	Molecular weight (MW)	mw		g/mol	f
	Molar volume ( $V_b$ )	mol_vol		ml/mol	f
	Boiling point (BP)	temp		°C	f
	Density compound	\		g/ml	f
<i>Isotherm parameters</i>	Freundlich parameter ( $K$ )	k		[ $(\mu\text{g/g})(\text{L}/\mu\text{g})^{1/n}$ ]	f/v
	Freundlich exponent ( $1/n$ )	xn	0.45	(-)	f
<i>Bed properties</i>	Radius particle ( $r_p$ )	rad		cm	f
	Porosity particle ( $\varepsilon_p$ )	epor		(-)	f
	Pore to surface diffusion ratio (SPDFR)	psdfr		(-)	f
	Particle density ( $\rho_p$ )	rhop		g/ml	f
	Apparent particle density ( $\rho_a$ )	rhof		g/ml	f
	Length bed	L		cm	f
	Diameter bed	diam		cm	f
	Weight bed	wt		g	f
	Flow rate	flrt		μg/min	f
<i>Raw data</i>	Tortuosity particle ( $\tau_p$ )	tortu		(-)	f
	Influent concentration c(t)	infl		μg/L	f/v
<i>Numerical solver</i>	Effluent concentration c(t)	effl		μg/L	f/v
	Radial collocation points	nr	14	amount	f
	Axial collocation points	nz	19	amount	f
<b>State variables</b>					
<i>State variables</i>	Concentration (t,x)	c		μg/L	v
<b>Output parameters</b>					
<i>Calculated output</i>	Effluent concentration c(t)	c		μg/L	v
	Liquid diffusion coefficient ( $D_l$ )	difl		cm <sup>2</sup> /s	f
	Film mass transfer parameter ( $k_f$ )	kf_v		cm/s	f
	Surface diffusion coefficient ( $D_s$ )	ds_v		cm <sup>2</sup> /s	f
	Pore diffusion coefficient ( $D_p$ )	dp_v		cm <sup>2</sup> /s	f
	Viscosity of water ( $\mu_l$ )	vw		g/(cm*s)	f
	Density of water ( $\rho_l$ )	dw		g/cm <sup>3</sup>	f
	Bed porosity ( $\varepsilon_b$ )	ebed		(-)	f
	Empty bed contact time (EBCT)	ebct		(s)	f

\*Type of parameter: fixed (f) or variable (v)

## 4 MODELLING PFAS REMOVAL USING GAC

The performance of GAC can be evaluated using a modelling study and the results can support decision makers to choose it, as a favourable technology. Burkhardt et al., (2022) evaluated the adsorption of 16 PFAS compounds under different scenarios through modelling. The pore and surface diffusion model from USEPA (chapter 3) was therefore utilized. PFAS removal was applied at pilot scale so model parameters could be calibrated based on experimental data. A dataset with other conditions, i.e.

winter instead of summer, was created and used to validate the model. The Freundlich isotherm was applied with Freundlich parameters  $K$  and  $1/n$  (Burkhardt et al., 2022a).

One of the PFAS compounds considered here was PFHpA. Its adsorption onto F400 GAC was studied in a pilot column with raw water influent coming from the Cape Fear River, North Carolina, USA (Burkhardt et al., 2022a). Compound properties, bed properties and concentration values were derived from the article and listed in **Table 8**. Parameters that could not be derived from the article were taken from the 'TCE' example. This dataset was included, as an Excel sheet, in the GitHub repository of USEPA. Properties related to the GAC granules were not mentioned and thus assumed to be similar to the adsorption system TCE-F400.

The available dataset for the single solute PFHpA is interesting since it can be used to test the open-source model. All input parameters were fed to the PSDM model, which was done by filling in the input Excel sheet. As a first step in this thesis it was decided to test and replicate the model and check if the same breakthrough curve is obtained as in the PFAS article (**Figure 20**). The simulation results served as a starting point for further research. Model mechanisms were better understood after investigation of the Python script. In the following steps, small extensions were made to the model and a scenario analysis on the Freundlich parameters was performed.

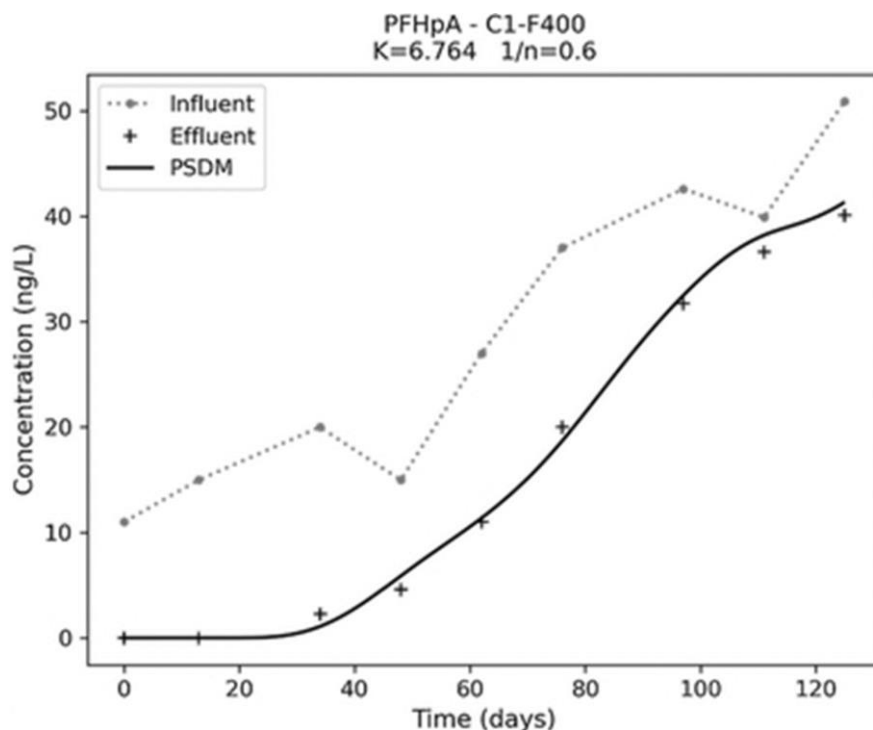


**Figure 20** Influent and effluent data of micropollutant PFHpA in pilot adsorption column.  
Solid line represents the PSDM model fit for the BTC (Burkhardt et al., 2022a)

**Table 8 Input parameters for modelling the adsorption of PFHpA and TCE (Burkhardt et al., 2022a)**

Parameter (Burkhardt, 2020)		PFHpA	TCE	Unit	
<i>Compound properties</i>	Molecular weight (MW)	364.06	131.39	g/mol	
	Molar volume ( $V_b$ )	203.158	102	ml/mol	
	Boiling point (BP)	175	87	°C	
	Density compound	1.792	1.53	g/ml	
<i>Isotherm parameters</i>	Freundlich parameter ( $K$ )	6.764	5026.04	[ $(\mu\text{g/g})(\text{L}/\mu\text{g})^{1/n}$ ]	
	Freundlich exponent ( $1/n$ )	0.6	0.43	(-)	
<i>Bed properties</i>	Radius particle ( $r_p$ )	0.0513	0.0513	cm	
	Porosity particle ( $\varepsilon_p$ )	0.641	0.641	(-)	
	Pore to surface diffusion ratio (SPDFR)	5	5	(-)	
	Particle density ( $\rho_p$ )	0.803	0.803	g/ml	
	Apparent particle density ( $\rho_a$ )	0.62	0.62	g/ml	
	Length bed	120	276.5	cm	
	Diameter bed	10	304.8 (10 ft)	cm	
	Weight bed	4349.95 (4.35 kg)	9e6 (20000 lb)	g	
	Flow rate	984.21	2146200	ml/min	
	Tortuosity particle ( $\tau_p$ )	1	1	(-)	
<i>Raw data</i>	Influent concentration c(t)	day0 13 34 48 62 76 97 111 125	0.011 0.015 0.02 0.015 0.027 0.037 0.0426 0.0399 0.0509	50 000	µg/L
	Effluent concentration c(t)	day0 13 34 48 62 76 97 111 125	0 0 0.0023 0.0046 0.011 0.02 0.0317 0.0366 0.0401	/	µg/L
<i>Numerical solver</i>	Radial collocation points	8	8	amount	
	Axial collocation points	11	12	amount	

## RESULTS AND DISCUSSION

### 5 TESTING THE PSDM BY USEPA MODEL

In this chapter, mechanisms of the PSDM model by USEPA, see **Chapter 3**, were tested and investigated in Python. For this purpose, example data from the GitHub repository itself or experimental data from the PFAS article (Burkhardt et al., 2022a) (**Chapter 0**), were used as input to feed the model. The implementation of the PSDM model into Python, that was used here, is open-source and available at: [https://github.com/USEPA/Water\\_Treatment\\_Models/tree/master/PSDM](https://github.com/USEPA/Water_Treatment_Models/tree/master/PSDM) (Burkhardt, 2020).

#### 5.1 Isotherm fitting tool

The PSDM by USEPA model (Burkhardt, 2020) includes a fitting tool for isotherm parameters in the '*Example\_isotherm.py*' script. An example dataset consists of datapoints for  $C_0$ ,  $C_e$  and carbon mass. This dataset is normally derived from a lab experiment with a beaker, single-solute polluted water and activated carbon. An initial concentration ( $C_0$ ) is added to a certain mass of carbon and after some time, equilibrium concentration ( $C_e$ ) is measured. If the mass of carbon was zero, then  $C_e = C_0$  because no adsorption took place. If a high mass of carbon was added to the batch experiment, the equilibrium concentration is typically low to zero because there was high adsorption capacity.

Based on the experimental dataset, the PSDM model automatically fits the desired isotherm. This is done by the *isotherm\_fit* function in *PSDM\_tools.py*. The function contains the isotherm equation of Freundlich, which is the default one, and makes use of the *curve\_fit* from *scipy.optimize* (SciPy -, n.d.) for finding the right fit onto the dataset. This is an isotherm equation with two equilibrium parameters and is important for the model to later calculate adsorbed concentrations at the surface of the GAC, which is assumed to be in equilibrium. Datapoints, best fit by the isotherm model and estimated isotherm parameters are shown in **Figure 21**.

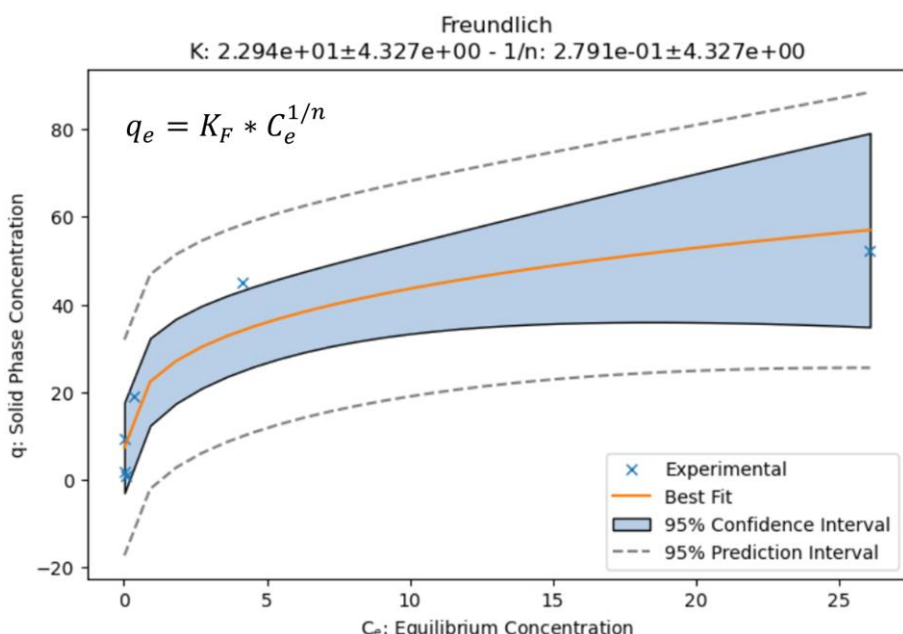
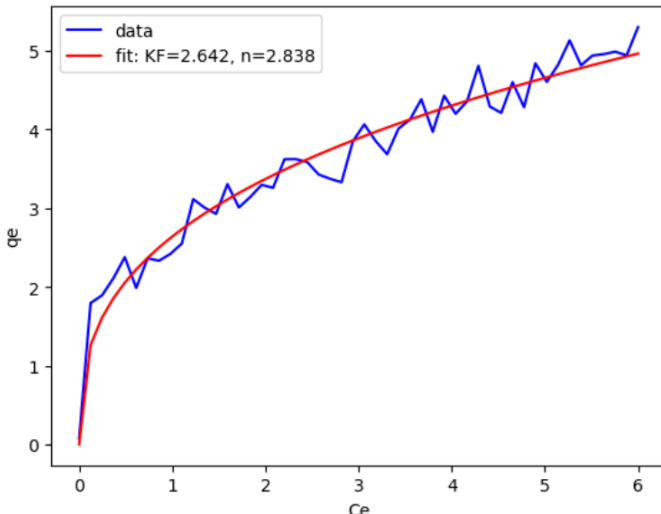


Figure 21 Isotherm fitting tool from USEPA (a) example dataset from batch equilibrium experiment  
(b) best fit Freundlich isotherm with equilibrium parameters K and 1/n

The `curve_fit` function from `scipy.optimize` was tested apart from the PSDM tools too, in a notebook that shares the name of this section. Its functioning was tested with a generated dataset which was formed based on a Freundlich isotherm ( $K_F=2.7$ ,  $n=3$ ) with some additional noise. The Python script was created with help of ChatGPT and the result can be seen in **Figure 22**. The estimated isotherm curve fitted well and Freundlich parameters were estimated in a similar way as in the `PSDM_tools.py` script.



**Figure 22** Isotherm fitting test with ‘`curve_fit`’ from ‘`scipy.optimize`’  
**(a)** Python script  
**(b)** Freundlich isotherm curve fit with estimated parameters

## 5.2 Example modelling of compound TCE

Executing the BTC model can be done from the notebook (`section_name.ipynb`). Example input data is found in `Example_TCE.xlsx`, where the input parameters from **Table 8 (TCE)** are classified under different sheets. The model estimates a breakthrough of 27 days after fresh or regenerated GAC was added. The BTC, estimated by the USEPA PSDM model, is shown in **Figure 23**. The prediction is not linked to any experimental data but is rather an example to show what the model output looks like.

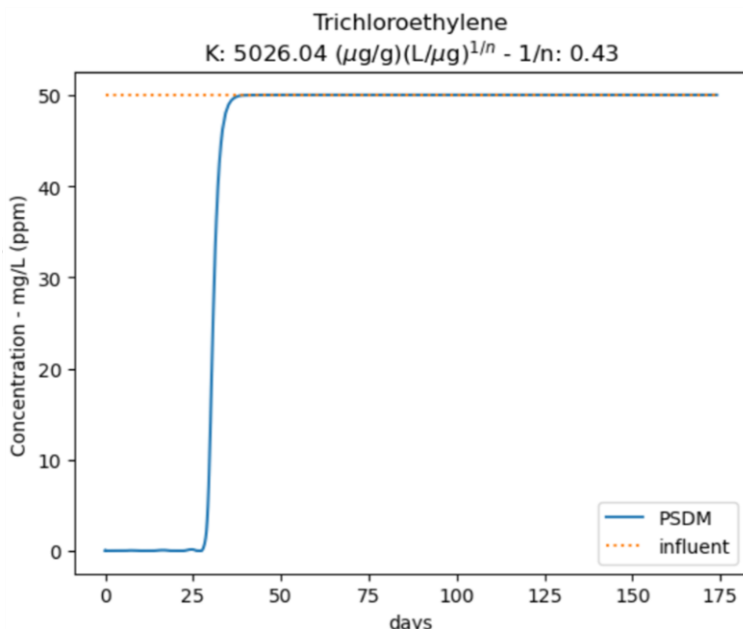


**Figure 23** Example breakthrough prediction for the compound TCE  
executed by the USEPA PSDM model (Burkhardt, 2020)

## 5.3 Pilot modelling of compound PFHpA

To test the PSDM model with a realistic case study, the PFAS pilot study (**Chapter 0**) was used. Input parameters from **Table 8 (PFHpA)** were inserted under the different sheets in *Input\_PFHpA.xlsx*. Fouling was also taken into account in the same way as in the research (Burkhardt et al., 2022a). Specifically, *chem\_type* was set to ‘PFAS’ and *water\_type* to ‘Rhine’. The USEPA fouling approach will be discussed in **section 5.4**.

### 5.3.1 Estimation of the breakthrough curve

**Figure 24** shows both the original model estimate (from the paper of Burkhardt et al., 2022) and the replicated model estimate (in this thesis) resulting from the USEPA Python code. To make the replication, the isotherm parameters K and 1/n, derived from the research, were given with the model input. On the contrary, the experimental effluent dataset was not given. The objective here was to get an estimate of the effluent curve. Parameters that were not given in the paper were taken from the previous ‘TCE’ example (**Table 8**), since also there the bed consists of F400 GAC. These were properties related to the GAC granules. The model parameters were not ‘calibrated’ and were rather derived from the reference study (Burkhardt et al., 2022a). However, this test demonstrated that the open-source model functioned very accurate and realistic, inspiring further investigation starting from this point of research.

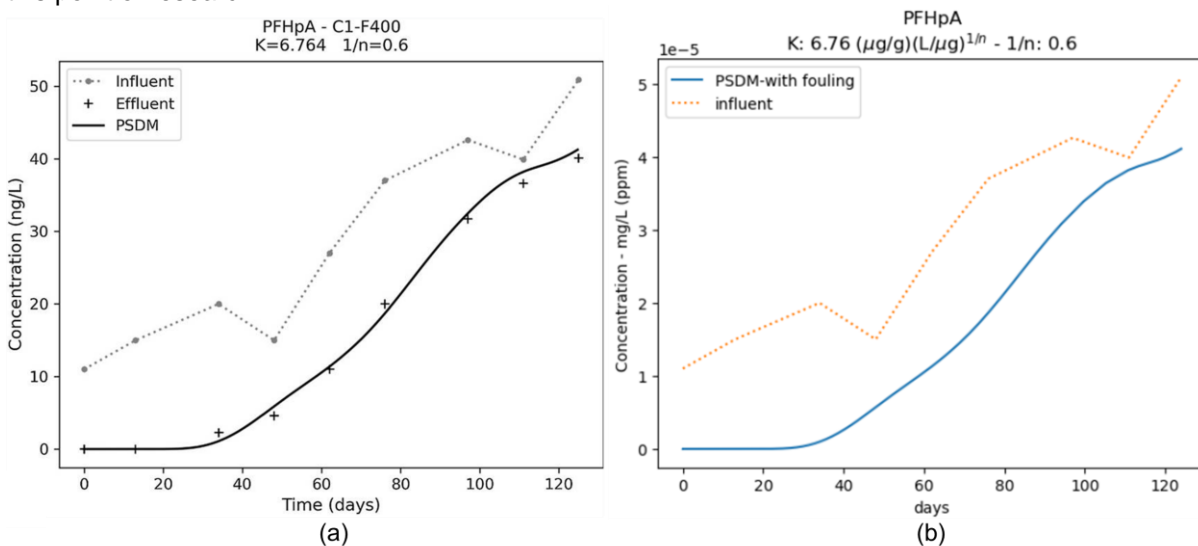


**Figure 24** Breakthrough curve model prediction for fixed-bed adsorption of PFHpA:  
(a) prediction from scientific paper of Burkhardt et al., (2022), (b) replication in Python

### 5.3.2 Estimation of isotherm parameters

Originally, the purpose of using the PSDM model in the case of **Figure 24(a)** was to estimate the Freundlich isotherm parameters K and 1/n through the automated fitting tool. To do so, experimental influent and effluent data was fed to the model. For this thesis, the same tool was also applied by hiding isotherm parameters K and 1/n and introducing the effluent experimental dataset. Estimation of the isotherm parameters by the automated fitting tool can be seen in **Figure 25**. It can be concluded that, next to the BTC estimation, estimation of equilibrium parameters was also functioning very well. The predicted isotherm parameters were close to the ones estimated by the original research paper. The red line is the best fit, which was found using the *run\_psdm\_kfit* function. It took 23 iterations to fit the model, which was known by defining a new parameter *psdm\_teller* that counted the number of runs.

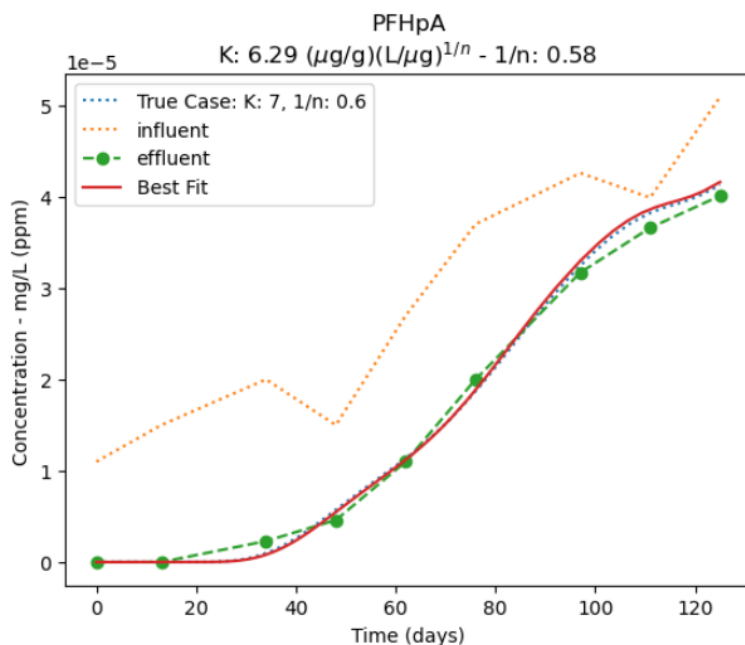


**Figure 25 Equilibrium parameters prediction by automated fitting tool of the PSDM model by USEPA.**  
(Burkhardt, 2020)

## 5.4 USEPA fouling approach

There are many problems that can cause a lower capacity of the carbon, from which the effects of NOM have been found to be the most important (Magnuson & Speth, 2005). Some examples are:

- Competition for adsorption sites from other contaminants
- Competition from background natural organic matter (NOM)
- Preloading of NOM onto AC
- Other: temperature, pH, low MP concentration leading to desorption...

The USEPA fouling approach is based in the study of Magnuson & Speth, 2005, where fouling is mathematically described with preloading by NOM. GAC capacity is reduced over time due to an increased preloading. Fresh carbon is initially organic-free, but its capacity reduces as more NOM accumulates. As mentioned in **section 2.3.1**, the Freundlich  $K_F$  is a constant for a given sorbate related to the sorption capacity. The idea of this fouling approach is to present a time dependent Freundlich  $K$  ( $K_t$ ), as this parameter represents the adsorption capacity. The reduction is empirically described in equation (25).  $K_t$  is divided by  $K_0$  that represents organic-free water and parameters  $rk1$ ,  $rk2$ ,  $rk3$  and  $rk4$  are calculated based on water- and compound-specific parameters (Magnuson & Speth, 2005).

$$\left(\frac{K_t}{K_0}\right)_{TCE} = 0.01 * [rk1 - rk2 * t + rk3 * \exp(-rk4 * t)] \quad (25)$$

This is empirically determined in a preloaded batch experiment for trichloroethylene at equilibrium and can be seen in **Figure 26**. Fouling is simplified by assuming that the Freundlich  $K$  diminishes over time. To find  $\left(\frac{K_t}{K_0}\right)$  for another solute, compound-specific correlation factors  $b1$  and  $b2$  are determined (Magnuson & Speth, 2005):

$$\left(\frac{K_t}{K_0}\right)_{contaminant} = b1\left(\frac{K_t}{K_0}\right)_{TCE} + b2 \quad (26)$$

Because it is time-consuming to determine parameters  $b1$  and  $b2$  for all compounds, it is assumed that the compound belongs to one of nine major groups (see later in **Figure 28**). This is simplification that makes the calculation more practical. Determination of compound-specific parameters ( $b1$  and  $b2$ ) is done by use of quantitative structure-property relationships (QSPRs), which are shown in equations (27) and (28).

$$b1 = -0.0624 \log K_{ow} - 1.15 \log \kappa_2 - 0.166 N_{am} + 1.37 \quad (27)$$

$$b2 = 0.0441\alpha + 0.406 D_{z(hybrid)} - 0.250 \quad (28)$$

Where fouling properties for the compound are (Burkhardt et al., 2022b; Magnuson & Speth, 2005):

- $K_{ow}$  = octanol-water partition coefficient
- $\kappa_2$  = second-order shape index
- $N_{am}$  = sum of number of primary and secondary amine groups
- $\alpha$  = molecular polarizability
- $D_{z(hybrid)}$  = largest hybrid component of the dipole moment perpendicular to the long molecular axis

Jarvie et al., (2005), reviewed how background organic matter (BOM) present in the water reduces the GAC capacity for SOCs. Reduction of the Freundlich capacity parameter  $K$  is illustrated both experimentally and modelled by use of equation (25) for the TCE compound (**Figure 26**).

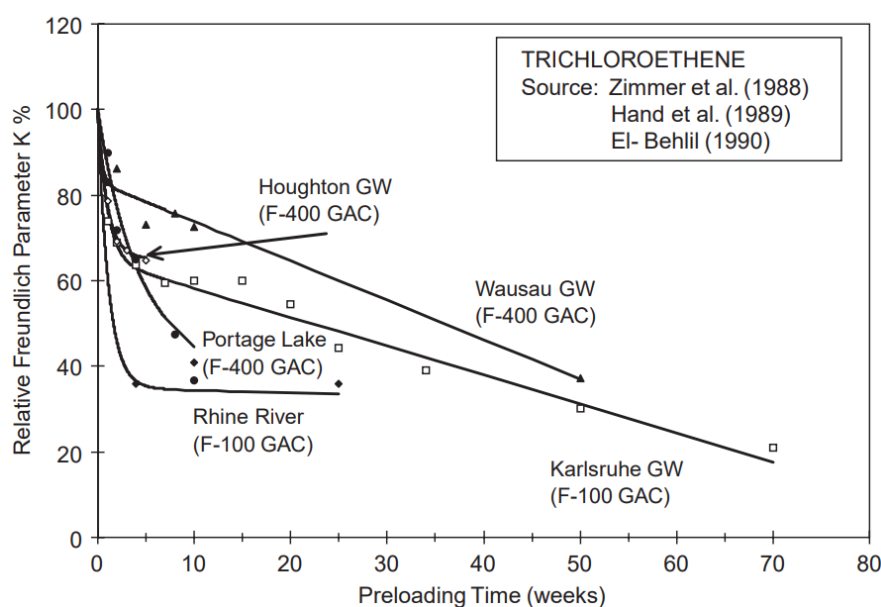


**Figure 26 Reduction of Freundlich K for TCE and for various background waters (Jarvie et al., 2005)**

In the PSDM by USEPA code, parameters  $rk1$ ,  $rk2$ ,  $rk3$  and  $rk4$  from equation (25) were calculated dependent on water-specific parameters  $a1$ ,  $a2$ ,  $a3$  and  $a4$  and compound-specific parameters  $b1$  and  $b2$ . The parameters  $a1$ ,  $a2$ ,  $a3$  and  $a4$  are empirically determined for different background waters. An empirical correlation can now be used to calculate the fraction  $(\frac{K_t}{K_0})_{contaminant}$ , which is defined as ' $k\_mult\_pd$ ' in the implemented code. This way, fouling can be simulated by reducing the Freundlich K parameter.

The fouling approach by USEPA was analysed by investigating the fouling parameter values during the pilot simulation of compound PFHpA (**section 5.3**). Printed fouling parameters are shown for organic-free water and NOM preloaded river water in **Table 9**. Model equations used to predict the time-dependent Freundlich K parameter are also shown.

**Table 9** USEPA fouling parameters and equations in Python for removal of PFHpA from ‘Rhine’ river water and organic-free water (Burkhardt, 2020). Fouling is simulated by reducing Freundlich K. All parameters are dimensionless

		Fouling (Rhine)	Organic-free	Equation
Water-type parameters	a1	0.35	1	
	a2	-6.15 e-8	0	
	a3	0.65	0	
	a4	-8.93 e-5	0	
Chemical-type parameters (PFHpA)	b1	0.44	1	
	b2	0.36	0	
Empirical parameters for K reduction	rk1	0.514	1	$b1 * a1 + b2$
	rk2	-2.706 e-8	0	$b1 * a2$
	rk3	0.286	0	$b1 * a3$
	rk4	-0.39 e-4	0	$b1 * a4$
Array with $(\frac{K_t}{K_0})_{PFHpA}$	k_mult_pd	[0.796, 0.739...]	[1,1,1...]	$rk1 + rk2*t + rk3*exp(rk4*t)$

**Figure 27(a)** indicated that influence of fouling was significant and it is important to consider this during adsorption simulations. First breakthrough occurred almost 60 days earlier when considering fouling (orange curve compared to the blue one). **Figure 27(b)** confirmed there is no Freundlich K reduction for organic-free water in the case of no fouling in the model and clearly displayed the declining orange curve. Reduced K ended up being more than half of the organic-free K. The function has a very similar shape as the ‘Rhine River’ function in **Figure 26**, where capacity reduction was fastest in the first weeks of the simulation. However, it was unclear what units the time axis of the obtained graph had, as it was not corresponding to 124 days of simulation. This issue was investigated in **section 6.1.2**.

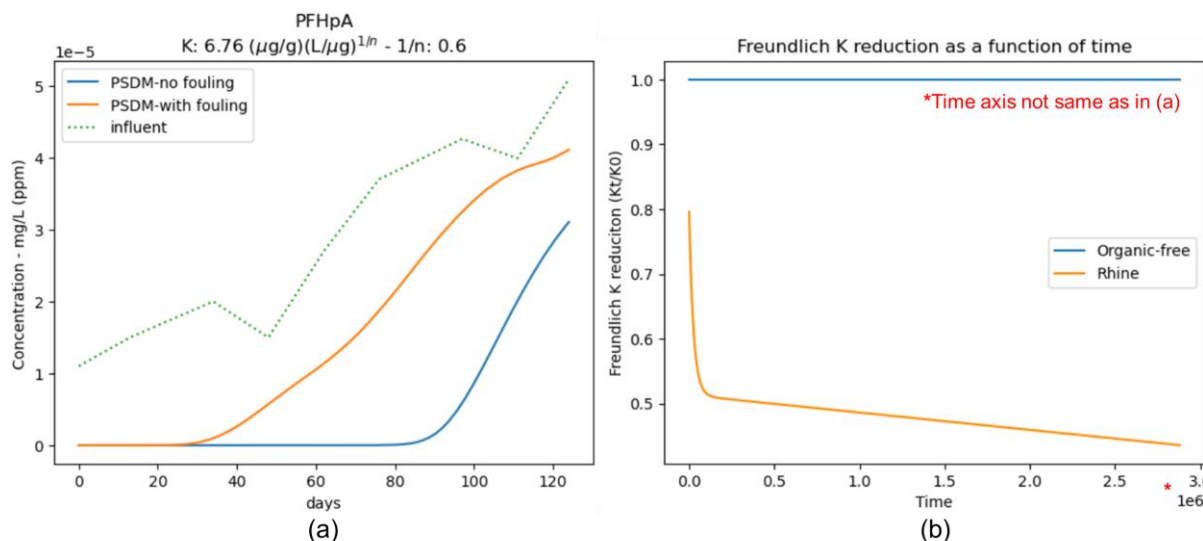


**Figure 27 Comparison of fouling vs no fouling for fixed-bed adsorption of PFHpA:**  
**(a) breakthrough curve model prediction, (b) Freundlich K reduction**

## **6 EXTENDING USEPA PSDM MODEL**

In this chapter, small extensions and alternatives were added to the PSMD by USEPA model (Burkhardt, 2020). Model input data used here were again derived from the PFAS paper for PFHpA (Burkhardt et al., 2022a) and from USEPA's GitHub for the TCE example (Burkhardt, 2020):

[https://github.com/USEPA/Water\\_Treatment\\_Models/tree/master/PSDM](https://github.com/USEPA/Water_Treatment_Models/tree/master/PSDM).

### **6.1 Extending the USEPA fouling approach**

#### **6.1.1 Implementing the QSPR fouling equations**

In the PSDM model of USEPA, equations (27) and (28) were not included in the code. They were calculated manually in advance and the values b1 and b2 were typed out for nine groups in the code, (**Figure 28**). Since the group of PFAS consisted of many examples, that is a time-consuming effort.

```
'chemical': {'halogenated alkenes': [1.0, 0.0], #default
    'trihalo-methanes': [1.0, 0.0],
    'aromatics': [0.9, 0.1],
    'nitro compounds': [0.75, 0.25],
    'chlorinated hydrocarbon': [0.59, 0.41],
    'phenols': [0.65, 0.35],
    'PNAAs': [0.32, 0.68],
    'pesticides': [0., 0.05],
    'PFAS': {'PFBA': [0.82, 0.12],
              'PPPeA': [0.67, 0.19],
              'PFHxA': [0.55, 0.28],
              'PFHpA': [0.44, 0.36],
              'PFOA': [0.34, 0.44],
              ...
    }
}
```

**Figure 28 Groups and subgroups of CECs with compound-specific parameters b1 and b2 that were manually inserted (Burkhardt, 2020). Yellow = for the compound PFHpA**

The aim of this section was to include equations (27) and (28) in the code, so b1 and b2 could be automatically calculated for any compound, based on new input of fouling parameters  $K_{ow}$ ,  $\chi_2$ ,  $N_{am}$ ,  $\alpha$  and  $D_{z(hybrid)}$ . This way, the compound did not have to be assigned values of a certain group manually in advance.

The 'compound properties' sheet in *Input\_PFHpA.xlsx* was extended with these compound-specific fouling properties. Then, the amount of equations in the model were extended by implementing the QSPR relationships, equations (27) and (28), that make use of these properties. The extra Excel data was processed through the *process\_input\_data* function and this way, the fouling parameters were introduced to the model. Parameters b1 and b2 were calculated for the respective compound, (**Figure 29**). These parameters were then used in the simulation to predict fouling with the same approach. Default values were still 1.0 and 0.0 for b1 and b2, respectively, and were used in the case of having *water\_type* as 'organic-free'. In such a case, it was important *k\_mult\_pd* remains 1 (see **Table 9**), so there is no Freundlich K reduction when free of NOM.

```

comp_data = process_input_data('7.1_Input_PFHpA.xlsx', sheet_name='Properties')

logKow = comp_data.loc['logKow']          # Fouling properties
κ2 = comp_data.loc['κ2']                  #
Nam = comp_data.loc['Nam']                #
alpha = comp_data.loc['α']                #
Dz_hybrid = comp_data.loc['Dz(hybrid)'] #

b1 = -0.0624 * logKow - 1.15 * np.log10(κ2) - 0.166 * Nam + 1.37
b2 = 0.0441 * alpha + 0.406 * Dz_hybrid - 0.25

```

**Figure 29 Python code for calculation of b1 and b2 through QSPRs**

Fouling properties of PFHpA were found in the supplemental information of Burkhardt et al., (2022b). The calculation resulted in 0.43565 and 0.360309 for b1 and b2, respectively. They were close to the values obtained by the reference paper (0.44 and 0.36) that were separately calculated, as in **Figure 28** (highlighted in yellow). As the compound-specific fouling parameters b1 and b2 remained almost the same, the BTC of PFHpA was also identical.

The compound-specific fouling parameters b1 and b2 were thus successfully and automatically calculated by the added QSPR equations, instead of manually calculating and inserting them for some groups. By this extension, new compounds did not have to be assigned a group but their fouling parameters  $K_{ow}$ ,  $\kappa_2$ ,  $N_{am}$ ,  $\alpha$ ,  $D_{z(hybrid)}$  could be inserted in Excel file for automatic calculation of b1 and b2. This gave the user more insights about the theory behind this underlying fouling approach. Also, it allows to include rapid calculations for new compounds without assuming it follows a certain class. This results in a better approximation of the K reduction by NOM for the specific pollutant. However, it is only worth the effort if fouling parameters are readily available and reliable.

### 6.1.2 Time axis adjustment of Freundlich K reduction graph

This section concerns the time axis of the K reduction graph in **Figure 27(b)**. The question arose whether this was corresponding to 124 days, as this is the length of the pilot experiment. After investigation of the code, it turned out the PSDM model calculates in seconds. The graph was made by plotting  $k\_mult\_pd$  for every second of the simulation. However, the simulation length is 2 880 000 seconds, which corresponds to 2000 days and this was the maximum amount of days possible in the PSDM model. The breakthrough curve (**Figure 27(a)**) was only plotted for 124 days because that was commanded from the input Excel file (*Input\_PFHpA.xlsx*). The aim was now to plot the K reduction graph for 124 days as well, so the time axis corresponds to the one of the breakthrough curve. The K reduction graph with right time axis can be seen in Appendix A (**Figure 42**). The original curve for 2000 days was not removed from this thesis as it also shows the linear part of the empirical equation (25).

### 6.1.3 Measuring K reduction: preloading Freundlich isotherms

This section relates to **Figure 26**, where the Freundlich K parameter was plotted as a function of preloading time, with experimental data and the model fit. It was unclear how the experimental data was obtained and this was further investigated by reading the references mentioned in the graph. These kind of experiments could potentially be useful when simulating GAC adsorption and this could lead to a more reliable representation of fouling.

The American Water Works Association did research on the influence of background organic matter (BOM) on GAC adsorption already in 1989 (Summers et al., 1989). The capacity of TCE was investigated, preloaded with organic matter. This was done both with a TCE-spiked GAC column and a preloaded GAC column without TCE spiking. The influent was *Rhine River* water. GAC was preloaded by accumulating NOM for a certain time. This was called the ‘preloading time’. Samples were taken from the unspiked preloaded GAC column at different preloading times (after 4, 10 and 25 weeks of preloading). These unspiked samples were then used to conduct a TCE isotherm. This way, the ‘preloading Freundlich isotherm’ was obtained for different durations of preloading. The set-up of the Hockenheim pilot plant can be seen in **Figure 30** (Summers et al., 1989).

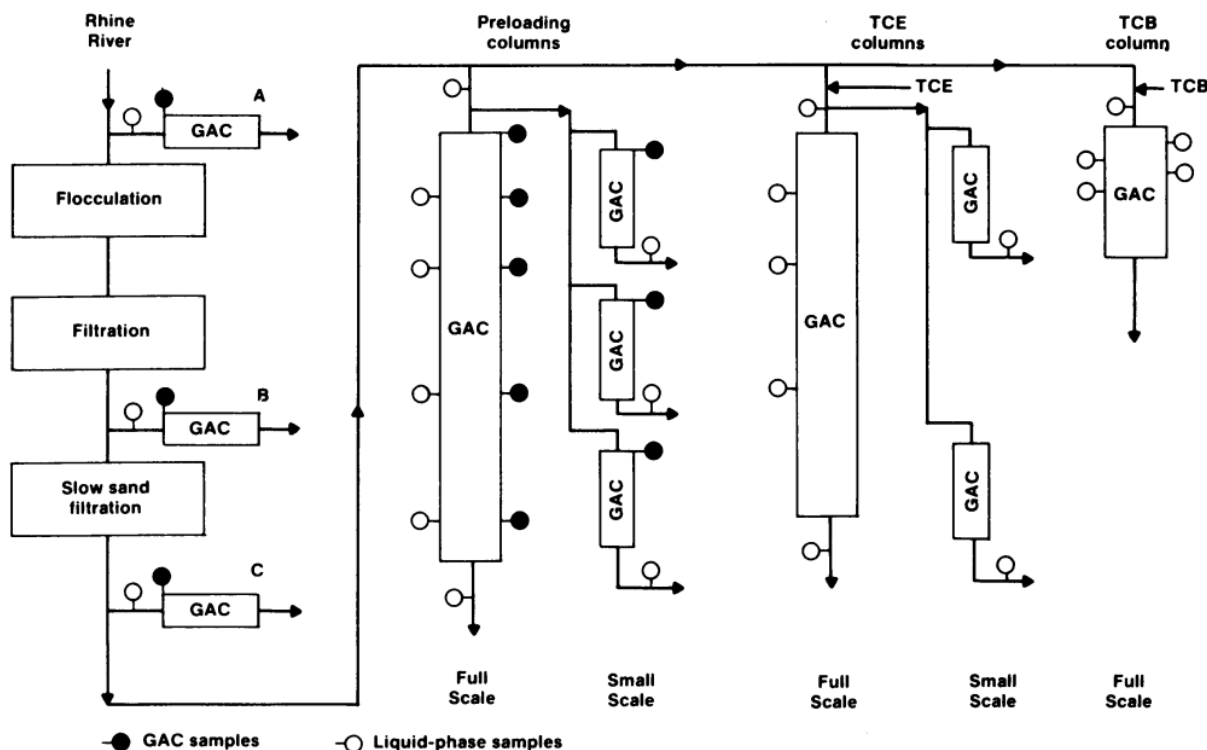


**Figure 30** Diagram of the Hockenheim pilot plant to study the impact of OM in the ‘Rhine River’ on GAC adsorption of TCE (Summers et al., 1989)

The resulting capacity of preloaded GAC for TCE of these unspiked samples, were very similar to capacities of TCE-spiked GAC columns. This way, it was concluded that preloading isotherms could be useful in better predicting GAC column adsorption (Summers et al., 1989). The three small-scale columns in the Hockenheim pilot plant were linked to the three ‘Rhine River’ datapoints in **Figure 32**, where the Freundlich K parameter was seen for 4, 10 and 25 weeks of preloading.

The derivation of the Freundlich K parameter from a Freundlich preloading isotherm can be seen in **Figure 31**. There, the TCE preloading isotherms shape in linear form (log-log scale) for different durations of preloading in Karlsruhe groundwater. In this scale, the y-intercept equals the Freundlich K, the slope of the isotherm equals  $1/n$ . The TCE equilibrium isotherm was plotted for various preloading times (in weeks). The data and the fit indicate that adsorption isotherms of TCE on preloaded GAC produce more or less parallel lines to the original single solute isotherm. Thus, a higher preloading time could be approximated by reducing the Freundlich K of the isotherm (Jarvie et al., 2005).

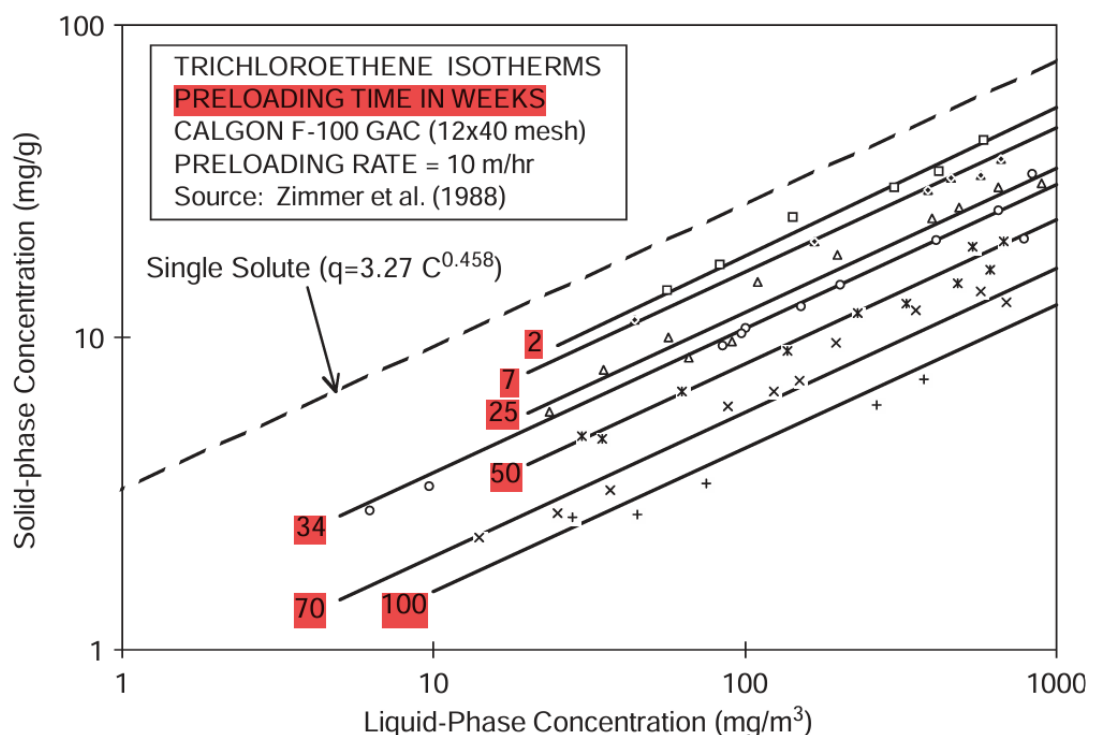


Figure 31 TCE equilibrium isotherms for various exposure times to Karlsruhe groundwater.  
Broken line is fresh GAC isotherm. Others are preloading isotherms, all linearized (Jarvie et al., 2005)

Reduction of the Freundlich K parameter over time seemed to be a good approximation for preloading isotherms of TCE. Now, the question is whether it is possible to feed the PSDM model with the K reduction function derived from experimental preloading isotherms. Instead of predicting the K reduction as a function of time, this information could also directly be derived from experiments (Figure 32) for the specific adsorption case.

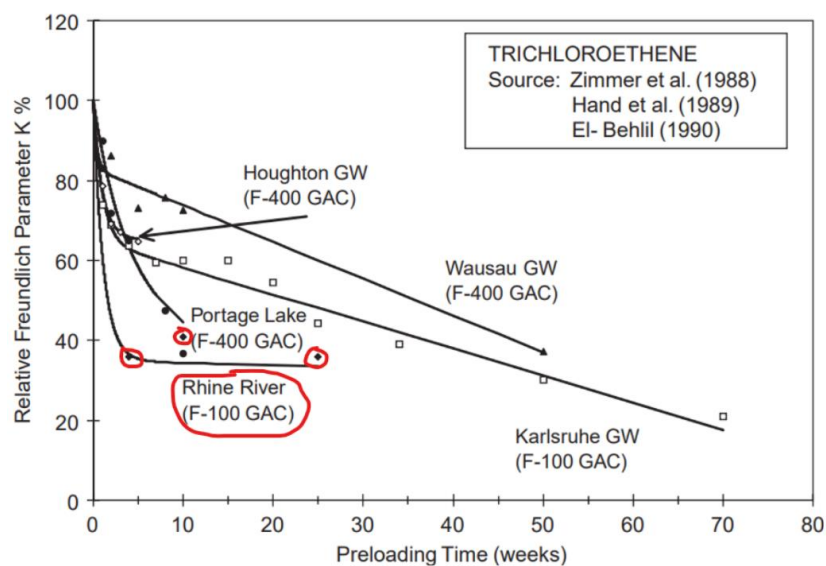


Figure 32 Reduction of Freundlich K for TCE and for various background waters (Jarvie et al., 2005)  
‘Rhine River’ data deviates from fit

## 6.1.4 Implementing a K fitting tool

In this section, a K fitting tool was implemented in the PSDM model. Instead of mathematically predicting the K reduction function a fit was made based on example data and the fitting parameters were fed to the model. In equation (29), the parameters rk1, rk2, rk3 and rk4 were no longer theoretically estimated, but were fitting parameters coming from the curve fit onto the K reduction datapoints.

$$\left(\frac{K_t}{K_0}\right)_{PFHpA} = rk1 + rk2 * t + rk3 * \exp(rk4 * t) \quad (29)$$

For the experimental K reduction curve, literature data was used, still from the PFHpA adsorption (Burkhardt et al., 2022a). There was no experimental data regarding Freundlich preloading isotherms and Freundlich K reductions. The mathematically predicted K reduction from the reference article was used for comparison. This way, it was checked if the K fitting tool worked properly and thus gave the same results as the original PFHpA simulation from the PFAS pilot plant (**Figure 27**). The fitted function had still the same values for parameters rk1, rk2, rk3 and rk4 as the ones predicted from the PFHpA simulation (**Table 9**). The function fitted onto the data is plotted in **Figure 33**.

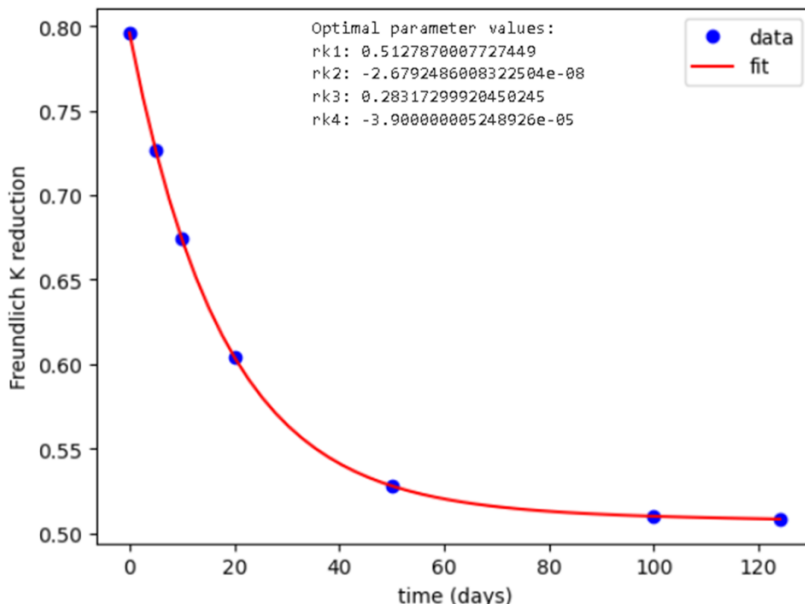


**Figure 33 K fitting tool where the K reduction function fits the data (demonstration).**  
Data derived from PFHpA pilot simulation for comparison (Burkhardt et al., 2022a)

This function was fed to the PSDM model (*psdm\_kft.py*). There, the parameters rk1, rk2, rk3 and rk4 from *k\_mult\_pd* (equation (29)) were replaced by the fitting parameters from the K fitting tool.

The result is a comparison of the original simulation, from the reference study, a simulation without fouling and a simulation where the K fitting tool was used (see Appendix A, **Figure 44**). From this, it was concluded that the K fitting function with parameters rk1, rk2, rk3 and rk4 was well implemented in the PSDM model, as the results were exactly the same as the reference article. This makes sense, because the parameters were made to be equivalent to the ones calculated by the article simulation. It was interesting to have a working fitting tool for K reduction as function of time, as this allows to introduce experimental data regarding the reduction of Freundlich K. Also, with this tool, some extra simulation tests could be conducted for further analysis.

### 6.1.5 Time-dependent vs constant Freundlich K reduction

A dataset with constant (reduced) K was given to the K fitting tool. This way, a comparison could be made between constant fouling and time-dependent fouling. The resulting graphs for breakthrough and K reduction can be seen in Appendix A, **Figure 45**. The breakthrough curves showed an unexpected behaviour. One would indeed expect that the gradually reduced K reduction from the article simulation gives better performance in the beginning, as there is less K reduction. However, after some time (when K reduction becomes almost equal as the constant reduced K), effluent concentrations are worse. When the bed is almost exhausted, effluent concentrations are suddenly higher for the article curve.

To make this a bit clearer, the same plots were made for a constant influent concentration of PFHpA (see Appendix A, **Figure 46**). There, the same behaviour was observed. Effluent concentrations were even higher than influent concentrations at a certain point. This *PSDM-article* (Burkhardt et al., 2022) curve was checked again for mistakes but seemed to be the true result when only changing the influent concentration to constant. Also, as the K fitting tool worked well for the original PFHpA simulation and only rk1, rk2, rk3 and rk4 were replaced by the fitting parameters, there seemed to be no reason the K fitting tool had false predictions at this point.

An explanation for this could be the following. Having a time-dependent Freundlich K reduction, means that K is reducing over time and does not have a constant reduced K from the beginning. Mainly in the beginning, K reduces and this means that the Freundlich isotherm is moving lower. Thus, adsorption capacity is lower. There can be less compound adsorbed and stored in the GAC. Because capacity is lower than previously, some of the adsorbed compounds cannot be stored anymore in the solid phase and following the mass balance, they need to be somewhere back in the liquid phase. This idea results in the fact that these compounds end up in the liquid when K is reducing, and together with the influent concentration, this leads to even higher solute effluent concentrations than in the influent.

It is important to investigate further the difference between time-dependent and constant Freundlich K reduction and the question might rise if the assumption of reduced Freundlich K is accurate enough to simulate fouling in reality.

### 6.1.6 Optimizing the K reduction curve

The advantage of the K fitting tool, next to using experimental data, is that any function can be used for the fitting curve. If K reduction data has a different shape, the empirical equation (equation (29)) or its parameters can be adjusted to optimize the fit. In **Figure 32**, it can be seen that the model does not always fit with the experimental data. There is a sudden increase that is not picked up by the model. In this section, the K fitting curve is optimized so it includes the sudden increase, when necessary. This means that the PFHpA simulation lasted only 17 weeks (124 days/7) and thus not covers the whole ‘Rhine River’ function form **Figure 32**. Data was artificially invented so there was a sudden increase in K in the end. The K fitting tool worked well and did include the increase in the end (see Appendix A, **Figure 47**).

The simulation can again be compared with the reference article simulation for PFHpA in Appendix A (**Figure 48**). There, the breakthrough curve decreased from the moment that  $K/K_0$  starts to increase, relative to the original article simulation. This makes sense, as an increased  $K/K_0$  means that there is less fouling and thus better adsorption. The same was done but with constant influent concentration of PFHpA (see Appendix A, **Figure 49**) and this resulted in similar conclusions.

### 6.1.7 Sudden increase of the K reduction curve

In this section, it is investigated where the sudden increase in the experimental data from **Figure 32** came from. There are several references mentioned in that graph. Without having access to all of them, another graph was found (**Figure 34**) that seemed to give more clarity about the phenomenon (Summers et al., 1989). The figure explains reduction in adsorption capacity, but here 0 (not 1) is equal to no capacity reduction, so the graphs is inverted compared to **Figure 32**. The curves in the graph are different for samples taken at different depths in the GAC bed. A temporary decrease can be observed after 10 weeks in the curve derived from the sample taken at 0.28 m column depth (orange circle).

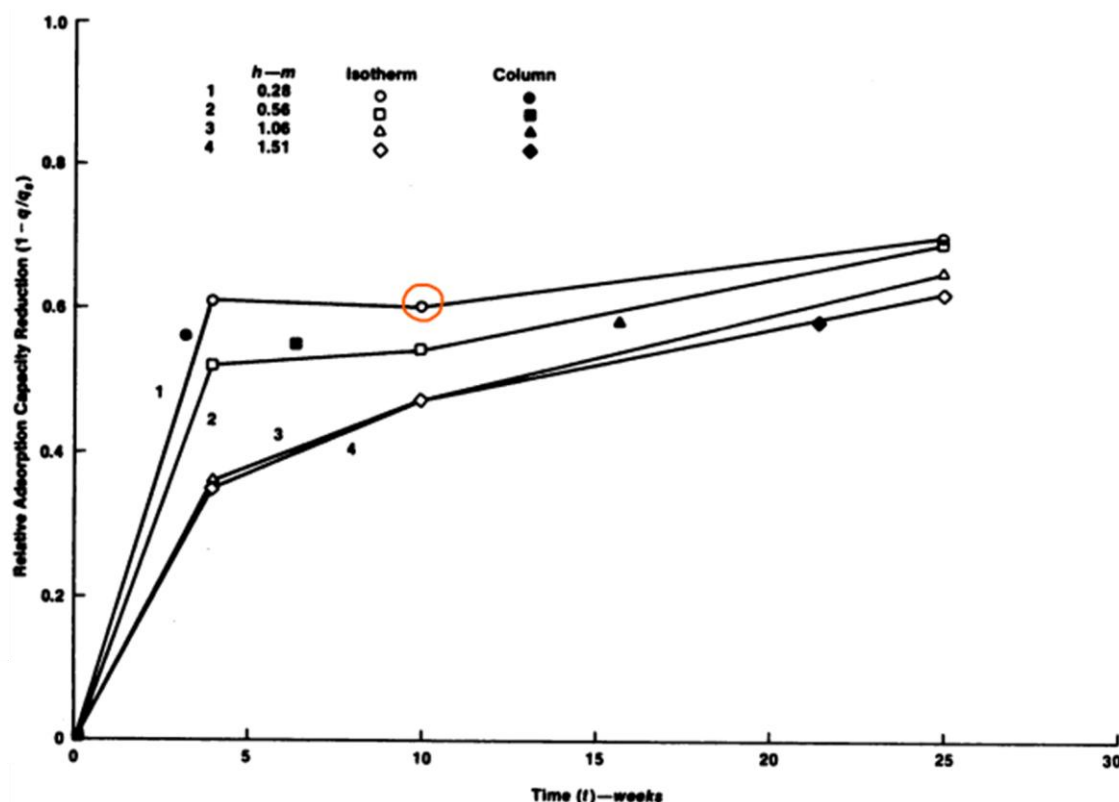


**Figure 34** Relative adsorption capacity reduction for TCE as a function of preloading time., calculated at different bed depths (Summers et al., 1989)

From this information, it can be derived that fouling does not occur uniformly over the column depth. The influence of fouling increases with decreasing column depth. This correlation may be explained by the fact that NOM is more retained at the top of the column, where the influent comes in, than at the bottom. This way, organic matter is not equally distributed over the column. The fact that there is a sudden improvement in adsorption capacity (or improvement in Freundlich K in **Figure 32**), may be explained by the following statement. NOM could first accumulate at the top of the column, but after some time, the organic matter might better distribute over the column depth. The flow brings the OM downwards and therefore, the amount of OM at the top could reduce a little bit, leading to less fouling there. However, this explanation might be incorrect as this is an assumption based upon this one graph (**Figure 34**). The article itself (Summers et al., 1989) does not comment on this phenomenon. In the PSDM model, fouling is assumed to be uniform over the column depth. Thus, a question might come up if this uniform K reduction approach is representative for fouling. A depth-dependent approach might be more accurate but also more complex. Also, measuring preloading isotherms as a function of depth requires more effort again. However, it might be worth the effort for further research.

## 6.1.8 Conclusions K reduction curve and K fitting tool

Preloading isotherms showed why reduction in the Freundlich K parameter can be a good approximation for representing fouling in the PSDM model. A K reduction curve was already implemented. However, the reduction was calculated based upon QSPPR equations and empirical equations for certain groups of compounds and background water types. Preloading isotherms can experimentally be determined for a specific adsorption case and data for the reduction of Freundlich K over time can be fed to the model. As data is getting more important in the water treatment sector, the measurement of preloading isotherms could be highly recommended considering the importance of fouling in GAC adsorption. The K fitting tool was successfully implemented and returned automatically the results for breakthrough. This way, it was demonstrated how the simulation could be more accurate with extra experimental data for specific cases. However, measuring preloading isotherms can be very time-consuming and complicated.

The K fitting tool allowed to have more control over the influence of NOM preloading in the model. Also, as the curve could take any shape, there could be experimented with fouling. This way, the difference between a time-dependent and constant fouling approach, but also the complexity related to it, was clear. This difference indicated that a dynamic fouling approach might be worth including. It was also demonstrated how the function parameters could change so it fits better to example data. The K fitting tool could help fine-tune fouling behaviour in the model in practice. For example, an increase in the K reduction curve was successfully included in the model. Finally, it was investigated where this increase came from. Although it is uncertain, it might be due to the movement of NOM through the column. This raises the question of whether a depth-dependent fouling approach could be relevant as a future research area.

It is not very straightforward if the current USEPA fouling approach is a good approximation of reality. During investigation, some thoughts came up. For example, if K is decreasing, previously adsorbed solutes might need to desorb according to the mass balance and decreasing capacity, leading to effluent concentrations that were temporarily higher than influent concentrations. Also, it was seen that fouling depended on column-depth. NOM accumulates first at the top of the fresh carbon bed and only after weeks of adsorption gets better distributed. However, the current fouling approach assumes that fouling occurs uniform over column-depth and that NOM distributes equally.

## 6.2 Alternative fouling approach

The fouling approach applied in the PSDM by USEPA model was based upon the reduction of the Freundlich capacity parameter K. This is a good approach, as it is based on experimental equations, but also needs time and effort. The parameters used in the fouling equations have some uncertainty and are now only available for certain (groups of) compounds.

An alternative fouling approach in this thesis was adopted by reducing the carbon bed weight instead of the Freundlich parameter. In fact, NOM preloading reduces the amount of carbon available for OMPs to adsorb onto. It is thus a simpler idea to reduce the carbon weight by adjusting one parameter.

Equation (30) was added to *psdm.py* in the initialization function of the *PSDM* class, so an additional parameter *Reduced bed weight* could be calculated.

$$\text{Reduced bed weight} = \text{original bed weight} * (1 - \left(\frac{\alpha}{100}\right)) \quad (30)$$

**Figure 35** shows example input data implemented in the model code for BTC prediction with fouling calculation. The number, e.g. 15, was extracted from the string input and defined as  $\alpha$  in the equation (30). The *run\_psdm\_kfit* function was executed for different *columns* including a column considering no fouling, a column using the original fouling approach and a column using the alternative fouling approach (presented in this section). For all of them, the example of PFHpA from the PFAS pilot study (Burkhardt et al., 2022a) was used. Furthermore, the code was added to the *Notebook* to automatically display a graph showing the BTC and a graph showing the Freundlich K parameter as function of time for each of the columns (**Figure 36**).

```
chem_type1 = 'PFAS'  
water_type1 = 'Rhine'  
  
chem_type2 = 'Fouling alternative (15%)'  
water_type2 = 'Fouling alternative (15%)'
```

**Figure 35** Input required for original and alternative fouling calculation

It can be seen from **Figure 36(a)** that the alternative fouling method, by carbon weight reduction, indeed moved the BTC towards the left. Thus, breakthrough occurred earlier as less carbon was available due to NOM preloading. However, 15% weight reduction seemed to be insufficient to fit the '*fouling (Rhine)*' curve, which perfectly fitted experimental data (**Figure 24**).

**Figure 36(b)** clearly confirms that there was no Freundlich K reduction for the *No fouling* or *Fouling alternative* curves. This is a check to be sure that the alternative fouling method was purely based on carbon mass reduction. As this reduction was not sufficient, parameter  $\alpha$  was calibrated onto experimental effluent data, which was earlier well-fitted by the '*fouling (Rhine)*' curve. The result is shown in **Figure 37**.

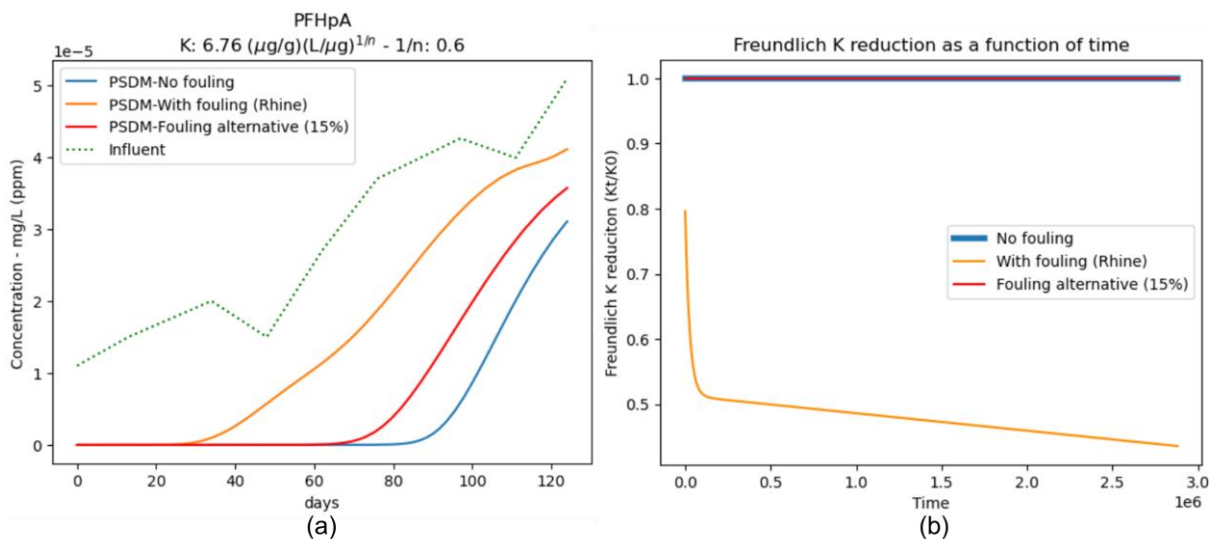


**Figure 36 Comparison of original fouling (K reduction), alternative fouling (15% carbon weight reduction) and no fouling for fixed-bed adsorption of PFHpA: (a) breakthrough curve model prediction, (b) Freundlich K reduction**

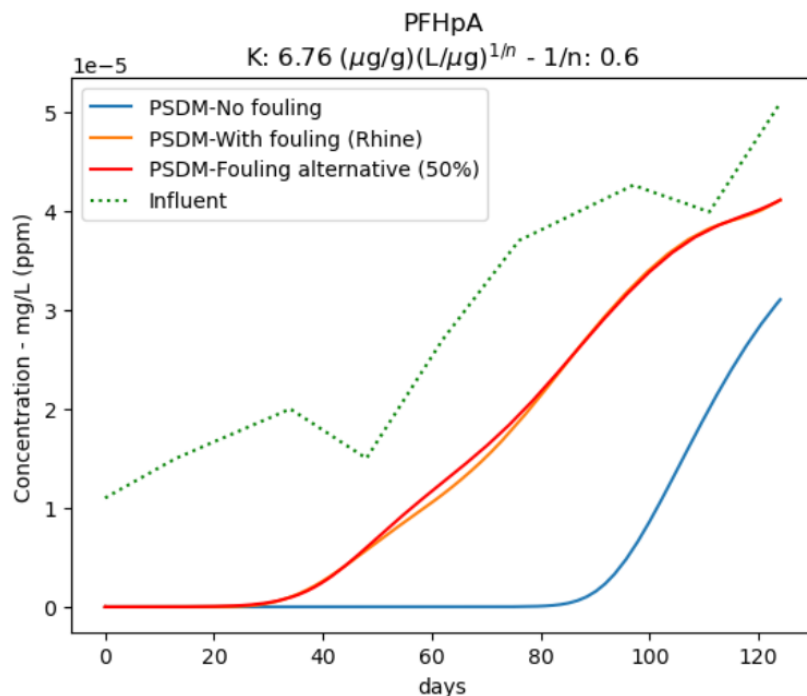


**Figure 37 BTC model predictions for various fouling approaches; No fouling, K-reduction (t) and carbon weight reduction (50%)**

It can be seen that reducing the amount of carbon with 50% resulted in a good fit. This leads to the conclusion that the impact of NOM on PFHpA adsorption from raw river water (Burkhardt et al., 2022b) was high and approximately halved the amount of carbon available for adsorption. A carbon weight reduction of 70% was also tested and can be seen in **Figure 38**. It was confirmed that with that much weight reduction, breakthrough occurred much faster.

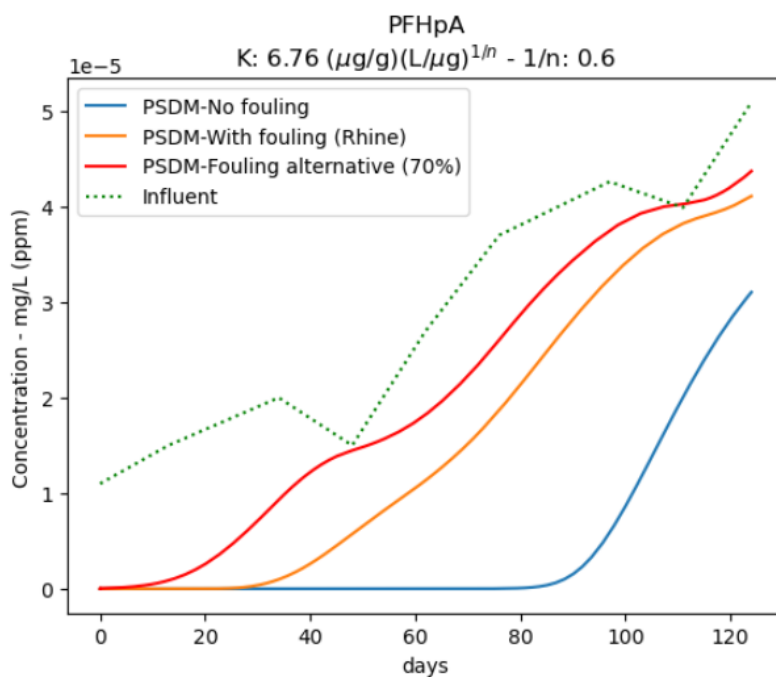


**Figure 38 BTC model predictions for various fouling approaches; No fouling, K-reduction ( $t$ ) and carbon weight reduction (70%)**

Advantages of the alternative method are that the number of fouling parameters is reduced and the approach is simplified. Disadvantages are that it is less theoretically grounded and capacity reduction by NOM is hard to estimate in terms of carbon weight. It also must be noted that the alternative fouling approach presented here was not time-dependent. The carbon bed weight initially was fixed to a lower value and kept constant during the simulation. This should make no significant impact in this study for predicting the effluent concentrations considering the fast time frame for the K reduction in the original fouling approach comparing to the time of simulation.

Finally, a comparison is made with the K fitting tool included, where Freundlich K was also fixed. The fixed, reduced K was chosen to have the same reduction as the weight reduction to make comparison possible. The BTCs can be compared in Appendix A, **Figure 50**. Relative to the organic-free curve, the fouling approaches gave more or less the same prediction with breakthrough after approximately 20 days. However, although the same constant reduction was applied for K as for carbon weight from the beginning, the BTCs were not identical. The reduced K predicted the first breakthrough a bit earlier than the approach with the weight reduction. The K reduction column does have its full volume, but the capacity is halved. The slope of the weight reduction curve was a bit steeper. This column, with only half of the volume, is faster exhausted once fewer carbon is occupied. It can be concluded that both fouling approaches have different effects, although having the same reduction factor.

In reality NOM does not distribute perfectly over the column; some places will be more affected than other places. The accumulation increases over time, but not uniformly over the column. Some carbon will remain fresh for a longer period, by which the local equilibrium occurs organic-free. Other places will be strongly preloaded so almost no adsorption is possible, the pores are blocked and the inner particle is not available. Other places will be partly preloaded. When the solute stream reaches equilibrium at the surface, there is less uptake because of the lowered capacity. Moreover, NOM can compete with the solutes for the adsorption sites in a mixed influent, or maybe can even make the previously adsorbed solutes desorb. It is important to remember that the above fouling approaches are strong simplifications of the complex reality and that they have a different effect on the model outcome.

## 6.3 Scenario analysis on the Freundlich parameters

In this section, it is explained how the PSDM model by USEPA was extended with an automatically returned visualization of some deviation of Freundlich parameters K and 1/n.

Data of compound PFHpA was again used as input for the model, the influent concentration was assumed constant for simplification. A deviation (%) for parameters K and 1/n were included under *percent\_K* and *percent\_xn*, respectively. Copies were made of the isotherm data object ‘*k\_data*’ and the deviated isotherm parameters were stored there. These copies were assigned to different columns. The *run\_psdm\_kfit* function was executed for these columns, each having its own isotherm data. First the original BTC was plotted, then the BTCs with deviated isotherm parameters were added to the same graph. The BTCs, with deviation of isotherm parameters, are demonstrated for the compounds TCE and PFHpA in **Figure 39** and **Figure 40**, respectively. The amount (%) of deviation for parameters K and 1/n can be modified, causing the graph to adjust automatically. The uncertainty here (10%) was just a simple demonstration to show the impact of a change in the parameters as the exact uncertainty of the isotherm parameters was not known.

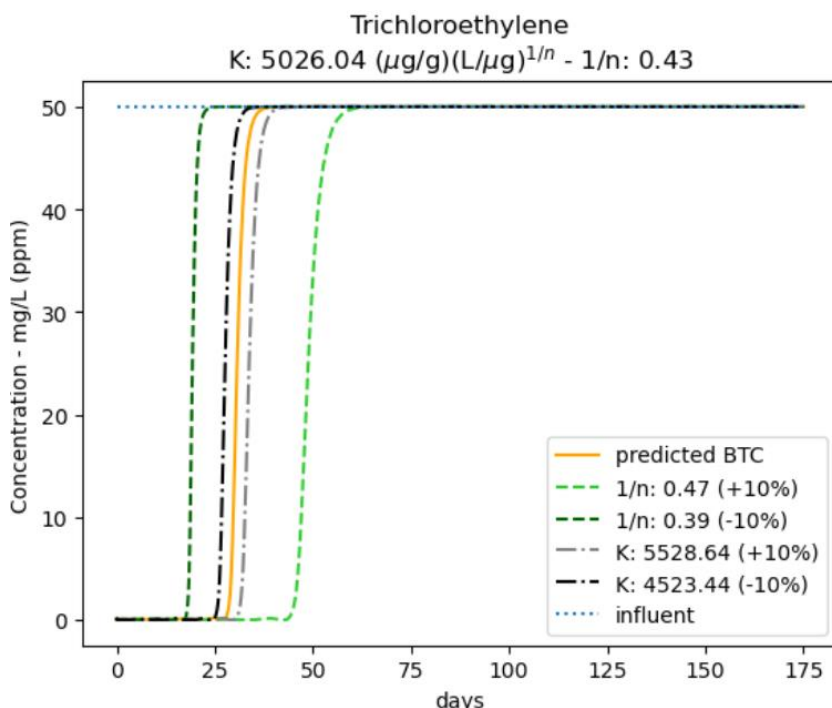


**Figure 39** BTC prediction and uncertainty analysis with isotherm parameter uncertainty of 10%. Compound = TCE

Uncertainty of the isotherm parameters seems to play a significant role in prediction of bed replacement intervals. Only 10% difference for the Freundlich 1/n parameter can result in more than 40% difference in breakthrough time. Considering the Freundlich isotherm relationship (equation (1)), it seems logical that higher values for isotherm parameters result in higher times before regeneration is needed. Specifically, equilibrium adsorption capacity increases along with the equilibrium parameters.

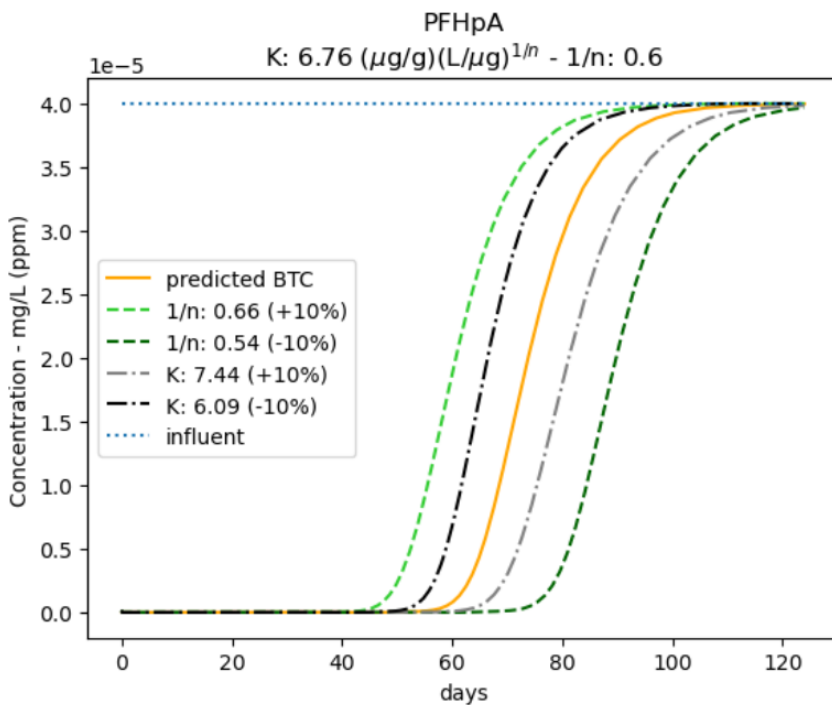


**Figure 40 BTC prediction and uncertainty analysis with isotherm parameter uncertainty of 10%. Compound = PFHpA**

For the compound PFHpA however (**Figure 40**), a counterintuitive behaviour for the parameter  $1/n$  could be observed. Increasing the parameter  $1/n$  did not lead to an increased adsorption capacity and thus increased breakthrough time, as was observed for TCE. Instead, the opposite occurs. This phenomenon was further investigated by plotting the Freundlich isotherm equations for both compounds, including 10% deviations. The script was also written so the isotherms were displayed automatically according to the amount of uncertainty.

**Figure 41** again represents the equation of the Freundlich isotherm and so one could expect that the equilibrium adsorption capacity  $q_e$  would increase with increasing equilibrium parameters. This however was not always the case. The difference could be explained by the equilibrium concentration  $C_e$ . Concentration is  $> 1$  in **Figure 41(a)** and  $< 1$  in **Figure 41(b)**. Because  $C_e$  is smaller than 1, increasing the exponent means decreasing the whole factor. This is why changing  $1/n$  had an opposite effect for the case of PFHpA.

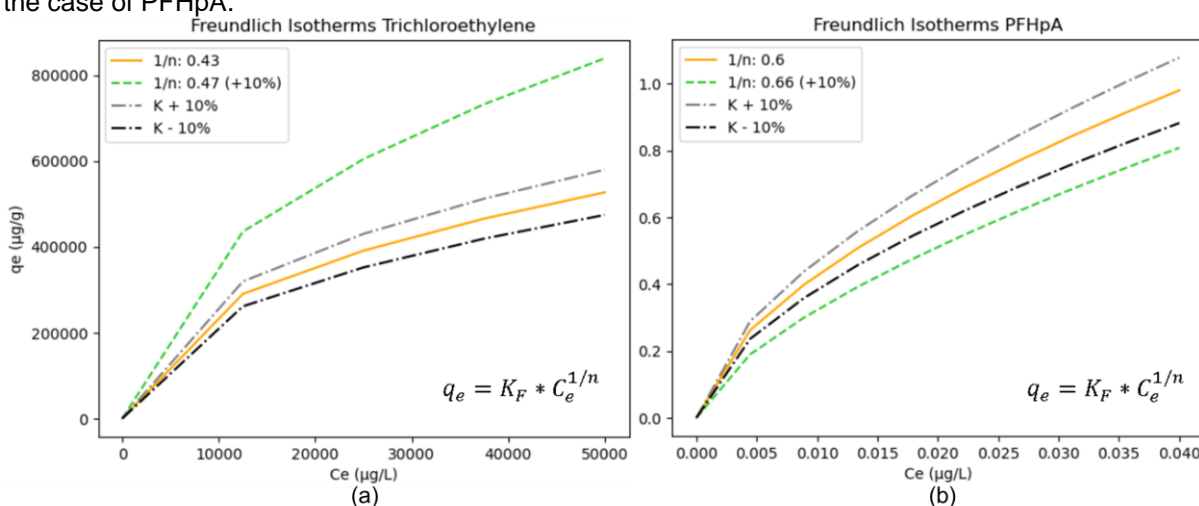


**Figure 41** Freundlich isotherm equations with parameter uncertainty for compounds (a) TCE & (b) PFHpA

## CONCLUSION AND PERSPECTIVES

The high diversity of organic micropollutants (from medicines, cosmetic products, etc.) present in our wastewater is of increasing concern. They appear in small concentrations but pose high risks to humans and the environment, as the planetary boundary for novel entities has been exceeded. It is clear that advanced treatment is needed as conventional wastewater treatment plants are not effective enough for removing these compounds. Several groups of treatment exist, from which adsorption features high efficiencies at relatively low costs. Adsorption comes with a wide range of options regarding adsorbents and set-ups. This thesis focussed on adsorption of the compounds TCE and PFHpA onto a fixed-bed column with granular activated carbon, without considering the biofilm growth.

The adsorption process of a single micropollutant in a fixed-bed granular activated carbon column is very complex. First, the solute transfers through the liquid undergoing convection and molecular diffusion. Then, it reaches the external film around one particle. In this boundary layer, external film diffusion occurs. If not adsorbed onto the external surface, the solute can go inside the particle, where intraparticle diffusion plays its role. This consists of the so-called pore and surface diffusion. Close to the surface, there is the local equilibrium between the liquid-phase concentration and solid-phase concentration, also called adsorption capacity. This is mathematically described by an isotherm and gives information about how much of the solute can be adsorbed. The adsorption-desorption reaction itself (onto the active site) can be of chemical or physical nature. It is important to include these theoretical mechanisms, especially when they are rate-limiting, in the model.

A fixed-bed breakthrough curve model consists of three components including the differential mass balance equation, the differential uptake rate equation(s) describing adsorption kinetics, and the isotherm equation describing equilibrium. Different isotherm equations can be used from literature. Also, several fixed-bed breakthrough curve models were discussed. The pore and surface diffusion model (PSDM) is a strong candidate for simulating adsorption in wastewater treatment plants. For porous materials like GAC, the adsorption of micropollutants is typically rate-limited by intraparticle diffusion. The PSDM is a versatile multi-phase model taking into account liquid diffusion, external film diffusion, intraparticle pore and surface diffusion and an equilibrium isotherm. However, the adsorption reaction is assumed to be instantaneous. Although this complex model still has strong assumptions, it is better suited than the other described (popular) models in this thesis, some of which lack physical significance and are more suitable as descriptive tools rather than predictive ones.

The PSDM by USEPA model was investigated and tested. First, the working of the USEPA isotherm fitting tool was investigated and then successfully replicated independently. The USEPA PSDM model was tested with a realistic case study from USEPA research (Burkhardt et al., 2022). There, adsorption of PFASs like PFHpA was tested in a pilot facility and simulated with this model. Input parameters were derived from that article text. The replicated breakthrough curve of the compound PFHpA was identical to the original study. The model features were demonstrated and this served as a good starting point for further research in this thesis. The USEPA fouling approach used in the pilot study was investigated by returning extra model parameters. The model was extended by implementing QSPR equations that were otherwise calculated independently, only for certain groups. This allowed for automatic and exact calculation of fouling parameters for new compounds instead of assuming they follow a certain group of compounds. Because the input sheet with compound properties was extended, this gave the user more control and insights about the theory behind the underlying fouling approach.

The USEPA fouling approach assumed a reduction of the Freundlich K parameter. This was based upon scientific experiments with preloading isotherms, where K seemed to reduce over time, and this reduction was mathematically predicted with empirical fouling equations. However, in previous research the fouling model did not fit the experimental data very accurately. A versatile K fitting tool was developed so the K reduction curve was better described. It was demonstrated how the reduction of K could be optimized according to case-specific experiments, i.e. preloading isotherms. The tool was successfully implemented in the USEPA PSDM model for automatic calculation of the results. This allowed to have more control and study better the influence of this fouling approach on the breakthrough curve. The difference between a time-dependent and constant fouling approach became clear. A dynamic fouling approach was indeed worth investigating. With the reduction of K, it could be seen that it led to desorption and thus resulted in an effluent concentration higher than the influent concentration. Also, it was seen that the USEPA fouling approach assumed uniform fouling over column-depth. However, from research, it was clear that preloading isotherms vary depending on the depth of the sample in the column and thus K reduces not uniformly in that regard. This was explained by the fact that organic matter initially accumulates more at the top of a fresh carbon bed. These observations revealed some weaknesses of the USEPA fouling approach.

An alternative fouling approach was implemented in the PSDM model by applying a desired weight reduction for the carbon bed. This allows for simulation of the carbon that is not available for MP adsorption due to complete preloading or pore blocking by NOM. For the pilot study case of PFHpA, it was concluded that the impact of fouling was high and approximately halved the amount of carbon available for adsorption. An advantage of this approach is that fewer fouling parameters are needed to calibrate. Disadvantages are that it is more simplified and capacity reduction by organic matter might be hard to estimate in terms of carbon weight. Also, this approach is not time-dependent.

A comparison was made between both fouling approaches with a constant reduced Freundlich K and carbon weight. Relative to the organic-free prediction for PFHpA, the fouling approaches more or less showed the same result. However, although the same fixed reduction was applied for K as for carbon weight from the beginning, the BTCs were not identical. The weight approach resulted in a steeper curve. The main conclusion was that both fouling approaches are strong simplifications of the complex reality regarding fouling and that they have a different effect on the model outcome.

Finally, a scenario analysis on the equilibrium Freundlich parameters K and 1/n was briefly discussed. The model was extended so a certain deviation could be inserted for both parameters and this lead to an automatic visualization of the influenced breakthrough curves. A counterintuitive behaviour of the parameter 1/n was observed for compounds TCE and PFHpA. This was due to the concentration value in micrograms per litre, which was significantly different for both compounds. This part was concluded with the fact that uncertainty in the Freundlich parameters has significant effect on the model outcome and it is therefore important to carefully determine these from batch equilibrium experiments.

Further research can regard the inclusion of biofilm growth onto the activated carbon granules. Also, a mixture of micropollutants can lead to competition with other compounds and it can be investigated whether single-solute isotherms still perform well in this case. The fouling approach can be improved since the discussed mechanism are strong simplifications of reality. It can be investigated whether a depth-dependent fouling approach is useful. Furthermore, including a combination of pore-blockage, (partial) preloading and competition by organic matter could make the fouling model more accurate. More experiments regarding the fouling phenomenon in real pilots can reveal better the fouling mechanisms and how these can be better approached in the model development.

## REFERENCE LIST

- Ahmadi, N., Abbasi, M., Torabian, A., van Loosdrecht, M. C. M., & Ducoste, J. (2023). Biotransformation of micropollutants in moving bed biofilm reactors under heterotrophic and autotrophic conditions. *Journal of Hazardous Materials*, 460, 132232. <https://doi.org/10.1016/j.jhazmat.2023.132232>
- Albuquerque, B., Heleno, S., Oliveira, M., Barros, L., & Ferreira, I. (2020). Phenolic compounds: Current industrial applications, limitations and future challenges. *Food & Function*. <https://doi.org/10.1039/D0FO02324H>
- Aliakbarian, B., Casazza, A., & Perego, P. (2015). Kinetic and Isotherm Modelling of the Adsorption of Phenolic Compounds from Olive Mill Wastewater onto Activated Carbon. *Food Technology and Biotechnology*, 53, 207–214.
- Aquafin. (2023). *Full-scale set-up for removal micropollutants*. <https://www.aquafin.be/en/full-scale-set-up-for-removal-micropollutants>
- Arvaniti, O. S., Dasenaki, M. E., Asimakopoulos, A. G., Maragou, N. C., Samaras, V. G., Antoniou, K., Gatidou, G., Mamaïs, D., Noutsopoulos, C., Frontistis, Z., Thomaidis, N. S., & Stasinakis, A. S. (2022). Effectiveness of tertiary treatment processes in removing different classes of emerging contaminants from domestic wastewater. *Frontiers of Environmental Science & Engineering*, 16(11), 148. <https://doi.org/10.1007/s11783-022-1583-y>
- Brandt, M. J., Johnson, K. M., Elphinston, A. J., & Ratnayaka, D. D. (2017). Chapter 10—Specialized and Advanced Water Treatment Processes. In M. J. Brandt, K. M. Johnson, A. J. Elphinston, & D. D. Ratnayaka (Eds.), *Twort's Water Supply (Seventh Edition)* (pp. 407–473). Butterworth-Heinemann. <https://doi.org/10.1016/B978-0-08-100025-0.00010-7>
- Burkhardt. (2020). *Water\_Treatment\_Models/PSDM at master · USEPA/Water\_Treatment\_Models · GitHub*. [https://github.com/USEPA/Water\\_Treatment\\_Models/tree/master/PSDM](https://github.com/USEPA/Water_Treatment_Models/tree/master/PSDM)
- Burkhardt, Burns, N., Mobley, D., Pressman, J. G., Magnuson, M. L., & Speth, T. F. (2022a). Modeling PFAS Removal Using Granular Activated Carbon for Full-Scale System Design.

*Journal of Environmental Engineering*, 148(3), 04021086.

[https://doi.org/10.1061/\(ASCE\)EE.1943-7870.0001964](https://doi.org/10.1061/(ASCE)EE.1943-7870.0001964)

Burkhardt, Burns, N., Mobley, D., Pressman, J. G., Magnuson, M. L., & Speth, T. F. (2022b).

Modeling PFAS Removal Using Granular Activated Carbon for Full-Scale System Design—

Supplemental information. *Journal of Environmental Engineering*, 148(3), 04021086.

[https://doi.org/10.1061/\(ASCE\)EE.1943-7870.0001964](https://doi.org/10.1061/(ASCE)EE.1943-7870.0001964)

Cantoni, B., Ianes, J., Bertolo, B., Ziccardi, S., Maffini, F., & Antonelli, M. (2024). Adsorption on activated carbon combined with ozonation for the removal of contaminants of emerging concern in drinking water. *Journal of Environmental Management*, 350, 119537.

<https://doi.org/10.1016/j.jenvman.2023.119537>

Das, S., Ray, N. M., Wan, J., Khan, A., Chakraborty, T., & Ray, M. B. (2017). Micropollutants in Wastewater: Fate and Removal Processes. In R. Farooq & Z. Ahmad (Eds.), *Physico-Chemical Wastewater Treatment and Resource Recovery*. InTech.

<https://doi.org/10.5772/65644>

Edefell, E., Falås, P., Torresi, E., Hagman, M., Cimbritz, M., Bester, K., & Christensson, M. (2021). Promoting the degradation of organic micropollutants in tertiary moving bed biofilm reactors by controlling growth and redox conditions. *Journal of Hazardous Materials*, 414, 125535.

<https://doi.org/10.1016/j.jhazmat.2021.125535>

European Investment Bank, & Bofill, J. (2023). *Microplastics and Micropollutants in Water: Contaminants of emerging concern*.

Guerra, P., Kim, M., Kinsman, L., Ng, T., Alaee, M., & Smyth, S. A. (2014). Parameters affecting the formation of perfluoroalkyl acids during wastewater treatment. *Journal of Hazardous Materials*, 272, 148–154. <https://doi.org/10.1016/j.jhazmat.2014.03.016>

Guillossou, R., Le Roux, J., Brosillon, S., Mailler, R., Vulliet, E., Morlay, C., Nauleau, F., Rocher, V., & Gaspéri, J. (2020). Benefits of ozonation before activated carbon adsorption for the removal of organic micropollutants from wastewater effluents. *Chemosphere*, 245, 125530.

<https://doi.org/10.1016/j.chemosphere.2019.125530>

Gutiérrez, M., Grillini, V., Mutavdžić Pavlović, D., & Verlicchi, P. (2021). Activated carbon coupled with advanced biological wastewater treatment: A review of the enhancement in micropollutant removal. *Science of The Total Environment*, 790, 148050.  
<https://doi.org/10.1016/j.scitotenv.2021.148050>

Hokanson, D. R., Hand, D. W., Crittenden, J. C., Rogers, T. N., & Oman, E. J. (1999, July 23). *Michigan Technological University (MTU) Researchers Develop New Software To Help Clean Up Contamination Sites*. ScienceDaily.

<https://www.sciencedaily.com/releases/1999/07/990723083614.htm>

Inglezakis, V. J., Fyrillas, M. M., & Park, J. (2019). Variable diffusivity homogeneous surface diffusion model and analysis of merits and fallacies of simplified adsorption kinetics equations. *Journal of Hazardous Materials*, 367, 224–245. <https://doi.org/10.1016/j.jhazmat.2018.12.023>

Issabayeva, G., Hang, S., Wong, M., & Aroua, M. (2017). A review on the adsorption of phenols from wastewater onto diverse groups of adsorbents. *Reviews in Chemical Engineering*, 34.  
<https://doi.org/10.1515/revce-2017-0007>

Jarvie, M. E., Hand, D. W., Bhuvendralingam, S., Crittenden, J. C., & Hokanson, D. R. (2005). Simulating the performance of fixed-bed granular activated carbon adsorbers: Removal of synthetic organic chemicals in the presence of background organic matter. *Water Research*, 39(11), 2407–2421. <https://doi.org/10.1016/j.watres.2005.04.023>

Khanzada, N. K., Farid, M. U., Kharraz, J. A., Choi, J., Tang, C. Y., Nghiem, L. D., Jang, A., & An, A. K. (2020). Removal of organic micropollutants using advanced membrane-based water and wastewater treatment: A review. *Journal of Membrane Science*, 598, 117672.  
<https://doi.org/10.1016/j.memsci.2019.117672>

Kim, S.-K., Im, J.-K., Kang, Y.-M., Jung, S.-Y., Kho, Y. L., & Zoh, K.-D. (2012). Wastewater treatment plants (WWTPs)-derived national discharge loads of perfluorinated compounds (PFCs). *Journal of Hazardous Materials*, 201–202, 82–91.  
<https://doi.org/10.1016/j.jhazmat.2011.11.036>

Krzeminski, P., Tomei, M. C., Karaolia, P., Langenhoff, A., Almeida, C. M. R., Felis, E., Gritten, F., Andersen, H. R., Fernandes, T., Manaia, C. M., Rizzo, L., & Fatta-Kassinos, D. (2019).

- Performance of secondary wastewater treatment methods for the removal of contaminants of emerging concern implicated in crop uptake and antibiotic resistance spread: A review. *Science of The Total Environment*, 648, 1052–1081.  
<https://doi.org/10.1016/j.scitotenv.2018.08.130>
- Kumari, P., & Kumar, A. (2023). ADVANCED OXIDATION PROCESS: A remediation technique for organic and non-biodegradable pollutant. *Results in Surfaces and Interfaces*, 11, 100122.  
<https://doi.org/10.1016/j.rsurfi.2023.100122>
- Ma, Y., Zhang, X., & Wen, J. (2021). Study on the Harm of Waste Activated Carbon and Novel Regeneration Technology of it. *IOP Conference Series: Earth and Environmental Science*, 769(2). <https://doi.org/10.1088/1755-1315/769/2/022047>
- Magnuson, M. L., & Speth, T. F. (2005). Quantitative Structure–Property Relationships for Enhancing Predictions of Synthetic Organic Chemical Removal from Drinking Water by Granular Activated Carbon. *Environmental Science & Technology*, 39(19), 7706–7711.  
<https://doi.org/10.1021/es0508018>
- Mohammadi, F., Bina, B., Rahimi, S., & Janati, M. (2022). Modelling of micropollutant fate in hybrid growth systems: Model concepts, Peterson matrix, and application to a lab-scale pilot plant. *Environmental Science and Pollution Research*, 29. <https://doi.org/10.1007/s11356-022-20668-2>
- Mudhoo, A., Otero, M., & Chu, K. H. (2024). Insights into adsorbent tortuosity across aqueous adsorption systems. *Particuology*, 88, 71–88. <https://doi.org/10.1016/j.partic.2023.08.022>
- Ngeno, E. C., Mbuci, K. E., Necibi, M. C., Shikuku, V. O., Olisah, C., Ongulu, R., Matovu, H., Ssebugere, P., Abushaban, A., & Sillanpää, M. (2022). Sustainable re-utilization of waste materials as adsorbents for water and wastewater treatment in Africa: Recent studies, research gaps, and way forward for emerging economies. *Environmental Advances*, 9, 100282. <https://doi.org/10.1016/j.envadv.2022.100282>
- Patel, H. (2019). Fixed-bed column adsorption study: A comprehensive review. *Applied Water Science*, 9(3), 45. <https://doi.org/10.1007/s13201-019-0927-7>

Patel, H. (2022). Comparison of batch and fixed bed column adsorption: A critical review. *International Journal of Environmental Science and Technology*, 19(10), 10409–10426.

<https://doi.org/10.1007/s13762-021-03492-y>

Persson, L., Carney Almroth, B. M., Collins, C. D., Cornell, S., De Wit, C. A., Diamond, M. L., Fantke, P., Hassellöv, M., MacLeod, M., Ryberg, M. W., Søgaard Jørgensen, P., Villarrubia-Gómez, P., Wang, Z., & Hauschild, M. Z. (2022). Outside the Safe Operating Space of the Planetary Boundary for Novel Entities. *Environmental Science & Technology*, 56(3), 1510–1521.

<https://doi.org/10.1021/acs.est.1c04158>

Piazzoli, A., & Antonelli, M. (2018). Application of the Homogeneous Surface Diffusion Model for the prediction of the breakthrough in full-scale GAC filters fed on groundwater. *Process Safety and Environmental Protection*, 117, 286–295. <https://doi.org/10.1016/j.psep.2018.04.027>

Pocostales, J. P., Alvarez, P. M., & Beltrán, F. J. (2010). Kinetic modeling of powdered activated carbon ozonation of sulfamethoxazole in water. *Chemical Engineering Journal*, 164(1), 70–76. <https://doi.org/10.1016/j.cej.2010.08.025>

Ramos, R., Ocampo, R., Flores-Cano, J. V., & Padilla, E. (2014). Comparison between diffusional and first-order kinetic model, and modeling the adsorption kinetics of pyridine onto granular activated carbon. *Desalination and Water Treatment*, 55, 1–10.

<https://doi.org/10.1080/19443994.2014.920278>

Rizzo, L., Malato, S., Antakyali, D., Beretsou, V. G., Đolić, M. B., Gernjak, W., Heath, E., Ivancev-Tumbas, I., Karaolia, P., Lado Ribeiro, A. R., Mascolo, G., McArdell, C. S., Schaar, H., Silva, A. M. T., & Fatta-Kassinos, D. (2019). Consolidated vs new advanced treatment methods for the removal of contaminants of emerging concern from urban wastewater. *Science of The Total Environment*, 655, 986–1008. <https://doi.org/10.1016/j.scitotenv.2018.11.265>

Sabri, A., & Abbood, N. (2019). Adsorption Study of Nitrate Anions by Different Materials Using Fixed Bed Column. *Engineering and Technology Journal*, 37. <https://doi.org/10.30684/etj.37.1C.25>

Saidulu, D., Majumder, A., & Gupta, A. K. (2021). A systematic review of moving bed biofilm reactor, membrane bioreactor, and moving bed membrane bioreactor for wastewater treatment: Comparison of research trends, removal mechanisms, and performance. *Journal of*

*Environmental Chemical Engineering*, 9(5), 106112.

<https://doi.org/10.1016/j.jece.2021.106112>

Saleh, T. A. (2022). Chapter 4—Isotherm models of adsorption processes on adsorbents and nanoadsorbents. In T. A. Saleh (Ed.), *Interface Science and Technology* (Vol. 34, pp. 99–126). Elsevier. <https://doi.org/10.1016/B978-0-12-849876-7.00009-9>

SciPy -. (n.d.). Retrieved 2 June 2024, from <https://scipy.org/>

Şerban, G., Iancu, V.-I., Dinu, C., Tenea, A., Vasilache, N., Cristea, I., Niculescu, M., Ionescu, I., & Chiriac, F. L. (2023). Removal Efficiency and Adsorption Kinetics of Methyl Orange from Wastewater by Commercial Activated Carbon. *Sustainability*, 15, 1–17.

<https://doi.org/10.3390/su151712939>

Sharifian, S., & Asasian-Kolur, N. (2022). Polyethylene terephthalate (PET) waste to carbon materials: Theory, methods and applications. *Journal of Analytical and Applied Pyrolysis*, 163, 105496. <https://doi.org/10.1016/j.jaap.2022.105496>

Sharma, S., Balestra, S. R. G., Baur, R., Agarwal, U., Zuidema, E., Rigutto, M. S., Calero, S., Vlugt, T. J. H., & Dubbeldam, D. (2023). RUPTURA: Simulation code for breakthrough, ideal adsorption solution theory computations, and fitting of isotherm models. *Molecular Simulation*, 49(9), 893–953. <https://doi.org/10.1080/08927022.2023.2202757>

Sharma, V., & Feng, M. (2017). Water depollution using metal-organic frameworks-catalyzed advanced oxidation processes: A review. *Journal of Hazardous Materials*, 372.

<https://doi.org/10.1016/j.jhazmat.2017.09.043>

Silva, L. M. S., Muñoz-Peña, M. J., Domínguez-Vargas, J. R., González, T., & Cuerda-Correa, E. M. (2021). Kinetic and equilibrium adsorption parameters estimation based on a heterogeneous intraparticle diffusion model. *Surfaces and Interfaces*, 22, 100791.

<https://doi.org/10.1016/j.surfin.2020.100791>

Sookkumnerd, T. (2019). Numerical Modeling of Industrial-Scale Pulsed Bed Adsorber for Colorant Removal in Sugar Refining. *IOP Conference Series: Materials Science and Engineering*, 559, 012019. <https://doi.org/10.1088/1757-899X/559/1/012019>

- Spindola Vilela, C. L., Damasceno, T. L., Thomas, T., & Peixoto, R. S. (2022). Global qualitative and quantitative distribution of micropollutants in the deep sea. *Environmental Pollution*, 307, 119414. <https://doi.org/10.1016/j.envpol.2022.119414>
- Summers, R. S., Haist, B., Koehler, J., Ritz, J., Zimmer, G., & Sontheimer, H. (1989). The Influence of Background Organic Matter on GAC Adsorption. *Journal AWWA*, 81(5), 66–74. <https://doi.org/10.1002/j.1551-8833.1989.tb03207.x>
- The BAC Process for Water Purification*. (2000, December). Wastewater Digest. <https://www.wwdmag.com/wastewater-treatment/article/10917010/the-biological-activated-carbon-process-for-water-purification>
- Topolovec, B., Škoro, N., Puač, N., & Petrović, M. (2022). Pathways of organic micropollutants degradation in atmospheric pressure plasma processing – A review. *Chemosphere*, 294, 133606. <https://doi.org/10.1016/j.chemosphere.2022.133606>
- Trojanowicz, M. (2020). Removal of persistent organic pollutants (POPs) from waters and wastewaters by the use of ionizing radiation. *Science of The Total Environment*, 718, 134425. <https://doi.org/10.1016/j.scitotenv.2019.134425>
- Vanoppen, M. (2023). 6 Activated Carbon Filtration. In *Environmental Technology: Water*. UGent-BW.
- Wang, J., & Guo, X. (2020). Adsorption isotherm models: Classification, physical meaning, application and solving method. *Chemosphere*, 258, 127279. <https://doi.org/10.1016/j.chemosphere.2020.127279>
- Wang, J., & Guo, X. (2023). Adsorption kinetics and isotherm models of heavy metals by various adsorbents: An overview. *Critical Reviews in Environmental Science and Technology*, 53(21), 1837–1865. <https://doi.org/10.1080/10643389.2023.2221157>
- Webb, P. A. (2001). *Volume and Density Determinations for Particle Technologists*.
- Westerhoff, P., Yoon, Y., Snyder, S., & Wert, E. (2005). Fate of Endocrine-Disruptor, Pharmaceutical, and Personal Care Product Chemicals during Simulated Drinking Water Treatment Processes. *Environmental Science & Technology*, 39(17), 6649–6663. <https://doi.org/10.1021/es0484799>

- Worch, E. (2008). Fixed-bed adsorption in drinking water treatment: A critical review on models and parameter estimation. *Journal of Water Supply Research and Technology-Aqua - J WATER SUPPLY RES TECHNOL-AQ*, 57. <https://doi.org/10.2166/aqua.2008.100>
- Xiaojian, Z., Zhansheng, W., & Xiasheng, G. (1991). Simple combination of biodegradation and carbon adsorption—The mechanism of the biological activated carbon process. *Water Research*, 25(2), 165–172. [https://doi.org/10.1016/0043-1354\(91\)90025-L](https://doi.org/10.1016/0043-1354(91)90025-L)
- Xu, Z., Cai, J., & Pan, B. (2013). Mathematically modeling fixed-bed adsorption in aqueous systems. *Journal of Zhejiang University SCIENCE A*, 14(3), 155–176.  
<https://doi.org/10.1631/jzus.A1300029>
- Yao, C., & Zhu, C. (2021). A new multi-mechanism adsorption kinetic model and its relation to mass transfer coefficients. *Surfaces and Interfaces*, 26, 101422.  
<https://doi.org/10.1016/j.surfin.2021.101422>
- Yin, R., & Shang, C. (2020). Removal of micropollutants in drinking water using UV-LED/chlorine advanced oxidation process followed by activated carbon adsorption. *Water Research*, 185, 116297. <https://doi.org/10.1016/j.watres.2020.116297>
- Zahmatkesh, S., Amesho, K. T. T., & Sillanpää, M. (2022). A critical review on diverse technologies for advanced wastewater treatment during SARS-CoV-2 pandemic: What do we know? *Journal of Hazardous Materials Advances*, 7, 100121.  
<https://doi.org/10.1016/j.hazadv.2022.100121>
- Zahmatkesh, S., Bokhari, A., Karimian, M., Zahra, M. M. A., Sillanpää, M., Panchal, H., Alrubaie, A. J., & Rezakhani, Y. (2022). A comprehensive review of various approaches for treatment of tertiary wastewater with emerging contaminants: What do we know? *Environmental Monitoring and Assessment*, 194(12), 884. <https://doi.org/10.1007/s10661-022-10503-z>
- Zhou, L., Qu, Z. G., Ding, T., & Miao, J. Y. (2016). Lattice Boltzmann simulation of the gas-solid adsorption process in reconstructed random porous media. *Physical Review E*, 93(4), 043101. <https://doi.org/10.1103/PhysRevE.93.043101>

## APPENDIX A: K FITTING TOOL

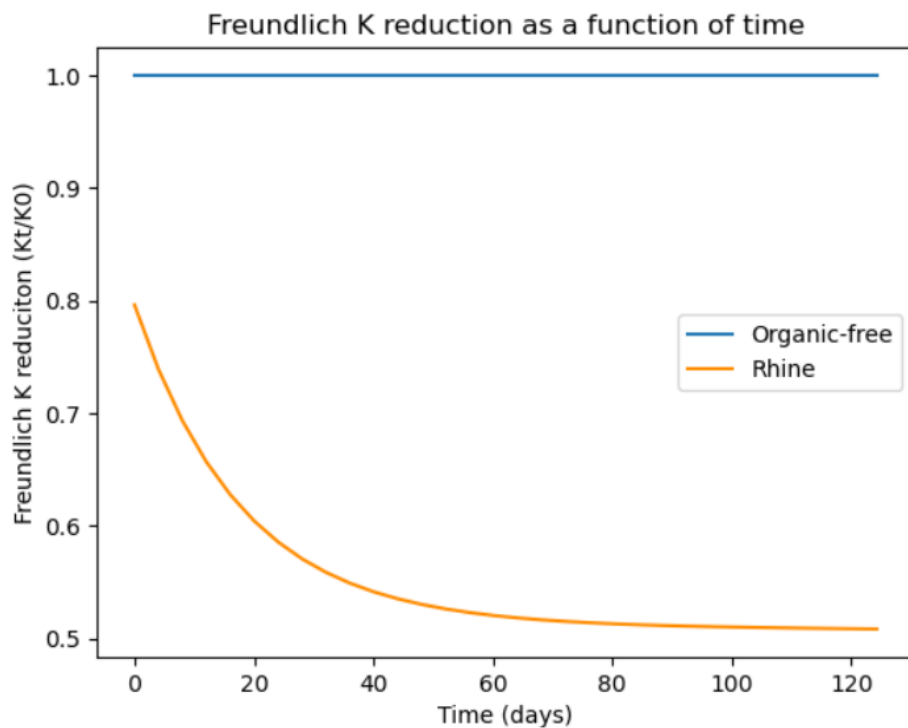


Figure 42 K reduction graph with adjusted time axis, corresponding to duration of pilot experiment (PFHpA) (Burkhardt et al., 2022a)

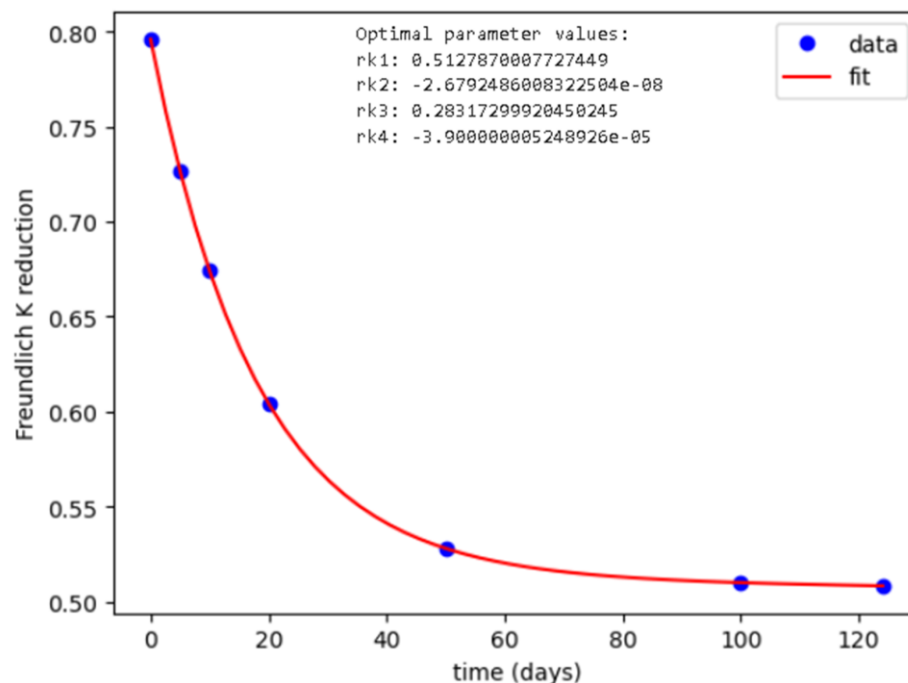


Figure 43 K fitting tool where the K reduction function fits the data (demonstration). Data derived from PFHpA pilot simulation for comparison (Burkhardt et al., 2022a)

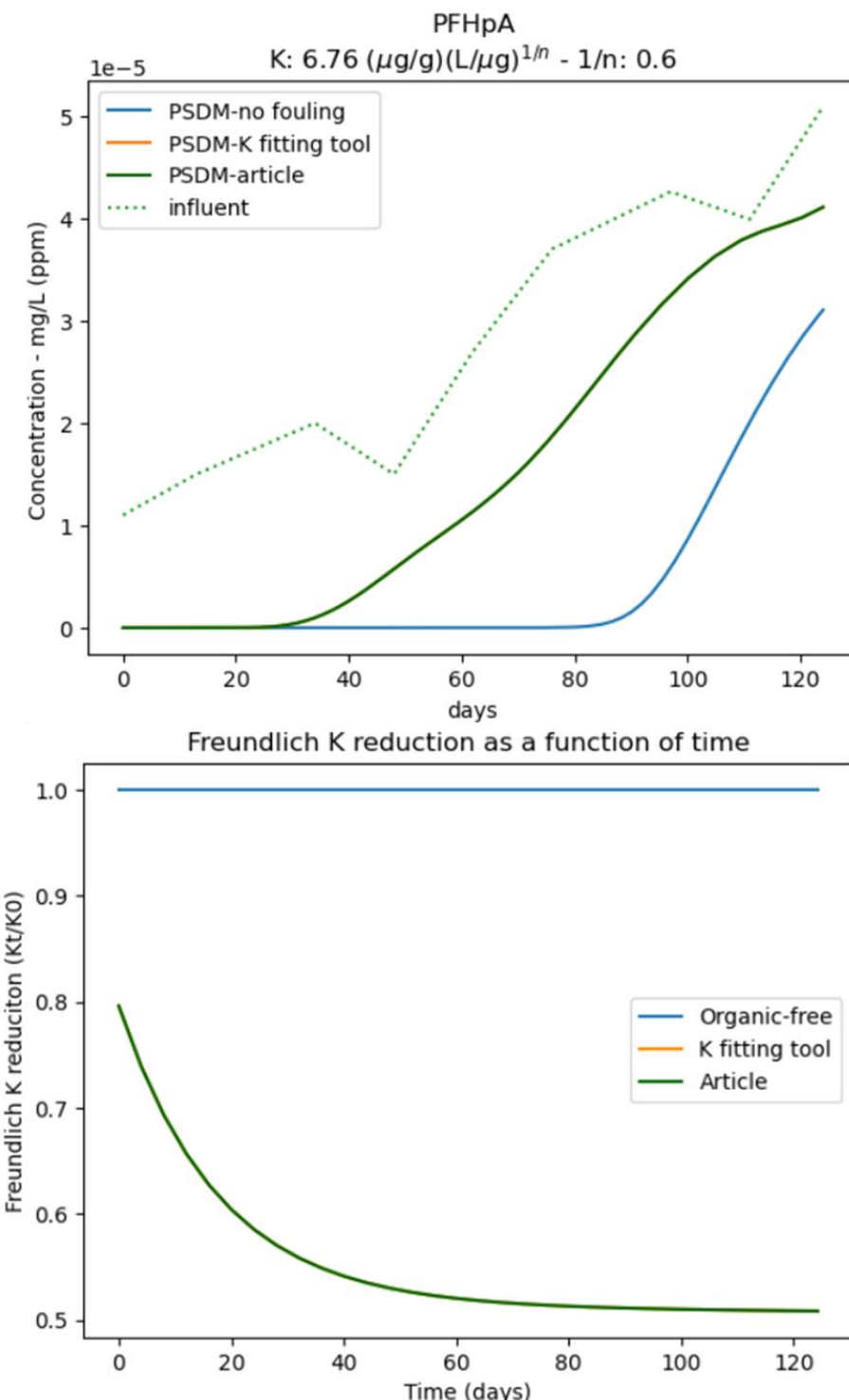


Figure 44 PSDM model output, i.e. breakthrough curves, and K reduction graph for organic-free, K fitting tool and reference article (Burkhardt et al., 2022a)

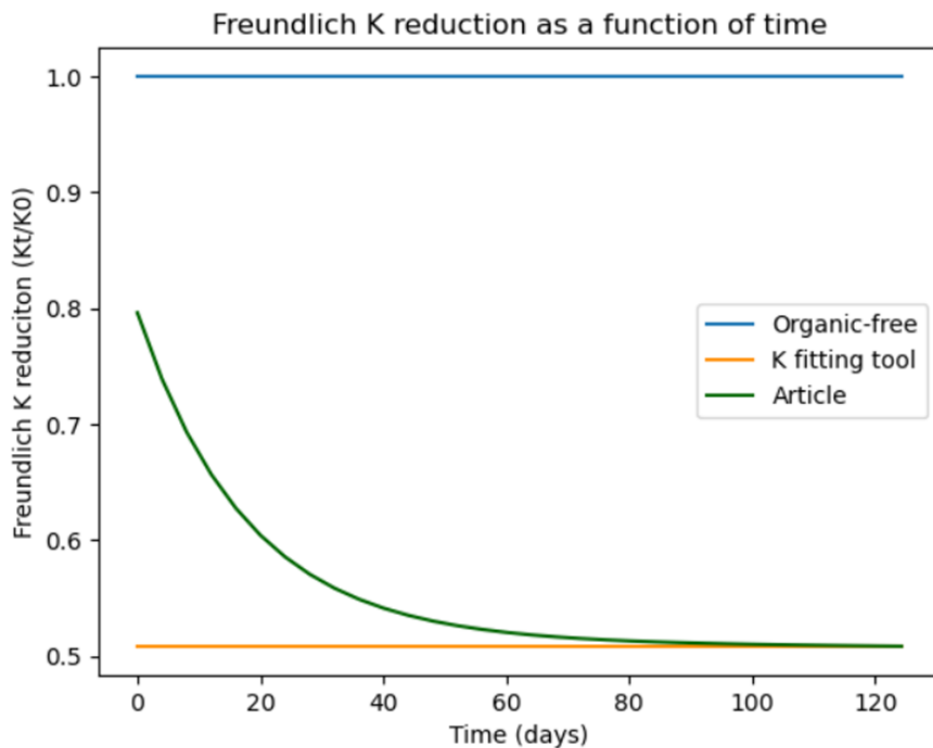
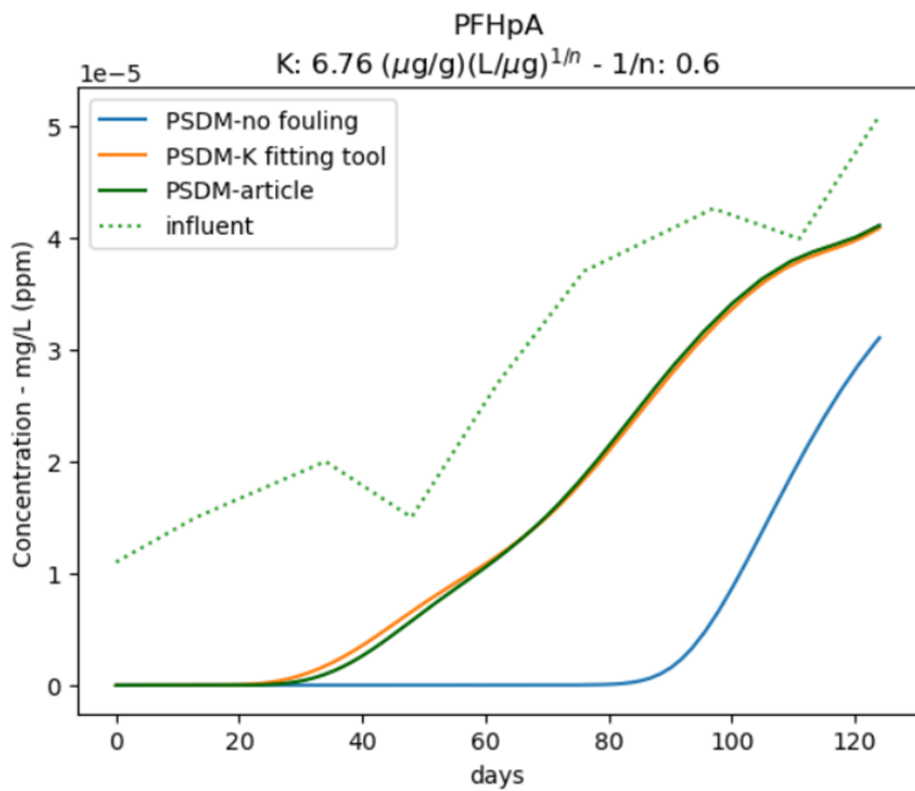
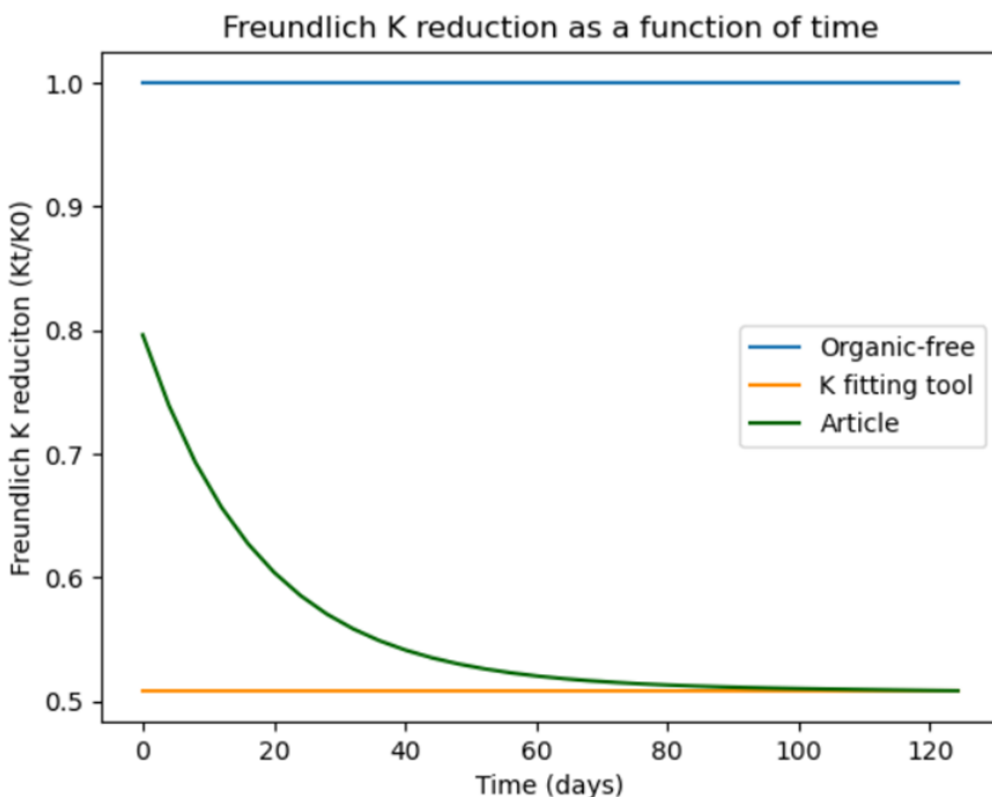
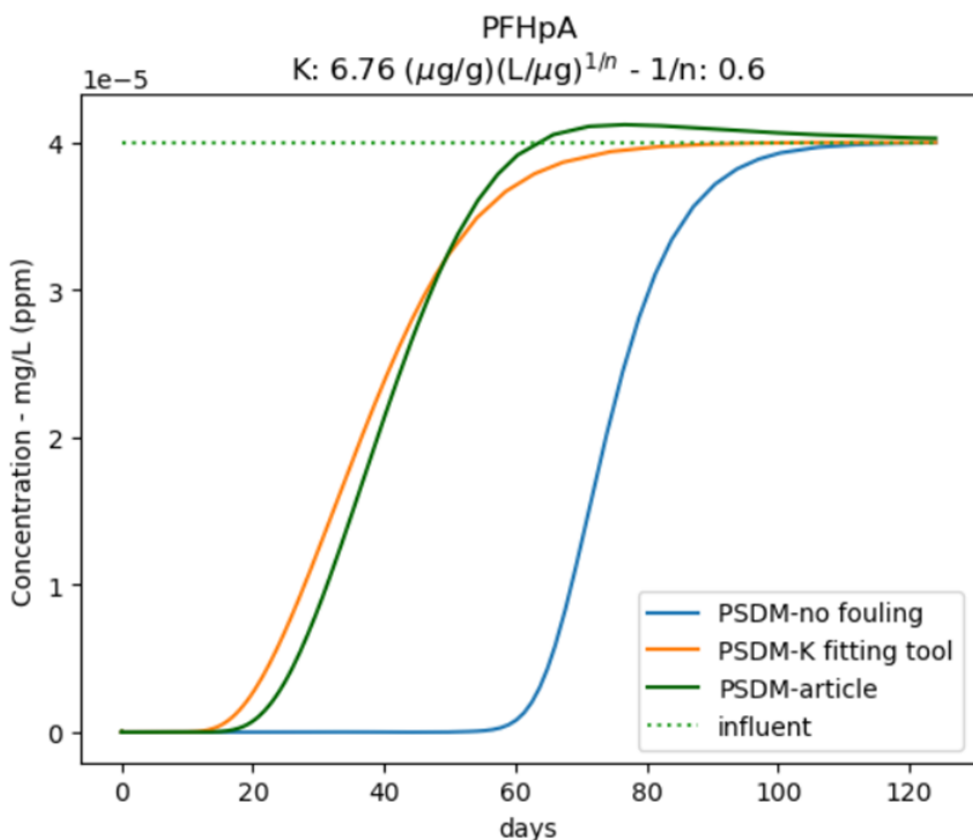


Figure 45 PSDM model output, i.e. breakthrough curve, and K reduction graph for organic-free, K fitting tool (constant reduced K) and reference article (Burkhardt et al., 2022a)



**Figure 46 PSDM model output, i.e. breakthrough curve, and K reduction graph for organic-free, K fitting tool (constant reduced K) and reference article (Burkhardt et al., 2022a). All simulations are done with constant influent concentration of PFHpA**

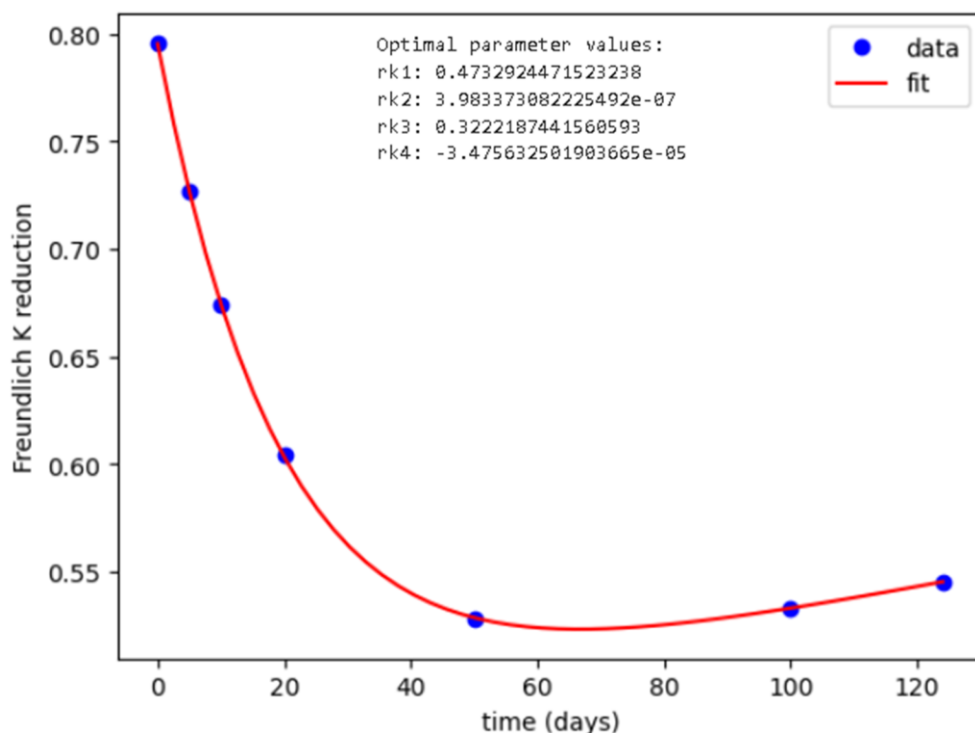


Figure 47 K fitting tool where the K reduction function fits the data.  
Data was made-up to demonstrate an increase of K in the end

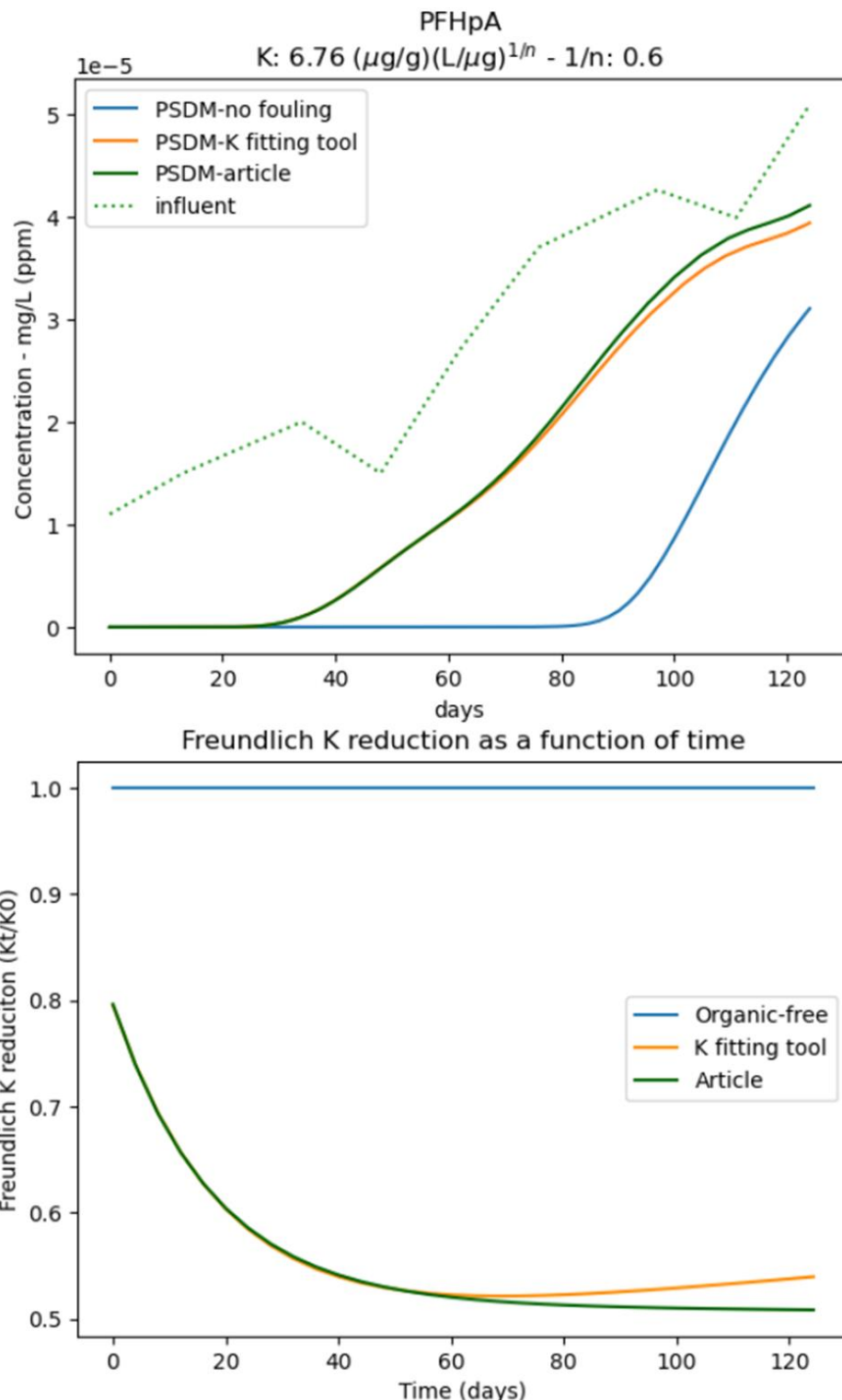
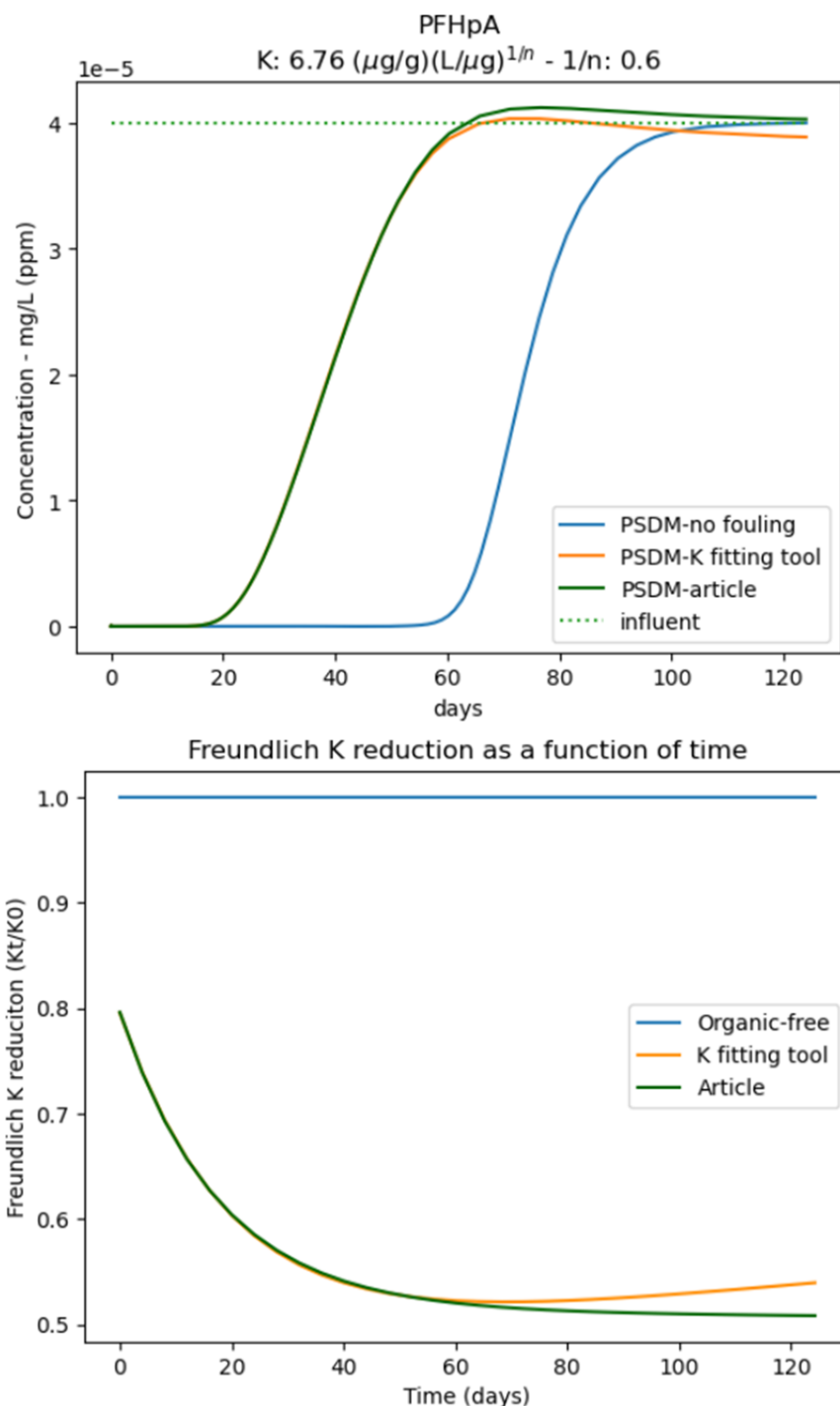
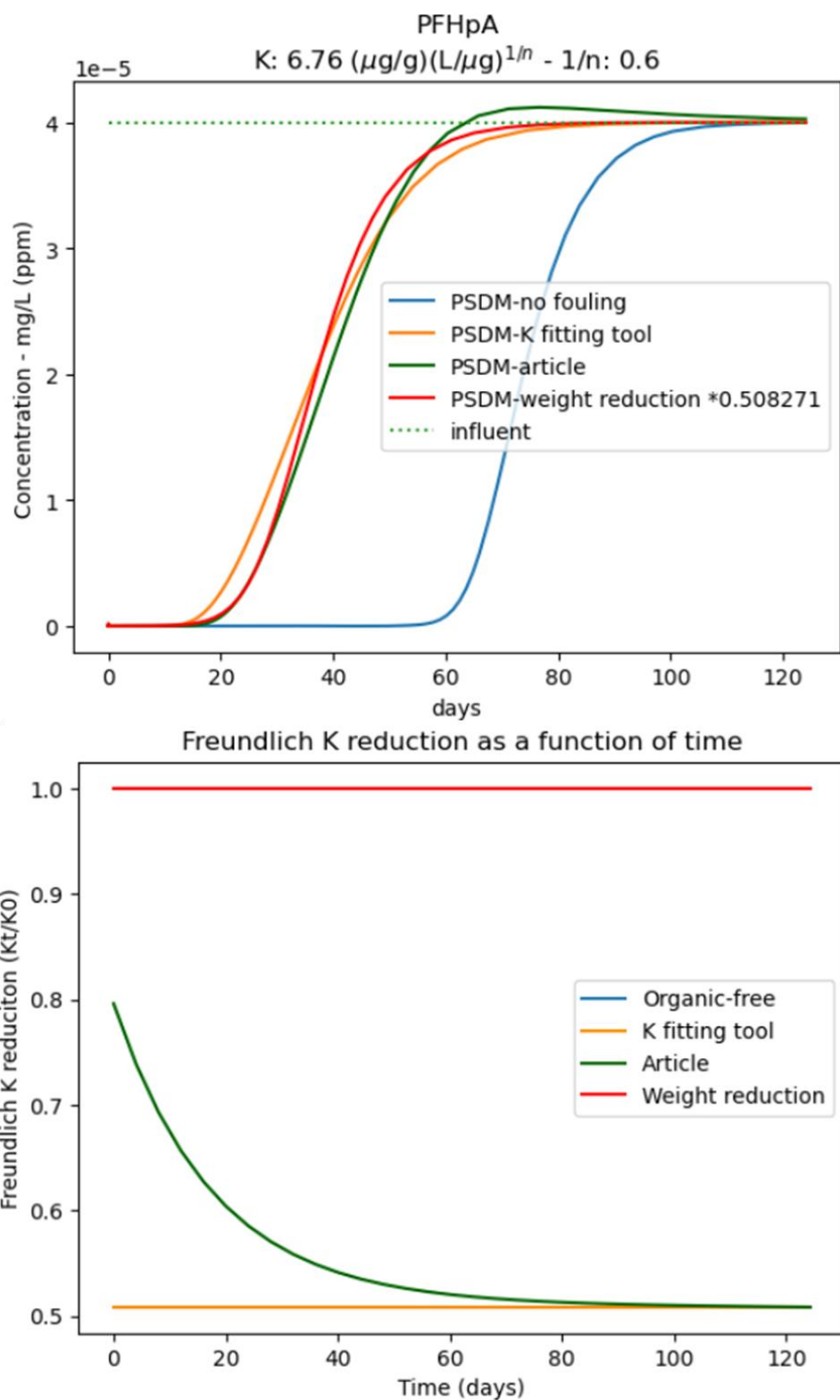


Figure 48 PSDM model output, i.e. breakthrough curve, and K reduction graph for organic-free, K fitting tool (increase in the end) and reference article (Burkhardt et al., 2022a)



**Figure 49 PSDM model output, i.e. breakthrough curve, and K reduction graph for organic-free, K fitting tool (increase in the end) and reference article (Burkhardt et al., 2022a).**  
**All simulations are done with constant influent concentration of PFHpA**



**Figure 50 PSDM model output, i.e. breakthrough curve, and K reduction graph for organic-free, K fitting tool (fixed), reference article (Burkhardt et al., 2022a), and weight reduction (fixed).**  
All simulations are done with constant influent concentration of PFHpA